POLITECNICO DI TORINO

Master Degree course in Biomedical Engineering

Politecnico
di Torino

Master's Degree Thesis

3D modelling of bioprinted porous bone implants

Supervisors:
Professor Francesco Baino
Professor Marco Mazza
Engineer Raphael Wenger

Candidate:
Roberta Gabrieli

A.y 2021/2022

POLITECNICO DI TORINO

Abstract

3D modelling of bioprinted porous implants

The anatomical and functional loss of a tissue is one of the most debilitating problems which involves a great cost to the international healthcare sector. A solution to the methods of traditional medicine is the new field of regenerative medicine. Tissue engineering aims at the development of artificial tissues through the use of biomaterials and specific cells. In the field of bone tissue, the use of scaffolds to promote tissue regeneration is a topic of great interest. The combination of additive manufacturing and computational methods led to the creation of bone scaffolds with complex microstructure and mechanical behavior comparable to that of bone.
In this study, some of the representative models of triply periodic minimal surface (TPMS) have been printed in 3D through the stereolithographic technique. Specifically, Schwarz Primitive and Gyroid surfaces have been created computationally; they are characterized by a complex geometry, a high pore interconnectivity and a curvature such as to play a key role in the mechanism of cell proliferation. There are several design parameters that can be varied in these structures and can consequently affect the performance of the scaffold. Morphological and mechanical analysis were performed to experimentally assess the properties of the scaffolds. Finally, the relationship between the relative density and the mechanical characteristics of the scaffolds has been analyzed in order to understand if the patterns created can be used for applications in bone tissue engineering.

Contents

Chapter 1

Introduction

In recent years, thanks to the sudden growth in the field of technology, new possibilities have opened up, leading to great improvements in all areas.

The development of artificial intelligence, nanotechnology, robotics, the use of virtual reality and 3D printing have led to a considerable acceleration in particular in the medical field.

Among these advances has been the introduction of 3D printing. In Pubmed there are more than 16,000 results in the last 5 years about the words '3D printing'.

3D printing is one of the most promising technologies that can be used in all sectors, from aerospace, automotive and construction, to the medical sector. It is seen as an alternative to the traditional production system, so much so that with the introduction of this technology we speak of "the fourth industrial revolution". [1]

It is a technology that allows physical objects to be produced from a virtual model created with specific software. It includes of a series of processes that consist of depositing material in layers (one by one), building the final object.

It is one of the most revolutionary technologies, in medical field; it was first introduced in 1990 in the dental sector but today it is also used in the development of medical equipment and in the creation of customised devices and prostheses. [2]

In dentistry, in addition to the production of fixed prostheses or dental braces, it is possible to take oral scans and subsequently print them out in order to adapt each piece to the individual patient with careful precision.

By way of 3D printing it is possible to reproduce every anatomical district in detail by constructing actual anatomical models for simulating surgical procedures. These are used by doctors for practice, pre-operative case studies and to improve the results of operations.[3]

The usability and low cost of 3D printing has enabled the creation of new surgical instruments and devices to improve the accuracy of surgical procedures.

Another field where 3D printing is very successful is orthopaedic prosthetics. Thanks to the introduction of 3D printing, it is possible to realize patient-specific prosthetic devices where a 3D scanner creates a digital model of the limb's morphology. This mainly results in the respect for the patient's anatomy and physiognomy and a better recovery of previously lost functionality. [3]

The use of increasingly innovative materials has enabled less difficult prosthetic replacement and at the same time a better wearability and appreciable results in terms of quality of life.[4]

New advances in printing methodologies and materials for prostheses and orthoses allow production in short time and with affordable prices, meeting the ever-increasing demands for these devices.

An alternative solution to implanting a prosthesis as a cure for damaged or degenerated tissue is the use of transplantation or grafting of physiological materials.

Although transplantation allows recovery of the function of the part to be replaced, it presents the problem of rejection, i.e. a negative immune response of the body to the transplanted part.

Today, the demand for replacement devices and artificial organs is increasing considerably, mainly due to the increase in the average age worldwide. But both the high costs of a cutting-edge prosthesis and the shortage of tissue and organ donors have led to the development of a new discipline, tissue engineering. [5]

Advances in innovative biomaterials research and cell culture methodologies have enabled the repair of damaged tissues through the production of systems capable of permanently replacing portions or entire parts of damaged tissue in the body.

It is a subject that combines engineering techniques and methods with principles of biology, medicine and chemistry in order to maintain, restore and heal tissues or organs.[6]

At the 1st NSF congress in 1988, the term Tissue engineering was introduced for the first time to identify *"the set of principles and methods of the medical and engineering sciences*

to establish the fundamental relationships between structure and function of healthy or pathological mammalian tissues and the development of biological substitutes to restore, maintain or improve tissue function.".[7], [8]

Over time, the following definitions introduced by the Langer and Vacanti scientists have been given:

'Tissue Engineering is that interdisciplinary field that applies the principles of engineering and the sciences that study life for the development of systems capable of restore, preserve and improve tissue functions' (Vacanti 1995).[9]

'Its primary objective is to restore tissue function through the implantation of 'living' elements that are capable, within a clinically acceptable timeframe to become an integral part of the organism into which they are introduced, with reduced margins of post-implant failure' (Langer 1999).[10]

Tissue engineering involves the creation of artificial tissues that through functionalisation with suitable cells are integrated into the host organism to enable tissue healing.

Essential components on which the work of tissue engineering is based are cells, growth factors mainly, the bioreactor and scaffolds.

Scaffold is a three-dimensional structure that is specially created similar to the architecture of the tissue that needs to replace and which, through the adhesion of specific cells, enables their proliferation and differentiation by stimulating tissue growth.

Scaffold is an artificial structure used for the regeneration of biological tissues as it creates a favourable environment for their growth. It is used as a temporary guide for the growth of new tissue.

What determines the success of a scaffold are the properties and physical characteristics similar to those of the natural tissue it is meant to repair. [7]

Certainly, as in the case of transplants and prosthesis, the main problem with implanting a scaffold is its possible rejection.

For this reason, a very important step in the production of the scaffold lies in the choice of its architecture and the biomaterial with which creating it. Scaffold must positively influence the mechanical and biological properties of the tissue and cells.

For the production of biomimetic and biocompatible scaffolds, 3D Bioprinting techniques has become increasingly popular.

Bioprinting refers to the method used to print biomaterials, cellular structures and engineered tissues that can be used directly on humans to repair or replace biological tissues.

The International Conference on Bioprinting and Biofabrication in Bordeaux (3B'09) in 2009 expressed itself in these terms:

"Bioprinting can be defined as the use of computer-aided transfer processes for patterning and assembling living and non-living materials with a prescribed 2D or 3D organisation in order to produce bioengineered structures serving in regenerative medicine, pharmacokinetic and basic cell biology studies."[11]

The aim of this work is to model scaffold for applications in bone tissue through bioprinting techniques.

Firstly it must be considered the use of the scaffold in order to develop it successfully, so it must be produced to mimic the characteristics of the bone.

The object of study must have a three-dimensional and highly porous structure, it must be biocompatible and possess mechanical properties comparable to those of bone tissue.

In this work the development of the scaffold was proposed through a software that allowed 3D modeling. The software used was Python, which made it possible to freely browse through its libraries and functions in order to create a porous scaffold with a bone-like structure.

After choosing the scaffold parameters and creating the digital model, it has been created the three-dimensional scaffold by means of 3D printing. This was done using the stereolithography technique, a method that uses thermo-hardening materials which react by polymerising and hardening themselves when they are exposed to UV lasers.

Then it was carried out a morphological investigation on representative samples to assess their porosity and structural characteristics.

In the final part of the project, the models were tested mechanically, in traction and compression, to investigate whether the results obtained are compatible with the mechanical characteristics of the bone.

In conclusion, it was assessed whether the lattices produced mimic the characteristics of the bone, and if possible, to develop and apply a theory that can predict the mechanical properties of the scaffold produced through density information.

Chapter 2

State of Art

2.1 Bone tissue

Bone is a connective tissue specialized for the supporting function of the human body. The main function of the bone tissue is to support the body, supporting soft tissue, protecting the vital organs and to support the muscles allowing their movement.

Bone is a complex tissue with an active metabolism due to high vascularization.

It consists of mineralized extracellular matrix and various bone cells. Bone can be considered as a composite material consisting of an organic and a mineral component.

Indeed, both in the bone tissue and in the same extracellular matrix can be recognized organic (30-35%) and inorganic (65-70%) components.

The organic component of bone consists of osteocytes, osteoblasts, osteoclasts and osteoprogenitor cells, which provide growth, production and resorption of bone tissue.

The organic component of extracellular matrix is made up by fibers of collagen type I, responsible for bone flexibility and elasticity.

The extracellulular matrix part consisting of minerals is the inorganic phase of bone tissue. It includes mainly calcium phosphates in the form of hydroxyapatite crystals, gives the bone properties such as hardness stability, mechanical strength and compressive stiffness. [12]

The bone components and their functions are detailed in Figure 2.1.

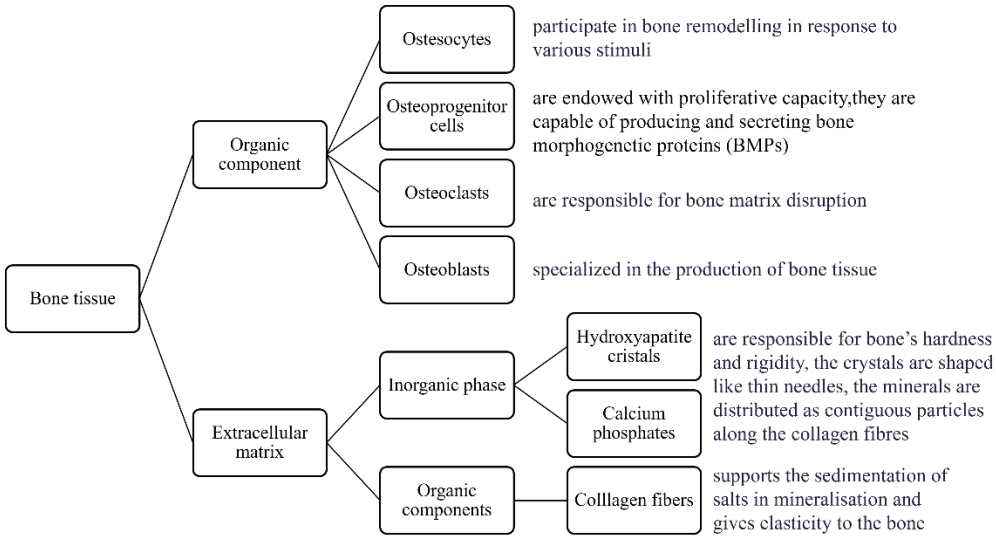

Figure 2.1 Bone components and functions

These components are arranged to form two types of bone: cortical bone and trabecular bone, whose percentages vary in the various bones. The bone structure is shown in the Figure 2.2.

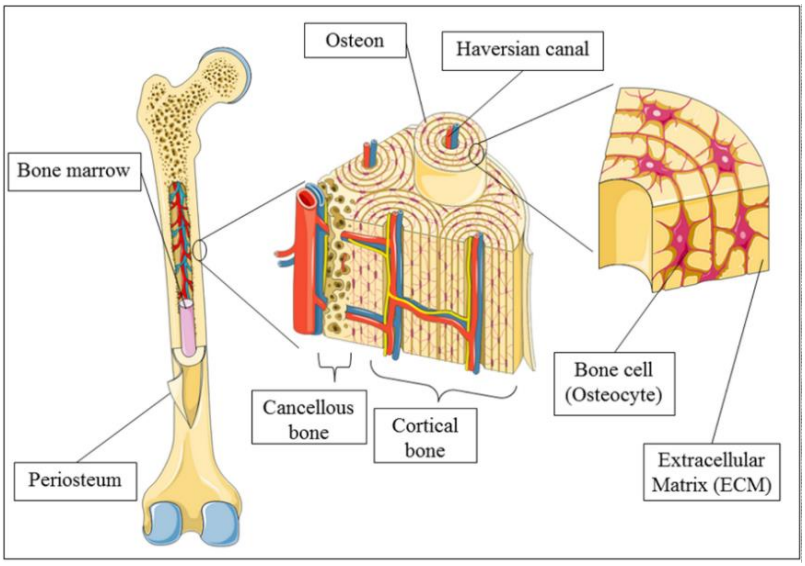

Figure 2.2 Bone structure

The cortical bone is mainly found in the outer part of the bone, it is called compact because it has reduced porosity.

The cortical bone has a porosity between 5% and 30%, it is made up of a fundamental unit, called osteon, and lamellae, consisting of collagen fibres adhering to each other and small lacunae containing osteocytes. The lamellae are arranged concentrically to Havers' canal within which are the blood vessels responsible for supplying nutrients to the tissue.

It has an anisotropic behaviour, with a preferential loading direction, the longitudinal one, which has superior mechanical properties to the others.

It is the hardest and most resistant component of bone, characterised by compressive strength of 100-230 Mpa, and Young's modulus of 7-30 Gpa.

While trabecular or cancellous bone is located in the inner part of the bone and it has a higher porosity between 30% and 90%.

Cancellous bone is characterised by collagen lamellae with deposited hydroxyapatite as in cortical bone, but with the absence of Havers' canal. The lamellae are arranged without specific orientation. There are large gaps between beam-like bone structures (trabeculae) that are arranged to form a lattice to maximise mechanical strength using the least amount of bone**.** Also the spongious bone has an anisotropic behaviour, in this case due to the orientation of bone trabeculae which change according to the imposed load and their spatial arrangement.

It is less rigid and less resistant than cortical bone, despite this, its architecture makes it more elastic and lighter, capable of withstand loads, characterised by lower compressive strength of 2–12 MPa and Young's modulus of 0.5-0.05 GPa. [13]

Bone can be defined as a fragile but ductile material at the same time. When subjected to external stress, it presents an initial linear elastic deformation, in which a small application of forces is sufficient to produce large deformations. Then follows an almost constant plateau until the fracture.

Bone is not a static tissue but it is characterised by dynamic remodelling, maturation, differentiation and resorption throughout life.

All these processes take place through a dynamic process involving osteoclasts and osteoblasts, which are responsible for maintaining healthy bone.[14] With bone remodelling, it means the process of structural adaptation that allows bone to continuously change and self-healing.[15]

Wolff's law states that bone constantly adapts to externally transmitted stresses and loads by remodelling itself. It is able to respond to organic and mechanical stimuli, both static and dynamic, through the modulation and adaptation of its internal structure.

German surgeon Julius Wolff, in the 19th century, states that *'Every change in the form and function of bone or of their function alone is followed by certain definite changes in their internal architecture, and equally definite alteration in therir external conformation, in accordance with matematical laws.'*

It means that to an increase in the load applied to the bone, the bone will respond by adapting through a process of remodelling over time and it will make it resistant for that load; this happens because the trabeculae are able to adapt and thicken. At the same time, if the loads transmitted to the bone decrease, the bone becomes weak and loses its supporting properties. [16]

When osteometabolism, i.e. the balance between the two types of cells, fails, bone diseases occur. The most common disease is osteoporosis, caused by a loss of minerals that leads to progressive brittleness of the bone. In addition, there are diseases due to infections, bone tumours, hormone deficiencies, genetic components or bone fractures. Most fractures do not require surgery, thanks to the bone's high regenerative capacity, but unfortunately large bone defects and in severe cases, where bone function is lost, surgery is required.[17]

2.2 Bone defect repair

Critical bone defects lead the bone to an extreme condition in which it cannot heal itself. [15] These defects adversely affect revascularization and the ability to differentiate tissue, resulting in a spontaneous fracture of the bone that progresses to break completely.

Fortunately, since the second half of the twentieth century, high medical achievements have been achieved in the repair of bone tissue.

Treatment varies according to the type of disease, among the useful interventions there are prosthetic therapy, the use of graft and tissue engineering, as illustrated in Figure 2.3.

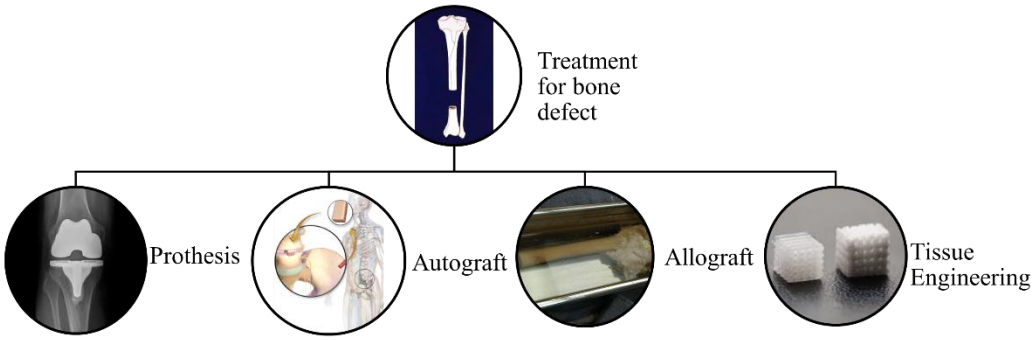

Figure 2.3 Main treatment for bone defects

Prosthetic therapy is the best solution that is implemented in case of severe pathology characterized by heavily damaged tissue; it consists of an orthopedic surgical procedure in which the damaged tissue is replaced, reshaped or realigned. The use of prostheses and fixators allows to restore the lost functionality, In particular, prostheses are long-term artificial implants that replace a part of missing or damaged bone tissue and fixators are devices that support a part that is not completely damaged.[18]

Another technique of intervention involves the use of graft, that is, the transplantation of a part of tissue taken from a donor, used are used to stabilize, align and support the damaged bone to restore the lost function.

Different types of grafts can be distinguished according to the donor:

- Autograft consists in taking bone from another part of the patient's own body, is the gold standard of these treatments. Autologous bone is alive and it provides osteogenic cells as well as essential osteoinductive factors needed for bone healing and regeneration., but this treatment involves a larger surgical procedure, more discomfort and damage in a healthy body part.
- Allograft is a procedure in which the bone is taken from somebody else's body, the rate of graft incorporation is lower than with the autograft.and it could introduce the posibilities of pathogen transmission from donor to host and immune rejection.[19]

However, because of the limited sources of bone tissue, risk of transmission of pathologies and inability of materials to reshape and react to physiological conditions are needed more effective strategies to heal large bone defects.[20]

In the last years, regenerative medicine and tissue engineering have emerged as promising strategies for bone reconstruction.

TE is an alternative approach with a great potential in regenerative medicine, it was defined by Langer and Vacanti as *''an interdisciplinary field of research that applies the principles of engineering and the life sciences towards the development of biological substitutes that restore, maintain, or improve tissue function''*. [21]

The biological substitutes selected to promote growth of new bone must perform the important functions of cell adhesion, migration and differentiation, diffusion of vital cell nutrients and secreted products, vascularization, support of mechanical and biological functions.[14]
In particular, research in this field combines engineering methods with the use of appropriate cells and biochemical factors to heal or replace damaged tissue.
In bone tissue engineering it is used a scaffold to mimic the natural behavior of the bone, in particular it provides a specific architecture and environment for bone growth and development.[8]

2.3 Bone defect repair

In BTE, a biomaterial implant which is used for bone defect repair is called scaffold. A scaffold is a three dimensional artificial structure that provides bone development and growth.

To do this, scaffold is designed to mimic the behavior of bone tissue's ECM, it has a specific environment and structure to provide cell migration and adheration and to stimulate their proliferation and differentiation. It is essential that it promotes osteogenenesis and vascularization within it for the new bone growth. Scaffold must prevent inflammatory responses after its insertion and must communicate with the surrounding tissues. To facilitate this, the scaffold is functionalized and may contain cells, growth factors, that can release specific molecules, promote adhesion of bone tissue cells and could partecipate in the regenerative process actively.[19]

Above all, the scaffold is a temporary matrix that will be replaced by new bone over the time. For this reason it must have an architecture ables to supporting loads during the formation of new tissue and in its degradation does not release toxic substances.

The main goals of the scaffold are summarised in the Figure 2.4. and the main characteristic of the scaffold are presented in the Figure 2.5.

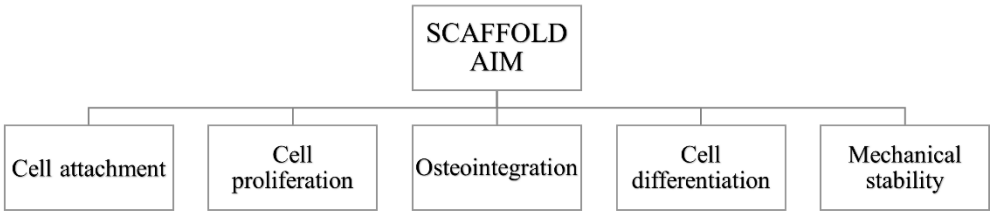

Figure 2.4 Scaffold aim

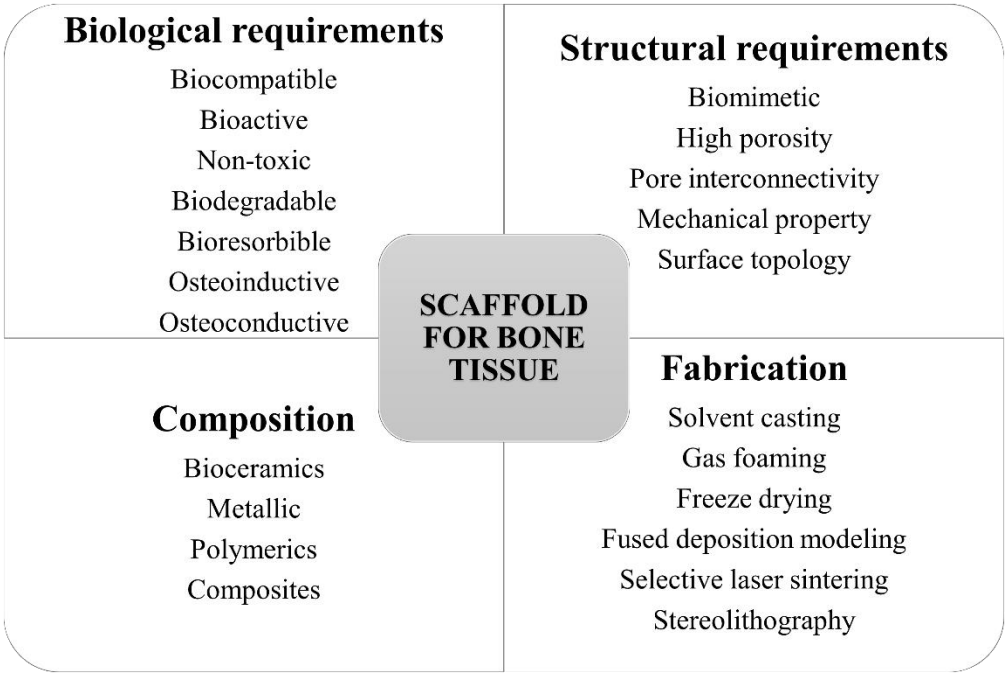

Figure 2.5 Scaffold for bone tissue engineering

2.3.1 Biological Requirements

To provide an optimal environment for cell growth, proliferation, and differentiation and tissue formation, scaffolds have to achieve certain important requirements.

Firstly scaffold must be biocompatible in order to interact with surrounding cells and tissues without causing inflammatory responses. Biocompatibility refers to the ability of biomaterial to minimize the risk of toxicity and allow integration onto the host tissue.

Biodegradability and bioresorbability are fundamental properties of the scaffold that allow the replacement of the scaffold with formation of new bone tissue without the need of second surgery to remove the implant.

It is important to have a controlled resorption rate because the scaffold must provides the mechanical stability during the replacement, so that the new tissue can gradually form itself. Additionally scaffold needs to degrade into products easily metabolized from the body and non-toxic.

It is desired that a bone scaffold could be osteoinductive and osteoconductive.

Osteoconductivity guides bone growth on scaffold surface, allows bone cells to adhere, proliferate and differentiate. Osteoconductivity is the ability of a scaffold to form mineralized matrix, create strong bond and eliminate the formation of fibrous tissue encapsulation.

Osteoinductivity induces the osteogenesis process stimulating osteoprogenitor cells to differentiate in the defect site. To improve osteoinductivity in bone scaffold is necessary to modify the surface for example with incorporation of osteogenic peptides.

Osseointegration refers to the anchor between implant and bone. A poor osseointegration influences mechanical stability and vascularization of the scaffold and the formation of a fibrous capsule around the implant which could leads to reject the implant.

Another biological requirements is scaffold's bioactivity. It is the ability to interact and crosstalk with surrounding living environment. As happens for osteoconductivity, at the same way bioactivity promotes cell migration, tissue neoformation avoiding host's immune response.

Biological requirements are affected by many factor including mechanical properties, structure and architecture of the implant and chemistry of biomaterial.[20],[22],[15]

2.3.2 Structural Requirements

Biomaterial surface is the first part that comes into contact with surrounding tissues immediately after implantation. It is modified by incorporation of bioactive molecules such as growth factors or antinflammatory drugs, to be released after implantation so as not to cause immune response and to promote cells adheration.

In order to have good adhesion and to make the biomaterial osteoconductive, the chemical and topographical properties of its surface must be considered.

First of all, the surface must be permeable to allow transfer of biological fluids and mass transport to permit exchange of nutrients and wastes, and cell migration. Also it has been demonstrated that a rough surface is able to imprison the fibrin matrix, which facilitates the migration of osteogenic cells to the materials surface.

Another critical feature is scaffold architecture. To promote bone regeneration it is necessary to consider non-homogeneous structure of bone and create a scaffold with a stratified, multilayered geometry to mimic the original structure of bone.

Firstly the exterior geometry of the scaffold must be suitable to cover the bone defect and then to facilitate tissue induction must have a controlled porosity distribution.

The ideal scaffold should have higly porosity with distribuited and interconnected pores in order to ensure an accurate diffusion of nutrients and gases, for the removal of metabolic waste, to allow cell growth and favor vascular invasion.

Porosity refers to the ratio of void volume to total volume, specifically it is overall the percentage of void space in a solid and scaffold for bone tissue has a porosity between 80-90%.

The level of porosity usually influences scaffold's mechanical stability, so, its value, should be balanced with the mechanical needs of the site that is going to be replaced, in particular there is a inverse correlation between porosity's degree and mechanical properties.

For example high porosity could compromises the integrity of the scaffold, because the mechanical strength is not sufficient to substain loads.

Also the porosity can influence the degradation rate of the scaffold, in particular high porosity involves acceleration of material's degradation.

On the contrary a great porosity, including higher interconnectivity of pores, leads rapid bone formation and facilitate the neovascularization. A higher porosity and pore size improve the available surface area to binding cells with scaffold and interaction with the surrounding tissue.

Scaffold with adequate degree of porosity is able to promote osteogenesis and ensure good mechanical properties.[23]

Related to the porosity, it is important to consider the pores size, which refers to the the diameter of individual voids in the scaffold.

Pores are necessary for bone tissue formation because they impact cell migration, nutrient transport, cell oxygenation. Especially pore size have been shown to influence cell attachment efficiency, ECM production and tissue vascularization.

Pores size depends on the type of bone tissue and the site they need to replace, normally are required pore size at least 40 μm, the ability to create smaller pore size is influenced by 3D printing resolution.

Pore size lower than 75 μm are useful to provides cell adhesion and production of ECM and improve scaffold osteoinduction.

Intermediate pores which the range is between 75-150 μm and pore size which are larger than 200 μm are more suitable for formation of unmineralized and mineralized bone tissues.

In particular pore size of 100-200 μm provide in large part osteoconduction and growth of new bone tissue. Pore larger than 300 μm are useful to have optimal tissue vascularization.

Generally, a range of pore size from 100 to 500 μm is considered ideal for bone tissue and blood vessels formation.

Another requirement to allow proper cell colonization is interconnectivity between pores.

Interconnectivity is essential to mass transport through their and to facilitate cell oxygenation, tipically pores with different size are connected through channels in the range of 15-50 μm.[24]

All the biological and structural requirements influence mechanical properties of scaffold.

Scaffold mechanical properties include tensile strength, stiffness, elastic modulus, fracture toughness, fatigue, and elongation percentage, they should be sufficient to provide mechanical support for new bone formation.

These properties must be tailor to fit the local conditions of the implant site and the local loading conditions and they shall be as close as possible to the original bone they replace.

Scaffold must have enough integrity and strength for provide support for bone formation and not lose their during its degradation, at the same time, mechanical properties must be adequate to minimise the risk of stress shielding or fracture. [19] ,[25]

2.3.3 Scaffold manufacturing

Different techniques have been developed to manufacture three-dimensional bone scaffolds, which are divided into two categories, conventional and additive manufacturing techniques.

Conventional techniques are the first to be used for the manufacture of bone scaffold in tissue engineering and they are mainly based on the use of solvents and solutes in liquid or non-liquid form.[26]

The main conventional techniques include solvent casting, freeze drying, gas foaming, sol-gel technique and thermally induced phase separation. All these techniques create 3D scaffold with randomly distribution of pores, they have restrictions to produce a controlled microarchitecture, the design of a specific pore size, interconnectivity and porosity is limited, these are not precise to production of the shape and the geometry within the scaffold.

These techinques are subtractive methods, since parts of the raw material are removed from an initial block to generate the desired conformations. Moreover, it is not possibile to include living cells or soluble factors within scaffold, because of the limitations in the scaffold production and the use of organic solvent and porogens in the process.[22]

Organic solvent are used to dissolve polymers and porogens are used to create pore structure, so many of them are toxic and their residues cause inflammatory response.

Despite the many disadvantages they are used because they offer a low-cost and accessible method for manufacturing scaffolds.[14],[27]

Rapid Prototyping or Additive Manufacturing are developed to overcome the limitations of conventional techniques, they have several advantages for producing scaffolds.

They have been used in various applications including controlled drug delivery system, manufacturing of medical device and engineering tissue.

Unlike conventional manufacturing techniques, Additive Manufacturing techniques are additive in nature, them do not involve the removal of materials from an initial block, but are based on the principle of fabricating 3D scaffolds through the deposition of overlapping layers according to pre-established model.

In particular manufacturing machines produce the desired scaffold through layer-by-layer fabrication. [22]

With RP techniques it is possible controlling the geometry and the material composition of the scaffold. With these approaches it is possible to create a complex microarchitecture of scaffold,in particular a geometry higly customizable and with a desired level of complexity is obtained. In addition, some of AM techiques have flexibility material and they consent the deposition of living cells or growth factors. [28]

The raw materials used in RP techniques can have different physical forms, such as solid-,liquid-and powder-based, because of that the raw materials are modified to be used in an additive manufaturing machine and then the machine produce the scaffold according to a pre-designed architecture.

The advantages of additive manufacturing techniques include increased speed and customization of the product. These techniques have few processing steps, require few manual operations and can therefore produce scaffolds in hours and days instead of weeks and months. [29]

It is possible to divide the additive manufacturing techiniques into three categories: (1) printing-based techniques, like 3D printing and wax printing; (2) nozzle-based techniques, such as melt extrusion/fused deposition modeling; and (3) laser-based techniques, such as stereolithography and selective laser sintering.

A brief overview of the methods is given in the Table 2.1.

Technologies	**Description**	**Biomaterial**	**Resolution/ accuracy**	**Strenghts**

FDM	Material extrusion, melted filament through a heated nozzle	Syntethic polymers	100-150µm ±0.5mm	Wide range of materials, low cost
SLS	Powder bed fusion, create a solid layer-by-layer, blending powder particles through termal energy source	Termoplastic powders	50-100µm ±0.3mm	Complex geometry, good mechanical properties
SLA	Vat polymerization, selectively curing a resin in a vat through a UV laser	Photopolimer resins	25-100µm ±0.15mm	Smooth surface, excellent resolution, fine details

Table 2.1 Characteristic of scaffold Additive manufacturing methods

3D printing uses ink-jet printing technology to control deposition of a binder solution on a bed of powder at room temperature conditions.

The process begins with the preparation of the powder bed into a platform, through inkjet print head; the liquid droplets of binding agents are deposited into the powder layer and bond the particles together. Then the platform is lowered and more powder is left and the process keeps on binding powder layer by layer.

The layer by layer process goes on until the production of three-dimensional scaffold.

The unbound powder in the void spaces of each layer can then be removed by compressed air or by manually brushing it away.

The possibility to room temperature processing of 3DP technology allows the incorporation of a pharmaceutical and biological agents into the scaffold and thanks to the use of the powder in the process. It is possible to print a scaffold of different materials such as polymers, metals, ceramics and composite.

The only condition is the availability of the material in powder form.

Other advantages of this technology includes easy process, few time and set up, affordability and the possibility to produce a scaffold with high degree of customization, possibility of controlling porosity and macro shape, complete pore interconnectivity and possibility to enable production on a large scale.

Among the main disadvantages of 3DP, it must be consider the need of post-processing steps to improve the resulting mechanical properties. In addition, it is difficult to remove

trapped materials and because of medium resolution of the printing, the powder particles may not bind well.

Fused deposition modeling, a nozzle-based techniques, uses a heated nozzle to extrude filament material and deposit semimolten polymer into a platform following a path and which immediately solidifies.

The extruder head is computer-controlled and builds layer by layer the three-dimensional scaffold, controlling the direction and the spacing between every layer it is possible to obtain a scaffold with uniform and complex internal structure.

It is possible to create a scaffold with high porosity and controlled pore size, with good mechanical strengh. The FDM techniques do not use a solvent, have no trapped material and minimal material waste, but they have a medium resolution of printing.

The high processing temperature is a disadvantage of this technique because it involves a limited choice of material to produce scaffold.

In selective laser sintering (SLS), scaffolds are made by passing a laser over a thin layer of powder.

SLS uses small particles of thermoplastic, metal, ceramic or glass powders that are fused by a high power CO2 or a Nd:YAG laser beam. The process begins with the preparation of the powder bed, for each layer of the structure, a new layer of powder is deposited on the previous one. Every layer of powder is exposed to light following the cross-sectional information of the designed model, the laser causes the fusion of the neighboring particles and to the preceding layer before until the 3D structure is formed.

Post processing of the final part can include the removal of trapped or non-sintered particles to leave microporosity within the structure.

This technique is characterized by having many advantages as wide range of material choices, lower material cost, not using solvent. It is possible to obtain a complex scaffold structure with controlled porosity and size of pores, a good accuracy and good mechanical properties.

Disadvantages of SLS include the post processing phase necessary to remove trapped powder, the high operating temperature which involves the use of only thermally stable polymers and the complex and expensive equipment.

Stereolithography (SLA) uses an ultraviolet light or laser to irradiate the photo-sentitive liquid resin and solidify it selectively.

A SLA system consists of a tank of resin, a platform supporting the developing model which is brought near the surface of a liquid tank, a UV laser, which is used to solidify the first cross-sectional layer of the model to the platform and non exposed polymer which remains liquid. Once the layer is completely solidified, the platform is lowered.

The scaffold construction is carried out layer by layer by moving the platform vertically and at the end of the process the non polimerized resin is washed and the scaffold is cleaned and treated in an UV oven to reduce surface irregularities.

This technique allows to produce a complex 3D structure and with high resolution and accuracy, but it has a limited choice of materials, because only photopolymerizable materials must be used. Also it requires a postprocessing after the production of scaffold and for this reason it is an expensive tecnhique.[14],[28],[15],[19],[30]

The advantages and disadvantages of main methods in Additive Manufacturing are summarized in the Figure 2.6.

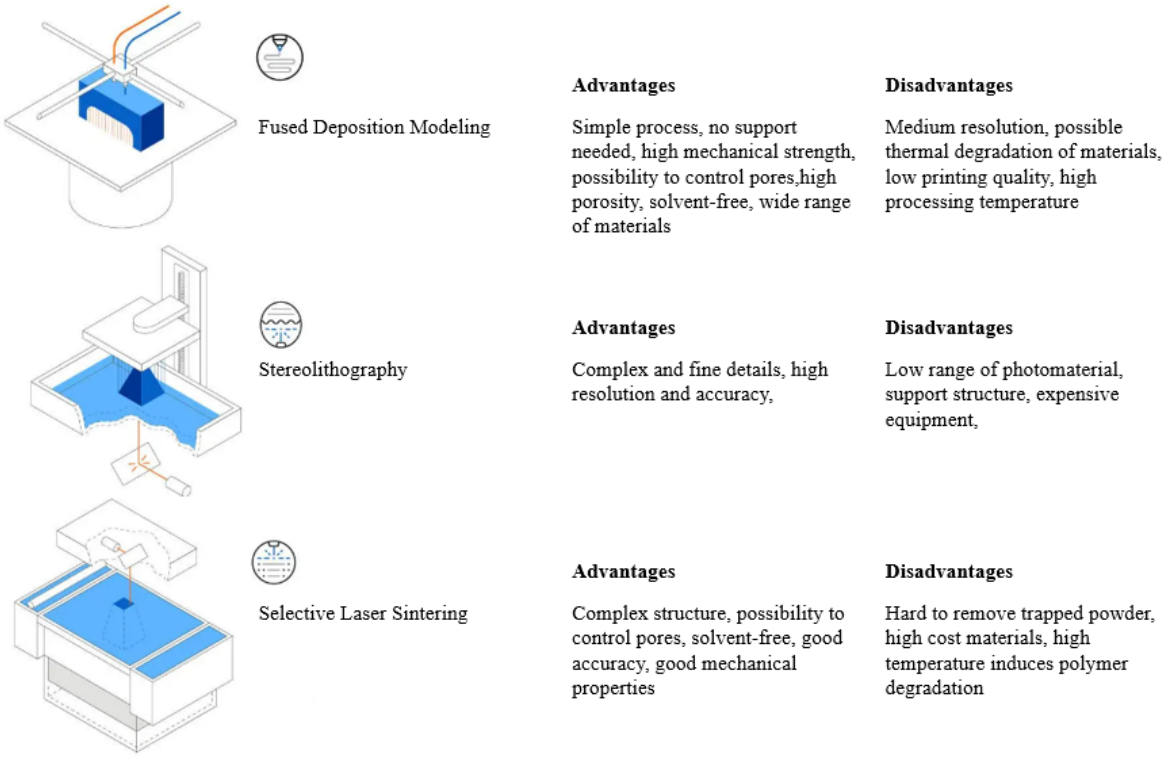

Figure 2.6 Comparison of Additive manufacturing methods

2.3.4 Scaffold material

The selection of the biomaterials for bone application is a important step which influences the properties of the final scaffold. As mentioned above, the materials commonly used for the production of scaffolds for bone tissue engineering are polymeric, metallic, ceramic and composite materials.

Each material is characterized by advantages and limitations for bone application and it needs to choice the material based by the biocompatibility, osteoinductivity and osteoconductivity and especially for the mechanical role it has to play in the human body. The main characteristics of these materials is summarized in the Table 2.2.

Material	**General properties**	**Disadvantages**
Metals	High strength, low elastic modulus, low density, corrosion resistance	Not biodegradable, not tissue replacement
Bioceramics	Bioactivity, chemically simile to bone, biocompatibility, osteoconductivity, non-toxicity, non inflammatory	Low strength, brittle
Natural polymers	Biocompatibility, biodegradability, support cell attachment, differentiation, complex structure	Rapid degradation, poor mechanical properties
Syntetic polymers	Biodegradability, high mechanical properties, biocompatibility, complex structure	Slow degradation, low bioactivity
Composites	High cell attachment, mimic bone tissue,good biological properties, biocompatibility	Poor mechanical properties

Table 1.2 General properties of materials for bone scaffold

Metallic biomaterials such as titanium and its alloys, magnesium and nitinol, are used for orthopedic implants, mainly applied as joint replacements and fracture-fixation implants, they have long been used to provide mechanical support because of their high strength, good biocompatibility and good fatigue resistence.

Metal implants present low elastic modulus, osteoconductivity and corrosion resitence, function as permanent implants, indeed unfortunately they are not biodegradble, so

usually is necessary to remove and substitute metallic implants. A lot of metal materials have high rigidity and show in vivo corrosion,

Titanium in particular is characterized by relase of metal ions and it is toxic for the bone repair, The surface of these metals is treated, modified with specific treatment, to overcome in vivo corrosion of the metal materials, and usually it is functionalized for increase bioactivity and controlled release of antinflammatory agent.

Just as metals are non-organic, there is a part of ceramic materials that is also inorganic and that is used in the biomedical field.

The inorganic ceramics that are used for bone tissue engineering are bioactive glasses, they have the particular modification of their surface when in contact with biological fluid that is the production of a layer of bioactive hydroxyapatite. This behavior takes part to the bioactivity of this material and it makes possible the bone repair because this layer facilitating the chemical bonding with the closer bone and then because of the controlled release of ions it improve cell differentiation and osteogenenesis.

The most commonly used bioceramics are HAp, TCP and their composites. Hydroxyapatite is high bioactive, biocompatible, non-toxic and it shows osteoconductivity but it is very brittle.

At the same time tricalcium phosphate has the same properties, it is readily available, it is not osteoinductive but it is able to form strong chemical bonds to closer bone and supports a great fixation and osteogenic differentiation in vivo.

Bioceramics have high resistence to corrosion, they are strong in compression but brittle in tension, they are characterized by a slow degradation and they have usually function of coatting the implants, or are used as partial component of bone scaffold.

Polymer-based scaffolds provide more facility of production and modification, they can have different physical forms, such as fibers, solid of gels, and they are able to be modified to improve their physiochemical properties.

In bone tissue engineering there are two types of biodegradable polymers, natural and synthetic polymers.The first includes polysaccharides such as hyaluronic acid, alginate, or proteins such as silk, collagen, fibrin.

They are definetely biocompatible and with controlled biodegradability, they have bioactive behavior and the ability to interact with closer tissue, in particular they are able to provide cell attachment and growth.

These materials have low immunogenic potential because they are obtained from natural sources, either from animal or vegetal source, therefore they need to be sterilized to prevent risk of infection. Unfortunately the sterilization affects the degradation rates and the physical properties of polymers.

Poor mechanical properties is the major problem of the natural polymers, they do not provide sufficient architectural support to grow bone.

On the contrary the synthetic polymers have greater strength, they can be a support for new bone growth and have adequate mechanical properties.

Unlike natural polymers they are easily reproducible in large-scale production, they have a high processability and versatility, so they can be used to produce scaffolds with desired macroscale and microscale design.

PLA, polyglycolic acid (PGA), poly-lactic-co-glycolic acid (PLGA) copolymers, and polyPCL are the biodegradable polymers used in BTE, they are biocompatible, but compared with natural polymers they have inferior bioactivity and this involves less interaction with cells.

As discussed above these materials have some limitation to mimics the behavior and the properties of the bone. The bone is composed mainly of organic collagen fibers and inorganic apatite, so the best solution is to combine two different materials.

Composite material is made up by a combination of ceramics and polymer, or of synthetic polymers with natural polymers or metals and polymers, to develop the best characteristics for the bone scaffold.

Usually composite materials are made up by polymers/ceramics or polymers/ metals, polymers provide toughness, compressive strength and biocompatibility, and inorganic phase improves the mechanical properties and degradation rate.[14],[19],[15],[20],[29]

Chapter 3

Materials and Methods

This chapter presents and describes the technological tools used in work and their theoretical foundations. Depending on the subject area, different categories can be considered:

- Sample modelling
  It describes the formulas and the parameters used to create the lattices through Python software
- Sample printing
  It explains the 3D printing process and its main features
- Sample production
  It reports the choice of the parameters used for the scaffold production
- Morphological analysis
  It outlines the methods of operation of the microscopes used to assess the morphological characteristics of the samples and the principles of operation of computed microtomography
- Mechanical analysis
  It describes the process of mechanical characterization in compression and traction of samples

The study provides the realization of porous scaffolds that have mechanical and structural characteristics compared to those of the bone. The main structural requirements that characterize the scaffold microstructure are summarised below:

-Porosity

Scaffolds must have a high porosity, this affects cell growth and the supply of nutrients by the blood vessels. The literature suggests a porosity greater than 75% that stimulates cell proliferation with greater efficiency.[31]

-Pore's size

In bone tissue engineering, the optimal pore size, identified by some researchers, is between 200-500 μm. It is recommended to ensure a homogeneous distribution of the pores inside the scaffold to allow a uniform growth of tissue. [24]

3.1 Scaffold design

Scaffolds are created and implemented using Python.

Python is an object-oriented programming language that supports procedural and functional programming, and therefore it uses of functions and iterators. The functions and variables used in Python are simple and very powerful, easy to learn and intuitive.

It is a generic programming language, used for website creation, data analysis and even machine learning, it is possible to use it on different platforms such as Linux, Windows and Mac and it can also be integrated with other languages. For these reasons it is the main recommended programming language. [32]

Given a series of inputs to the program and applying instructions with specific syntactic rules, it is able to produce a set of output data. It also manages memory, adopts a garbage collection mechanism, automatically deletes unused objects to make space in memory and at the same time it is possible to use variables freely without having to declare them from time to time.

Python is a language highly used in various fields thanks to the numerous libraries, about 200 modules, that allows to perform and manage many operations and functions. Modules are files that contain very complex and long code that can give instructions and definitions and this allows a very organized and intuitive programming management.[33]

3.1.1 Libraries

Each library is purpose-specific and contains methods and instructions to facilitate programming.

Importing a library into the code allows to perform certain actions without having to write the full code of that particular function at each use. In addition to the standard Python

library, it is possible to download and install numerous add-on modules created by the python community for free thanks to PyPy, the Python Package Index.[34]

Here are the libraries used in this thesis work:

- Math
  It is the module consisting of trigonometric and mathematical functions.
- Pygmsh
  Pygmsh combines Gmsh with Python, it contains modules for meshing, to create complex geometries, solvers and post-processing.
- Numpy
  Numpy is an open source Python library used primarily for scientific computing. It means numerical Python, indeed it provides a mathematical library capable of performing calculations, arithmetic operations and solving mathematical problems.
- Matplotlib
  The matplotlib library allows you to create and draw 2D and 3D graphs in python language.
  It consists of various useful functions for graphical representation with different properties, mainly deals with the data visualization of the numpy library.
- Pyvista
  It is based on the visualization toolkit, it contains a set of useful and intuitive tools for 3D visualization, mesh analysis and processing in Python.
  This library is widely used for scientific plotting and research papers.
- Blender in Python
  Blender is an open source and free 3D graphics software.
  It is a program used to create animated 3D images, for which it deals with animations, modeling, 3D rendering of images and even video editing.
  It can be used on Python simply by calling its functions and tools.[33],[35],[36],[37]

3.1.2 Unit cell design

Initially, through the Pygmsh library in Python, a first model of scaffold is made.

The aim is to create a simple geometry to represent the scaffold with spherical pores.

Through the pygmsh.occ.Geometry() function, a cube, a sphere and three cylinders are created, oriented in the three Cartesian directions. Subsequently, through Boolean operations, the union of three cyclinders is made, which is later subtracted to the sphere and the cube. Below there are the functions used to create the geometries that compose the unit cell and to generate the final mesh.

sphere = geom.add_ball (center, radius)

cube = geom.add_box(x0, x1, y0, y1, z0, z1)

cil1 = geom.add_cylinder(center,axis,radius)

Where the centre of the ball is an array of 3 elements and the radius is a float number refers to the radius of the ball; cube's specifications describe the coordinates in the three directions; the centre of cylinder describes the 3 coordinates of the centre of the first circular face and axis is an array of 3 elements refers to the three vector of axis. The radius is a number refers to the radius of the cylinder.

The Boolean operations used are the union of the cylinders and the difference of the cylinders from the sphere/cube, and it is summarized in the single expression:

geom.boolean_difference(sphere,geom.boolean_union([cil1, cil2, cil3]))

Boolean operations operate with two lists of volumes, curves, or elementary surfaces.

The mesh obtained with the command below is shown in the Figure 3.1(a)

mesh = geom.generate_mesh()

After creating the single unit cell the work continues with the replication of the unit cell in several directions, such as to form a grid of unit cells (Figure 3.1(b)).

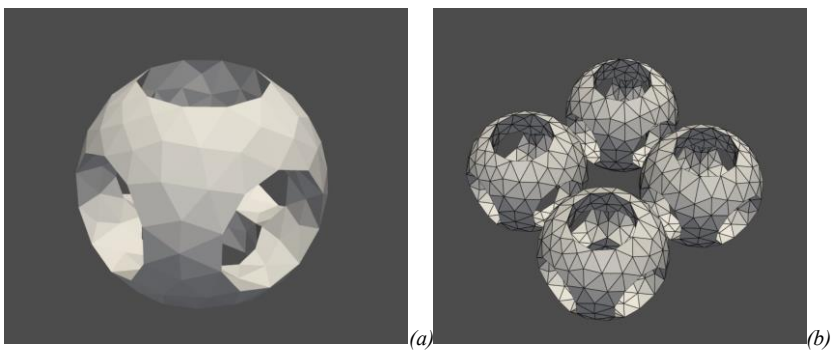

(a) *(b)*

Figure 3.1(a)Difference of cylinders from a sphere. (b) Grid of unit cell

Then a different unit cell is created, in which the sphere and three cylinders are joined in Boolean way and then subtracted from a cube, composing a lattice shown in Figure 3.2(a)(b).

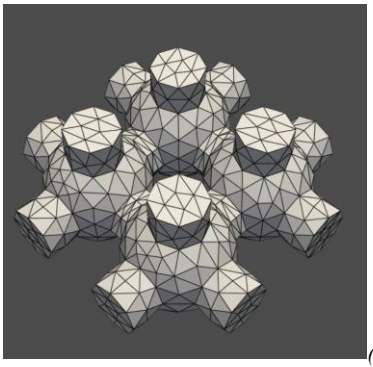
(a)
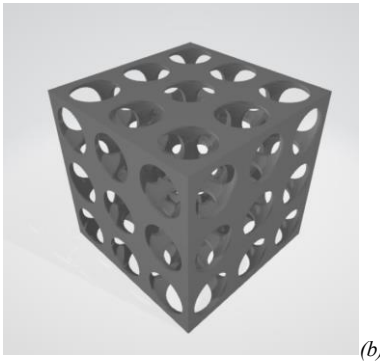
(b)

Figure 3.2(a) Union between cylinders and sphere. (b) Lattice obtain with the difference from a cube

The Pygmsh module requires excessive computational time to replicate objects in three directions, so work continued with Pyvista.

Pyvista allows the creation of the same unit cell previously created. In order to develop the prism in the various directions automatic, a get_prism function is created which it uses functions and Boolean operations similar to the previous ones for the creation of the unit cell. In the Figure 3.3 is reported the function get_prism.

```
def get_prism(dim_x,dim_y,dim_z,center,length):
    cx, cy, cz = center
    length_x, length_x, length_x = length
    for i in range(dim_x):
        for j in range(dim_y):
            for k in range(dim_z):
                prism = pv.Cube([cx + i * length_x, cy + j * length_y, cz + k * length_z], length_x, length_y, length_z)
                cyl1 = pv.Cylinder([cx + i * length_x, cy + j * length_y, cz + k * length_z], [1.0, 0.0, 0.0],
                                   length_x / 4, length_x * 2)
                cyl2 = pv.Cylinder([cx + i * length_x, cy + j * length_y, cz + k * length_z], [0.0, 1.0, 0.0],
                                   length_x / 4, length_y * 2)
                cyl3 = pv.Cylinder([cx + i * length_x, cy + j * length_y, cz + k * length_z], [0.0, 0.0, 1.0],
                                   length_x / 4, length_z * 2)
                cyl1 = pv.PolyDataFilters.triangulate(cyl1)
                cyl2 = pv.PolyDataFilters.triangulate(cyl2)
                cyl3 = pv.PolyDataFilters.triangulate(cyl3)
                prism = pv.PolyDataFilters.triangulate(prism)
                m1 = cyl1.boolean_union(cyl2)
                cyl = m1.boolean_union(cyl3)
                prism_with_hores = prism.boolean_difference(cyl)

                if i == 0 and j == 0 and k == 0:
                    merged_prism = prism_with_hores
                    merged_prism = merged_prism.merge(prism_with_hores)

                elif i != 0 or j != 0 or k != 0:
                    merged_prism = merged_prism.merge(prism_with_hores)
    return merged_prism
```

Figure 3.3 Function get_prism

The scaffolds obtained by sphere and cube are represented in Figure 3.4.

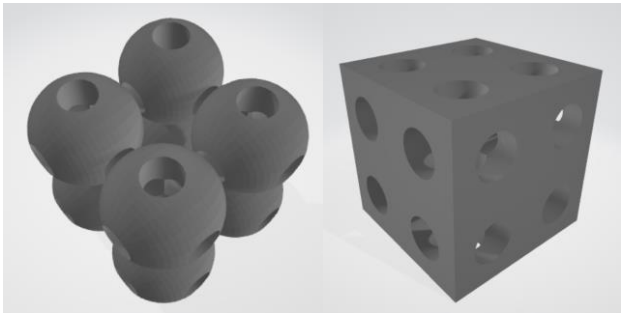

Figure 3.4 Scaffold obtained with Pyvista

3.1.3 Triply periodic minimal surface: TPMS

Through bibliographical research, it is noted that the structures most used for the creation of scaffold for bone engineering are the triply periodic minimal surface.

The first surface to be introduced was the Schwarz Primitive in 1865. The triply periodic minimal surface is defined mathematically as a surface that repeat in three dimensions with a large surface area. It is characterized by a minimal surface because it has a zero-mean curvatures over its entire surface.[38]

The TPMS can be defined as implicit, parametric and boundary way. In this study it is used the implict method, which used a trigonometric function in an implicit form to describe the TPMS structure.[31]

Using modules such as Numpy and Pyvista in Python, it is easily possible to represent TPMS surfaces and change their parameters.

Four unit cells are selected among the main TPMS structures for bone scaffold, the equations describing them are given below:

- Schwarz Primitive

$$\cos(\alpha x) + \cos(\alpha y) + \cos(\alpha z) = C$$

- Gyroid

$$\sin(\alpha x)\cos(\alpha y) + \sin(\alpha y)\cos(\alpha z) + \sin(\alpha z)\cos(\alpha x) = C$$

- Schwarz Diamond

$$\cos(\alpha x)\cos(\alpha y)\cos(\alpha z) - \sin(\alpha x)\sin(\alpha y)\sin(\alpha z) = C$$

- Schoen IWP

$$2[\cos(\alpha x)\ \cos(ay)\ +\ \cos(\alpha y)\ \cos(az)\ +\cos(\alpha z)\ \cos(ax)] - [\cos(2\alpha x) + \cos(2ay) + \cos(2\alpha z)] = C$$

The trigonometric function describes a constant-level isosurface set by C. When the equation is zero, C=0, the isosurface divides the 3D space into two sub-domains with the same volume. The part where the trigonometric function is negative or equal to zero is defined as the portion occupied by the surface; instead, the region where the function is greater than zero is defined as empty. [39]

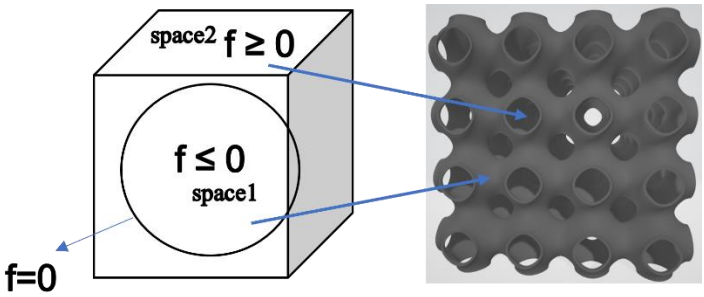

Figure 3.5 Sub-domains of the 3D volume

The parameters that can be managed in Python and that consequently affect the structural properties of the elementary cell are:

- C level set parameter; it controls the expansion of the surface in 3 directions and influences the density of the lattices.[40] It can assume constant value or be function of x, y, z, c(x,y,z). C has a value constant between -1 and 1. If C assumes positive or negative constant value, the surface expands or contracts in space. It is said that the structure has uniform porosity, the pores are the same in all directions.

  If C is a linear or quadratic function of x,y or z describes a surface with different porosity in the three directions; a porosity gradient is introduced where the pores vary in size according to the specific coordinate value, it is called graded scaffold.

Type of scaffold	C(x,y,z)
Uniform	C
Linear	C * z
Radial	C* ($x^2 + y^2$)
Quadratic	C*($x^2 - y^2$)

Table 3.1 Relationship between the type of scaffold and C

- *a* is equal to 2*π/L, where L is the length of the unit cell. *a* is used to define the periodicity of the cell which determines the size of the lattice.[41]

- *x, y,* and *z* define the spatial coordinates of the structures, are defined by Numpy, through the mgrid() function which allows to create dense 2D arrays with similar values.

  x, y, z = np.mgrid[xMin:xMax:100j, yMin:yMax:100j, zMin:zMax:100j]

  Xmin and Xmax indicate the number of elementary cells along the x direction, the same is done for the y and z directions; the complex number is used to define the number of points between the start and end values, called as step length or resolution. Increasing the complex number shows how the mesh, plotted with Pyvista, is finer and defines better the surface, but at the same time it requires a higher computational calculation.

The TPMS surfaces of the four selected structures are shown below.

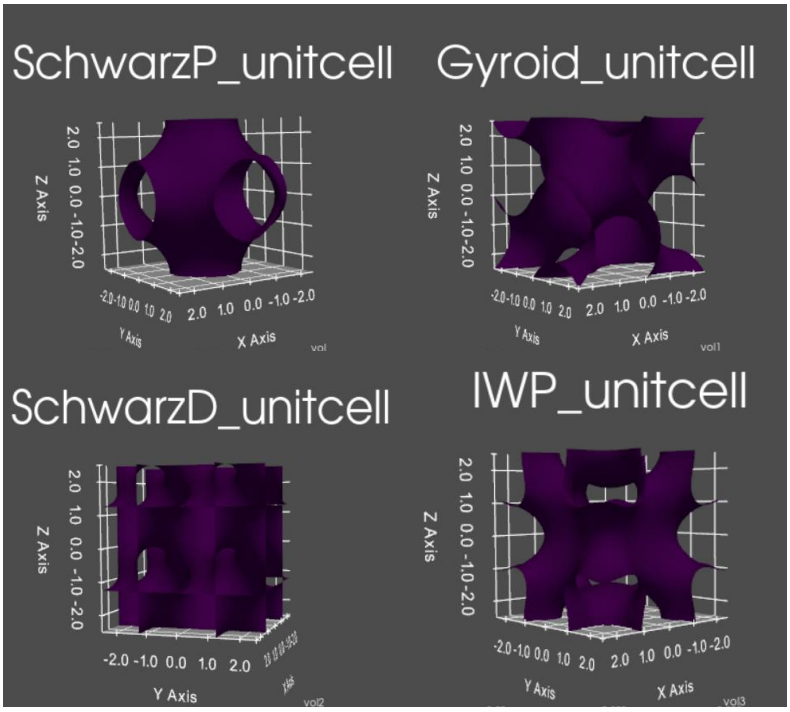

Figure 3.6 TPMS surface

With the use of Blender in Python, the thickness value is chosen to make the surface a solid structure. The following Figure 3.7 have a cell length value of 5mm, a C value equal to 0 and thickness equal to 0.2mm.

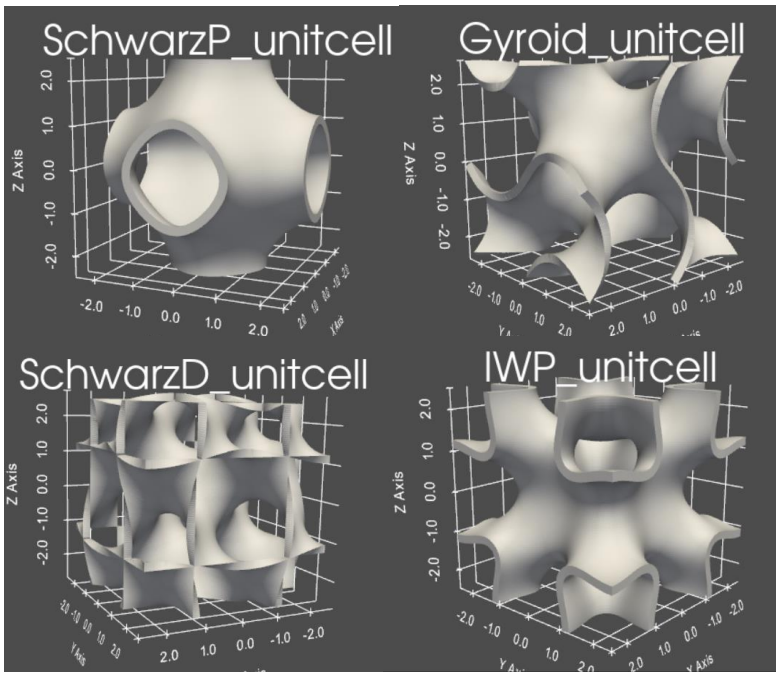

Figure 3.7 Solid TPMS

The unit cells have been replicated in three dimensions and with different values of C and thickness, to evaluate through the printer which parameters lead to the success or failure of the scaffold.

3.2 3D printer

The three-dimensional scaffold was produced through additive manufacturing, specifically through stereolithography.

3.2.1 Workflow SLA

In this study was used Form2 printer produced by Formlabs, visible in Figure 3.8.

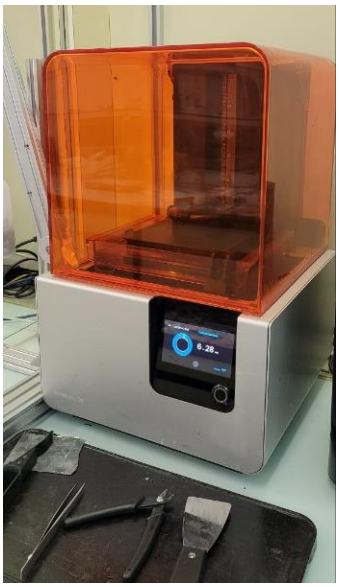

Figure 3.8 Form 2, stereolithography printer

The operation of the SLA printer involves at first a planning phase, then a printing phase and a final post-processing phase.

- PLANNING

In order to create the object, the printer needs an object file format which is in STL (standard triangulation language). It is a format in which the shape is accurately described and discretized in triangles.

The stl created file is imported into Preform; it is a software which permits to prepare a stereolithographic printing. The user interface of Preform is shown in the Figure 3.9.

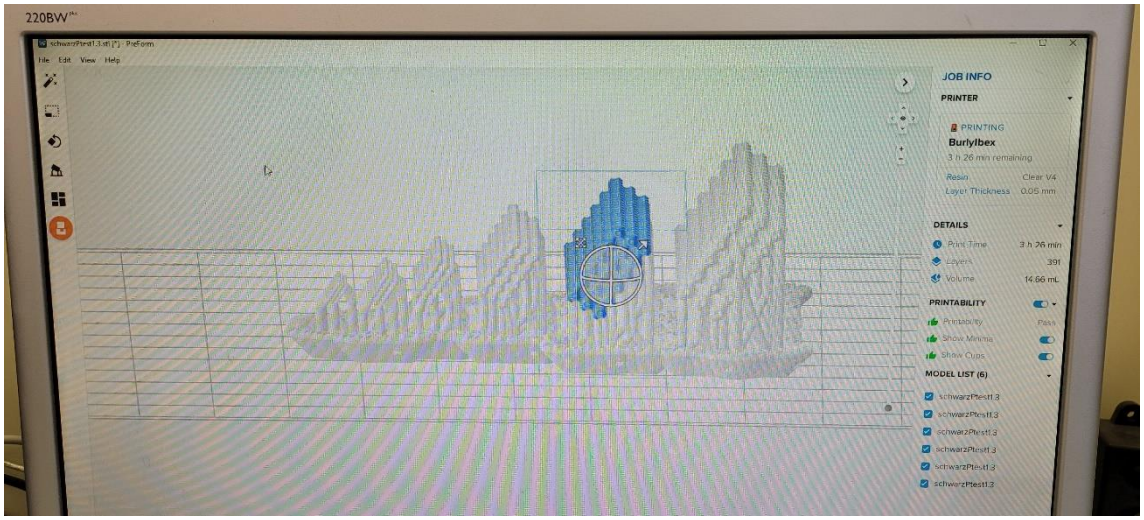

Figure 3.9 User Interface in Preform

The Preform algorithm allows to set the orientation, position and dimensional scale of the model. A specific orientation of the sample during printing is recommended because it affects the failure or not of the print. It is recommended to tilt the model to reduce contact between the tank and the workpiece, which could subject the model to greater force each time the platform is raised.

The base of the model often has marks left by the supports, which affect the surface finish, for this reason important details should be put in the opposite direction of the base.[42]

Preform automatically creates the supports that the sample needs during printing to avoid failure. It is possible to choose the density and size of these, in this case it is chose the smallest size, about 0.6mm, so as not to affect too much the shape of the sample.

At the end, the print material**,** the resins for stereolithography and the relative print resolutions are selected. For the first scaffolds are used a common resin, Clear one. The It is transparent and it allows to see inside of the printed parts, which is important for this research. It supports print resolutions of 100, 50 and 25 microns**,**

However if the resolution decreases, despite increasing in accuracy and precision, the time of printing becomes considerably longer.

After printing several samples and choosing the scaffolds to be printed for subsequent characterization, a biocompatible resin, Dental LT Clear Resin, is used. Class IIa biocompatible resin is used for prostheses and rigid dental appliances. It is transparent, so it is possible to analize the structure internally with mycroscopy and it is characterised by high fracture resistance, biocompatibility, and a good long term wear resistance. The biocompatible resin only supports print resolution along the Z axis of 100microns less than Clear Resin.[43]

Figure 3.10 Tank of Formlabs Biocompatible Resin

- PRINT

Once the project is uploaded, printing automatically proceeds without any supervision. Form 2 printer's components are shown in Figure 3.11.

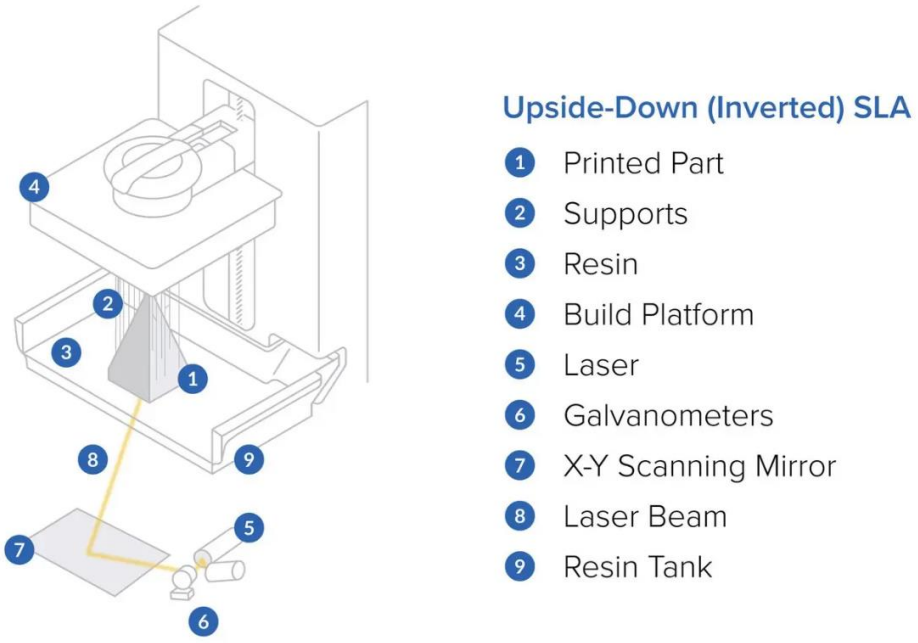

Figure 3.11 Components of Form2

The Form 2 works with liquid but thermosetting resins, which when exposed to light with a certain wavelength react and polymerize solidifying.

Through the sensors on the printer it is possible to monitor the status of the printer, in particular there is the resin tank sensor that detects the presence or not of resin and that allows its filling automatically.

When the resin is at the right level, the printing surface is lowered by immersing it in the tank with the resin.

The UV laser beam is projected into the resin that makes it harder only in the areas where it radiates. So, workpiece is built the bottom up.

The galvanometer allows the positioning of the laser on the Y axis, it directs it on a mirror to provide a beam that is constantly perpendicular to the printing plane.

At the end of each polymerized layer, the solidified resin remains attached to the build platform, the plate rises and the wiper mixes the remaining liquid resin.

The resin mixing system is important because it allows you to have less impurities in the print area.

The printing ends with the production of the upside-down model that remains attached to the build platform.[42],[44]

The process is placed at room temperature with automatic printing temperatures of around 30 ºC-35 ºC.

- POST-PROCESS

The printing process is completed with two machines, Form Wash, Figure 3.12(a) and Form Cure, shown in the Figure 3.12(b).

(a) *(b)*

Figure 3.12(a) Form Wash. (b) Sample insert in Form Cure

Firstly the object is placed in the container of the Form Wash, which performs the automatic washing of the sample through isopropyl alcohol. Washing is ready in 15 minutes. Parts of uncured resin are removed from the sample surface using a propeller that moves the alcohol to reach the inside of the workpiece. The workpiece is then allowed to dry at room temperature for a few minutes. For better removal of isopropyl alcohol trapped in the internal parts, a compressed air pump is used.

Then it is possible to keep on with the photopolymerization of the object in the Form Cure. The Form Cure chamber is heated to 60° and the 13 multidirectional LEDs inside trigger the post-curing reaction. The piece is placed on a turntable that provides uniform light exposure, the process takes about an hour.

Post-print processes allow to maximize material performance.

Finally, the supports in the object are removed with finishing tools.[45]

3.2.2 Technical specification

The technical specifications of the Form 2 stereolithography printer are given in Table 3.2.

Hardware	Dimensions	35x33x52 cm
	Weight	13 kg
	Operating Temperature	Auto-heats to 35°
	Power Requirements	100–240 V 1.5 A 50/60 Hz 65 W
	Laser specifications	EN 60825-1:2007 certified Class 1 Laser Product 405nm violet laser 250mW laser
Printing Properties	Build Volume	145 × 145 × 175 mm
	Layer Thickness (Axis Resolution)	25,50,100 microns
	Laser Spot Size	140 microns
	Supports	Auto generated Easily Removable

Table 3.2 Form2's technical specification

In the stereolithographic printer the level of detail of the piece is provided by the resolution. It is necessary to consider the resolution along the three directions, as the direction of printing is controlled by different mechanisms.Resolution XY is defined horizontal resolution and it is the minimum movement that a printer's laser can make within a single layer, the accuracy of the details is greater if the number is smaller.

Resolution XY relates to the minimum dimension of details and it is rarely present in the datasheets because it is possible to measure it under a microscope.

The minimum size of the details in SLA are about small as the diameter of the laser point, Form2's technical specifications indicate a 140 micron laser spot, therefore the minimum size of details can never be less than this number.

Form2's XY resolution has been shown to be 150 microns, only 10 microns more than the laser spot, this value can be influenced by microscopic contaminants, resin chemistry, laser refraction and more.

The resolution of the Z-axis is widely indicated in datasheet, allows differentiation between additive manufacturing techniques, it ia also defined layer thickness.

Layer thickness of Form2 is 25-200 micron for all resins, high **resolution have a price** because printing with 25 micron of resolution means making more repetitions than printing with a resolution of 100 microns, and this involves a longer printing time and more artifacts.

Printing models at lower resolutions, such as 100-200 micron, can lead to higher quality prints, but for specific and complex details it is convenient to use high resolution.[46],[47]

3.2.3 Sample production

This paragraph is introduced to describe the tests performed simultaneously in Python and with stereolithography to understand which parameters should be chosen and set in order not to cause the failure of the lattices.

The work is divided into tests that have different purposes.

Initially, to assess until what size is guaranteed that the lattice not to fail with printing, the scaffold is printed with different scale factors, through Clear Resin.

The characteristics chosen for the first lattices are:

- Elementary cell type Schwarz P
- Cell length 5mm
- C value equal to 0
- Thickness 0.3mm
- Replication in three dimensions X = 3, Y = 20, Z = 6

After importing the stl file into Preform, the scaffold, with a chosen print resolution of 0.025 mm, is reproduced with a scale factor of 0.15,0.2,0.3,0.4,0.5 as can be seen in

Figure 3.13. Figure 3.13 shows the lattices after washing and curing with Form Wash and Form Cure.

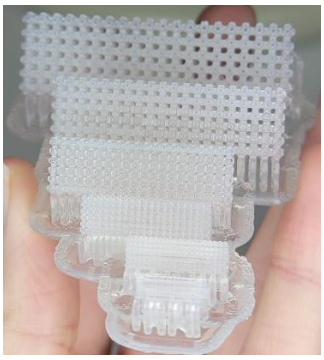

Figure 3.13 Lattices with different scale factors

Subsequent tests include the evaluation of scaffolds created using the four cubic-sized TPMS surfaces. The scaffold obtained with Python in the type Schwarz P, Gyroid, Schwarz D and IWP are shown in the Figure 3.14 from right to left.

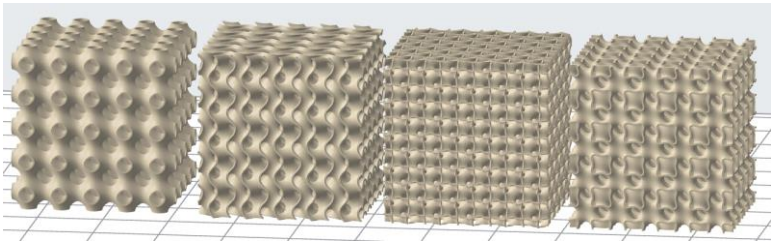

Figure 3.14 Cubic TPMS structure

Parameters set with Python:

- Cell length 5mm
- C value equal to 0
- Thickness 0.1mm, 0.25mm, 0.5mm
- Replication in three dimensions X = 5, Y = 5, Z = 5

This test involves printing each type of TPMS using three different scale factors, 0.2, 0.3 and 0.4.

The first test performed with Dental Clear Resin involves the creation of scaffolds, with a print resolution of 0.1mm, in the types Schwarz P and Gyroid with a theorical volume of 25x25x25mm^3. Porosity in this test becomes a key parameter to be taken into account in Python when choosing the parameters, as the intention is to create scaffolds with a similar percentage of porosity to spongious bone.

C, influencing the expansion or contraction of the surface, is chosen so as not to cause occlusion of the pores. In Figure 3.15 shows the change of the surface to the variation of C.

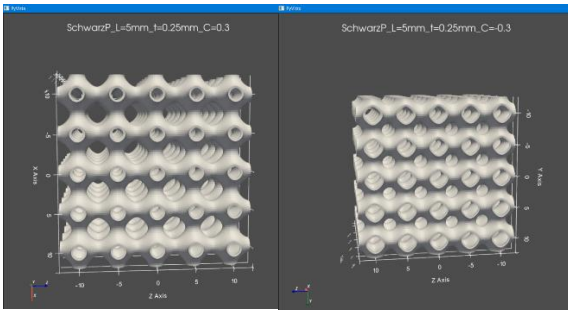

Figure 3.15 Schwarz P lattice with different value of C

The Table 3.3 shows the values set for the cell length, thickness and C for the two TPMS and their porosity values obtained in Python.

	Unit cell length (mm)	Thickness (µm)	C	Teorical porosity %
Schwarz P	5	0.25	0.3	88
	5	0.25	-0.3	88
	5	0.5	-0.3	76
	3.2	0.5	-0.3	61
Gyroid	5	0.25	0.6	86
	5	0.25	-0.6	84
	3.2	0.25	-0.6	74
	3.2	0.25	0.6	78
	3.2	0.25	0.9	83
	3.2	0.25	-0.9	75

Table 3.3 Parameters of Schwarz P and Gyroid unit cell

The study continues with the creation of Schwarz P and Gyroid scaffolds with biocompatible resin. The parameters chosen in Python for the two types of structures are shown in the Table 3.4, divided by the length of the elementary cell.

Unit cell length(mm)	Thickness(mm)	C	Theoretical Volume(mm^3)
2	0.1	0	10x10x10
2	0.2	0	10x10x10
3	0.1	0	10x10x10
3	0.2	0	10x10x10
3	0.3	0	10x10x10
3	0.4	0	10x10x10
3	0.5	0	10x10x10
4	0.1	0	12x12x12
4	0.2	0	12x12x12
4	0.3	0	12x12x12
4	0.4	0	12x12x12
4	0.5	0	12x12x12

Table 3.4 Parameter of Schwarz P and Gyroid scaffolds

The following Figure 3.16(a) shows the project created on Preform, containing almost all of the grids created. In the picture it is seen that the lattices are slanted, which is necessary to have a lower probability of failure during printing; in the Figure 3.16(b) the same samples are shown before post-processing through Form Wash and Form Cure.

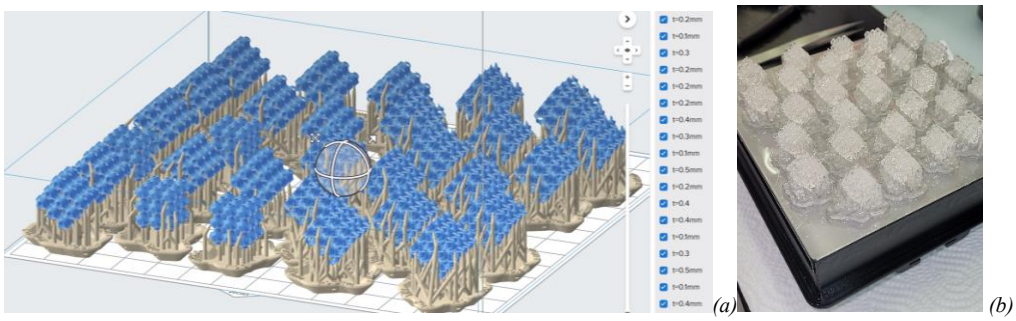

(a) (b)

Figure 3.16(a) Preform project (b)Printed samples

3.3 Porosity and density evaluation

After removing the supports from the moulded parts, an evaluation of the lattice density is carried out.

The analysis of density and porosity is important because the mechanical resistance, the durability of the workpiece and cell proliferation depend on it.

Lattices are chosen with certain parameters capable of having a high porosity, at least theoretically, from a value of 50% to 98%.

Having a high porosity is one of the objectives of the study, because for the scaffold for bone tissue this leads to increased cell migration, differentiation and subsequent angiogenesis within it.

The relative density of the lattices is calculated experimentally to be compared with that calculated in Python on the virtual model, in order to analyze the accuracy of the printer to create the structures.

Firstly through Python it is obtained the porosity and the relative density in percentage of each scaffold through the following formulas:

$$percentage\ porosity = \frac{pore\ volume}{total\ volume} x100$$

$$percentage\ density = \frac{solid\ volume}{total\ volume} x100$$

The total volume is the volume of the cube that includes both porous part and solid part, calculated for each single scaffold through the measurements of the extremes of its coordinates; the volume of the porous part is calculated by Python automatically making the difference between the total volume and the volume occupied by the surface.

Then experimentally the density is calculated through mass and volume measurements for each individual scaffold.

For mass calculation is used a balance with an accuracy of 10-4 g and a maximum capacity of 510 g, shown in the Figure 3.17(a).

The analytical balance is an instrument with high precision in the measurement of mass, is able to detect the minimum oscillation in weight of the object and for this reason is equipped with a windproof cage. The scaffold, placed inside the balance, is isolated from the external environment. It is good to calibrate the instrument before each measurement through the integrated system in the balance, in order to have a precise measurement.

The density measurement is calculated as follows

$$density = \frac{mass}{volume}$$

The mass is obtained through the balance, whereas the volume is calculated by making the product between the height, width and length of each individual sample.

In particular, the measures of length, width and height are obtained by averaging, for each size, three measures have been taken through a caliber, which is represented in Figure 3.17(b). The average is made to have a more accurate measurement of the size, as the removal of the supports is not occur precisely.

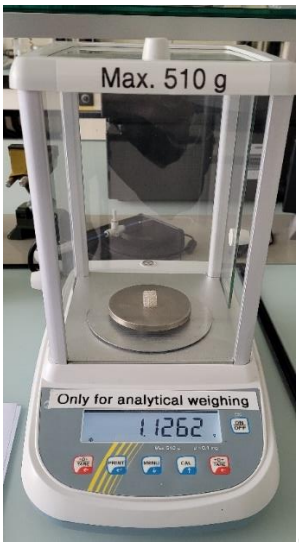

(a)

Figure 3.17(a) Analitical balance

(b)

Figure 3.17(b) Size measure with caliber

3.4 Morphological analysis

The work keep going with the morphological characterization of the samples through the microscopes and the Micro-CT.

3.4.1 Digital optical microscope

The digital microscope has the same functionality as an optical microscope but without an eyepiece that allows direct viewing. The optical microscope is characterized by the presence of a digital camera that transmits the image on a monitor in real time, precisely in the analysis software of the microscope.

The digital microscope used is the KEYENCE VHX-6000, by Keyence Corporation, represented in the Figure 3.18(a), at the laboratory in iPrint Institute at Haute école d'ingénierie et d'architecture in Fribourg.

Figure 1.18(a) KEYENCE VHX-6000 microscope

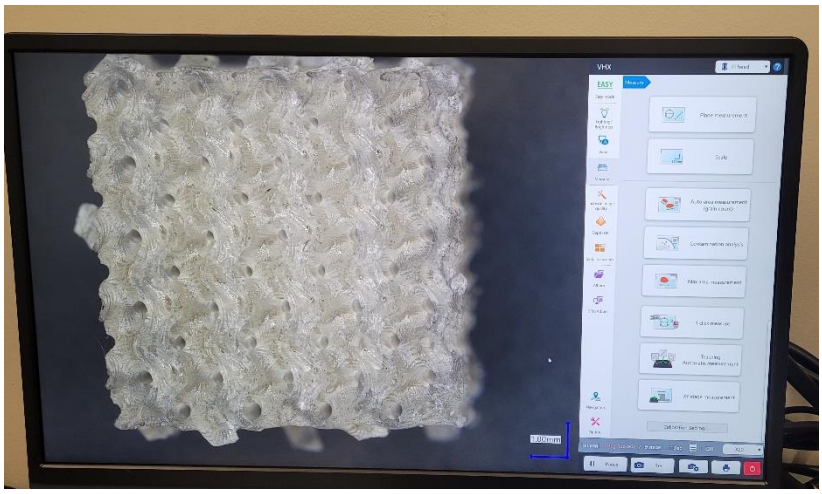

Figure 3.18(b) KEYENCE VHX-6000 User Interface

It is a new generation optical microscope that provides high resolution images.

It is characterized by a large sensitivity CMOS camera with a frame rate of 50 Frame/second and a 3D microscope that allows a magnification range from 0.1x to 5000x.[48]

It captures images completely in focus and in less time than traditional microscopes, providing images with wide depth of field up to 20x greater than conventional optical microscopes that allows for greater image quality and ease of use.

It allows to observe the object from different angles, allows the inclination of the objective and a rotation of 180, without the need to manually move the sample from its position.[49]

It has an intuitive user interface, shown in Figure 3.18(b) through which it is possible to make numerous analysis, measurements of the areas of interest and change lighting methods.

3.4.2 Electron scanning microscope (SEM)

The electron scanning microscope, SEM, is a technique that allows to generate images with resolutions that exceed the resolution limit of optical microscopy by exploiting the interaction between electrons and the atoms that constitute the sample under examination.

Essential components of SEM are the source of electrons that generate the electrons beam, a column consisting of a set of lenses that allow to manage the electrons beam, detectors that own the information generated by the interaction between the beam and the sample

and that allow to reconstruct the image, the support to place the sample and a vacuum system. A schematic representation of the bench SEM components are reported in the Figure 3.19.[50]

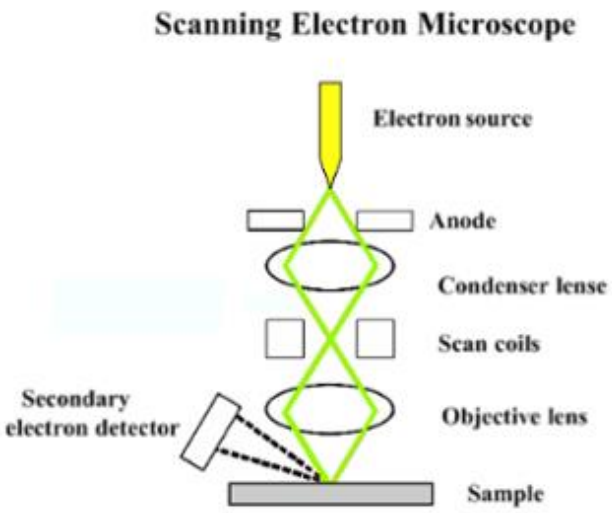

Figure 3.19 SEM components representation

For morphological analysis of samples is used the JCM-6000Plus benchtop SEM, from JEOL., shown in the Figure 3.20.

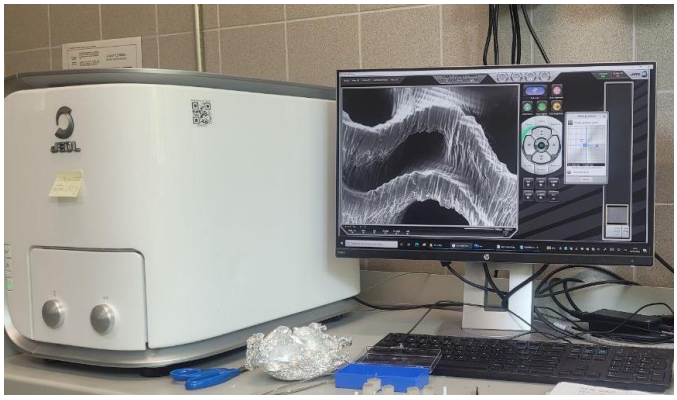

Figure 3.20 JCM-6000Plus benchtop and User interface

- Sample preparation

If the sample must be placed in the chamber stage, not only it must has a small size, but it must also be prepared in order to resist the conditions of high vacuum and the high-energy electron beam striking it.

The samples used in this thesis are non-conductive, so when scanning with electrons, they can pick up charges, which cause scanning defects and artifacts in imaging. For conventional SEM imaging it is recommended to link to ground the sample and makes it

electrically conductive at least superficially. Initially the samples were rigidly glued to a circular stub using a conductive glue with silver nanocluster. The glue used is electrodag 915 silver paint, it has a low viscosity, ideal to bind the sample to the stubs and to connect the samples to ground potential in order to avoid accumulation of electrostatic charges. The glue is shown in the Figure 3.21(a).

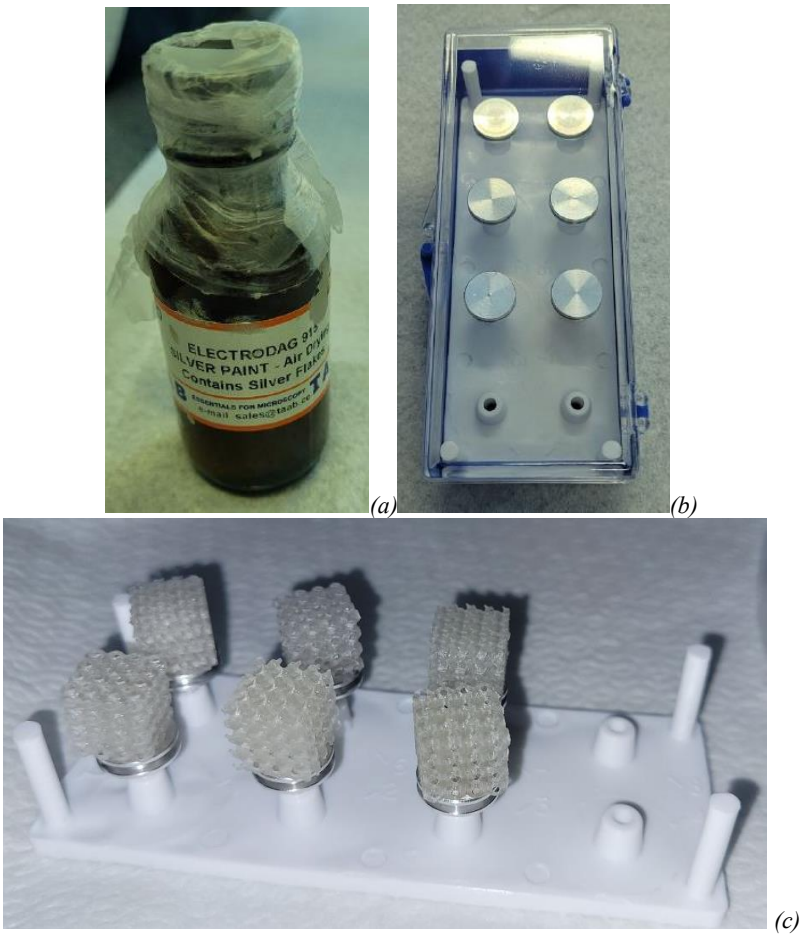

Figure 3.21(a) Electrodag 915 silver paint. (b) Circular stubs (c) Samples glued on the stubs

A sputter coater is used to coat the sample with a nanometric layer of platinum in order to make the samples electrically conductive. This increases not only the conductivity, but also the number of secondary electrons and consequently increases the resolution of the image. [51] The sputter coater machine is shown in the Figure 3.22(a), in the Figure 3.22(b) is shown how the sample are placed in the machine.

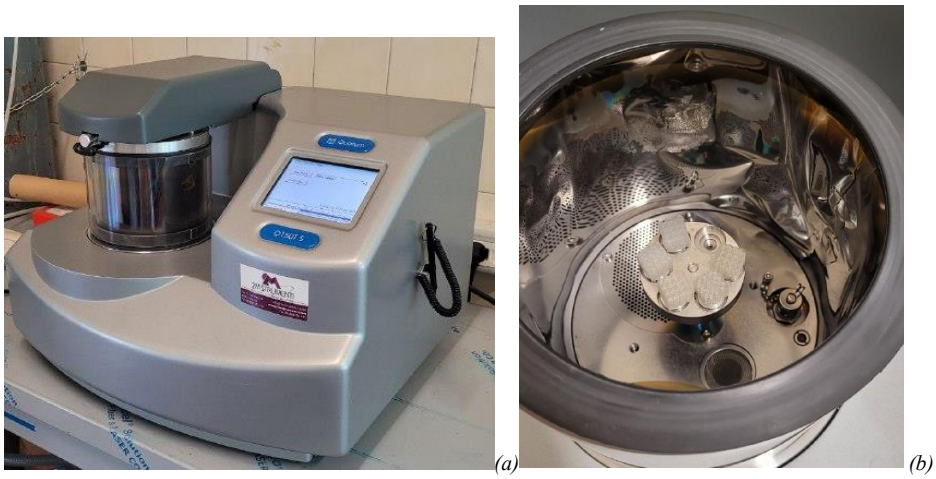

(a) (b)

Figure 3.22(a) Sputter coater (b) Sample positioning in the sputter coater

After coating, the samples are placed inside the sample stage, taking care to have the top of the scaffold protrude just 1mm outside the stage, as shown in the Figure 3.23(a). This is done to optimize the focus and brigthness settings in the SEM imaging software.

The sample preparation and the SEM aquisition is developed in Disat department at Politecnico of Torino.

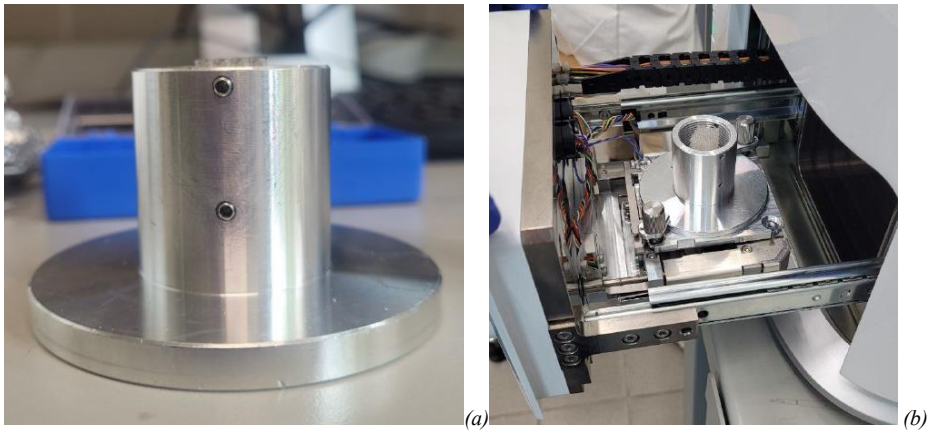

(a) (b)

Figure 3.23(a)Scaffold placement in the stage (b)Scaffold placement in the benchtop SEM

- Fundamental components

The electrons are generated from a source, in this case a thermionic source has been used, precisely a tungsten filament, which heated over a certain energy is able to emit an electron beam, the beam voltage is between 5kv and 15KV.

Through condensing lenses the beam is converged, electromagnetic lenses allow in fact to determine the size of the electron beam from which will depend the resolution of the image. Then the beam passes through an objective lens able to focus and deflect the beam on the sample so that it can be scanned.[52]

During the interaction of the beam with the sample, retrodiffuse electrons, secondary electrons and X-rays are emitted, which are detected by different detectors.

For imaging the first two types of electrons are used, through X-rays you can instead obtain compositional information and identify the elements that composed the sample.

The retrodiffused electrons, BSE, originate from the elastic collision between electrons of the primary beam and atoms of the sample, the number of retrodiffused electrons hitting the detector is proportional to their Z number and come from a deeper area of the sample.

These electrons come from a large area of the interaction volume and their collisions cause changes in the trajectory of the electrons, for this reason the BSE detector is concentric to the beam and is located above the sample so as to maximize the collection of electrons in different parts.

On the contrary, the secondary electrons, SE, have lower energies than the previous ones, they come from inelastic interactions between the primary beam and the sample that happen in the more superficial zones.

The SE detector called the Evengart-Thornley detector is a scintillator, located inside a Faraday cage, which has a positive charge that attracts secondary electrons. It is placed on the side of the electronic chamber with a certain angle of inclination such as to increase the efficiency of electron collection.[53]

In the Figure 3.24 are shown the different types of signals used in SEM and where they originate from are shown, Figure 3.24(a), and the typical location of electron detectors in Figure 3.24(b).

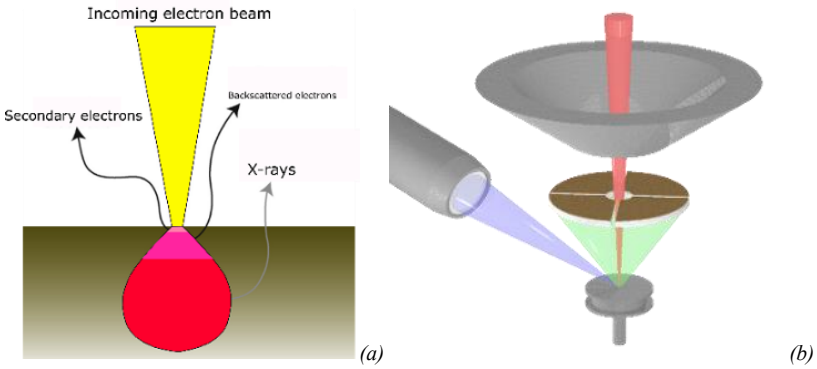

Figure 3.24(a) Origin of electron and X-rays (b) Position of electron detectors

Images obtained via BSE provide information on the composition and distribution of the elements in the sample and have a lower resolution than images obtained with SE, these last provide 3D images with detailed information about the surface of the sample.

In order for the electron source not to be contaminated by atoms or molecules, it is necessary to guarantee the vacuum in the entire microscope. Gas molecules can interfere with the electron beam by deflecting it and reducing image quality, so vacuum is essential to achieve a less noisy and high resolution image.

- Technical features of SEM

The two important features of SEM that affect image quality are resolution and magnification.

The SEM using an electrons beam with a very small wavelength can have images with very high resolution and therefore it can obtain a higher magnification.

According to an optical microscope for which the resolution depends on the diffraction limits or fineness of the lenses, in this case the resolution depends only on the size of the electronic spot.

Although SEM does not have high resolution to see individual atoms, it is able to watch large areas of the sample of interest.

The SEM magnification ranges from a minimum of 10 to a maximum of 3,000,000 times, is given by the ratio between the size of the display device and the actual size of the part of the sample on which the beam is scanned.

A larger magnification is due to a smaller area scanned on the sample.

Secondary electrons provide a range of magnification of x10 x60.000 and backscattered electrons provide an image with a magnification of x10 x30.000.

The magnification of the image in an SEM does not depend on the power of the lens as for optical microscopes, but it is controlled by the current provided by the scanning coils.

In addition, to have a sharper image it is useful to scan slowly stopping the beam for more time on the points of interest.[54]

3.4.3 Micro Computed Tomography

Micro-CT is an imaging technique that uses X-rays to scan the sample internally, creating cross-sections that are then stacked to create the virtual 3D model of the sample. It is a non invasive and non destructive technique that does not require specific sample preparation, which allows to use the sample for subsequent tests. [55] Micro-CT used to analize lattices is illustrated in Figure 3.25, it was possible to use Micro-CT in the laboratory J-Tech at Politecnico of Torino.

Figure 3.25 Micro Computed Tomography

With porous structures, as in this case, Micro-CT allows to study not only the external morphology of the sample but also to assess porosity, density, investigate pore shape, size and their interconnectivity.

One can observe the orientation of the fibres that compose the scaffold, the thickness of the walls and analyse the presence of defects in the sample. In addition to these characteristics, it is possible to create a mesh of the model, perform a FEM analysis, and simulate its mechanical properties and permeability.

- Micro-CT operation

The X-ray beam hits the sample directly, the detector opposite the source collects the radiation not absorbed by the sample and, through a collimator and scintillator, generate a two-dimensional X-ray image. The Figure 3.26 shows how micro ct works.

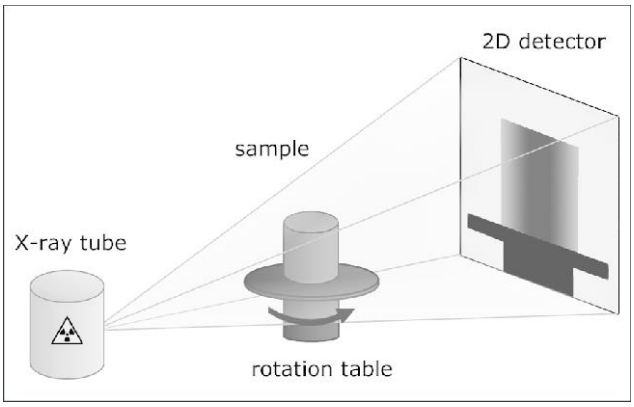

Figure 3.26 Operation diagram of Micro CT

To capture projection images at different angles, the object is rotated by fractions of a degree at a time until it reaches 180° or 360°.

Through the principle of filtered back-projection, the computer is able to stack the images of the sample and reconstruct its three-dimensional structure.

Depending on how the X-rays are attenuated by passing through the sample it is possible to deduce the internal structure and its properties.

The quality of the reconstruction of the object depends on the resolution of the scan ranging from 1 to 50 μm, with a high resolution, around 5 μm, it is possible to get a good quality reconstruction, but this requires a very high time for scanning and data processing.[56]

- Micro-CT interface

The sample is placed on a stand, in a position that during rotation it does not deviate too much from the image acquisition frame, at a specific distance from the source and detector.

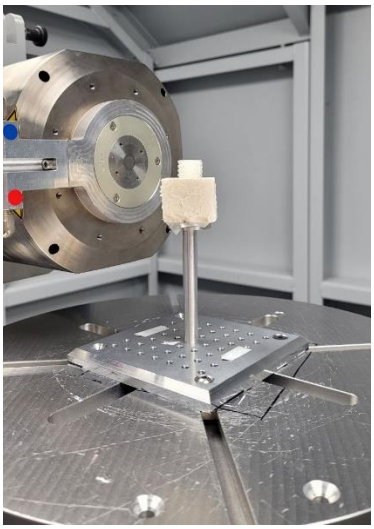

Figure 3.27 Positioning of the sample in Micro CT

The XClient app allows the user to set the intensity of the beam, ranging from 20kV to 300kV, the current in µA, the image acquisition speed and the exposure time to generate the image.

In this case, a voltage of 60kV and current of 100µA was set, so that the power is less than 10 W, as recommended by the machine specifications.

The Image settings have not been modified on the advice of the users of the machine.

Then the geometry settings must be set:

- SDD: distance between detector and tube, equal to 1800 mm
- SOD: distance between the object and the tube, equal to 150 mm
- Rotation: angle of rotation of the table, in °, anticlockwise, to achieve 800 projections
- Resolution: pixel size in µm, equal to 16.67 µm, calculated by the app automatically

$$Res = \frac{SOD}{SDD} * (resolution\ detector = 0.2 \frac{\mu m}{pixel})$$

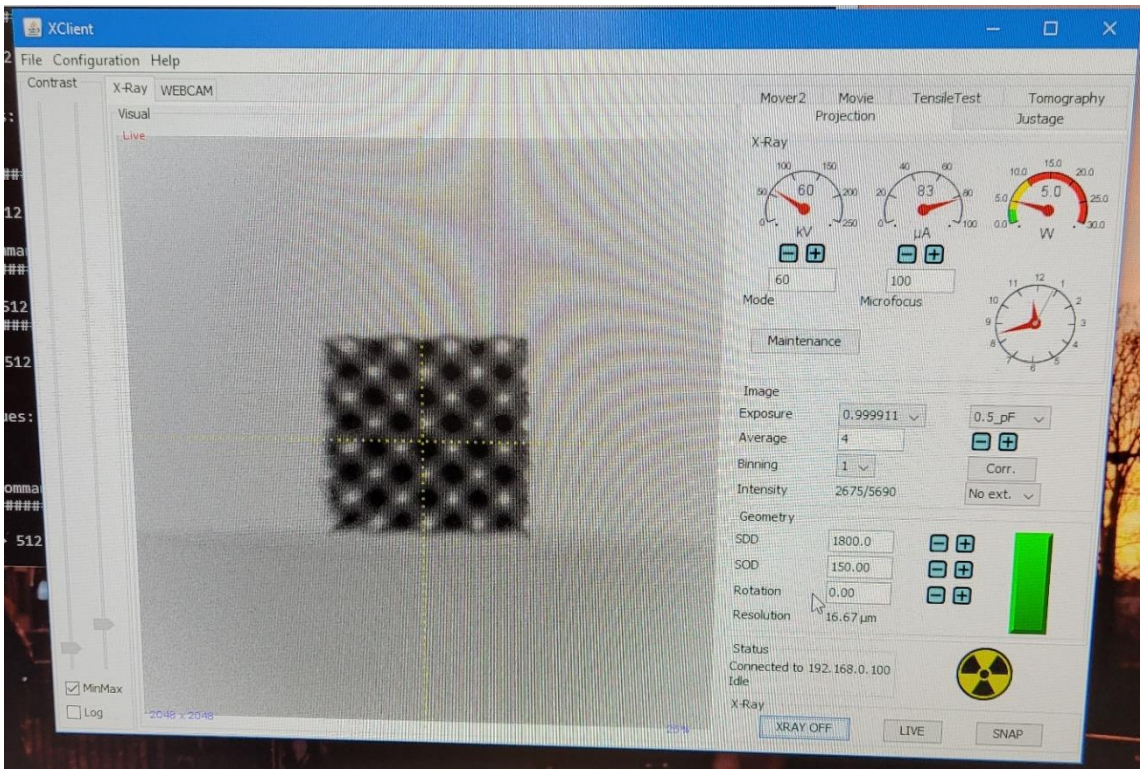

Figure 3.28 User Interface of App XClient

Once all tomography images have been acquired, the ImageJ software must be opened from the desktop to do the image reconstruction and check that the tomography is good.

Post processing of the reconstruction is performed through VGStudio max.

3.5 Mechanical analysis

The use of the mechanical testing machine is essential to understand the behaviour of the lattices subjected to compressive and tensile forces, to compare the mechanical behaviour between the different porous structures and, subsequently, to compare their behaviour with values and behaviour typical of bone.

For the mechanical tests, the Shimadzu Autograph AGS-X machine with a 10kN load cell is used, guaranteeing force accuracy, during the test, of up to ±0.5% of the indicated value. The mechanical test is performed at iRap Institute, at Haute école d'ingénierie et d'architecture in Fribourg.

Figure 3.29 Shimadzu Autograph AGS-X

Based on measured force and deformation data, the machine allows automatic real-time adjustment of the control parameters and, by offering high-speed sampling of 1msec, ensures that force variations are not lost.

Essential components of mechanical test machine:

- Load cell to control and measure the force applied to sample
- Crosshead
- Instruments for measuring the displacement of the crosshead
- Common joint for Tensile and Compression tests
- Computer to processing data

Operations must be carried out to ensure that the machine functions properly at each test. The instrument must be calibrated, this is done automatically, then the load and the initial strain must be reset.[57]

Before starting the test, the machine requires to insert the speed of the crossbar, the maximum force to be imposed on the specimen and the geometric characteristics of the samples. For the calculation of the elastic modulus in the deformation domains it was necessary to specify in the machine the type of material to be tested, in this case Polymer.

The measurements of specimens are taken for each characteristic size, as shown in the Figure 3.30, with a caliber.

Figure 3.30 Measure of the sample size with a caliber

For the tensile test, the dimensions of specimen thickness, gage width and length of narrow section were entered, while for the compression test, the dimensions of height, width and length.

In the Figure 3.31 is shown the user interface of the machine for inserting the geometric measurements of the samples.

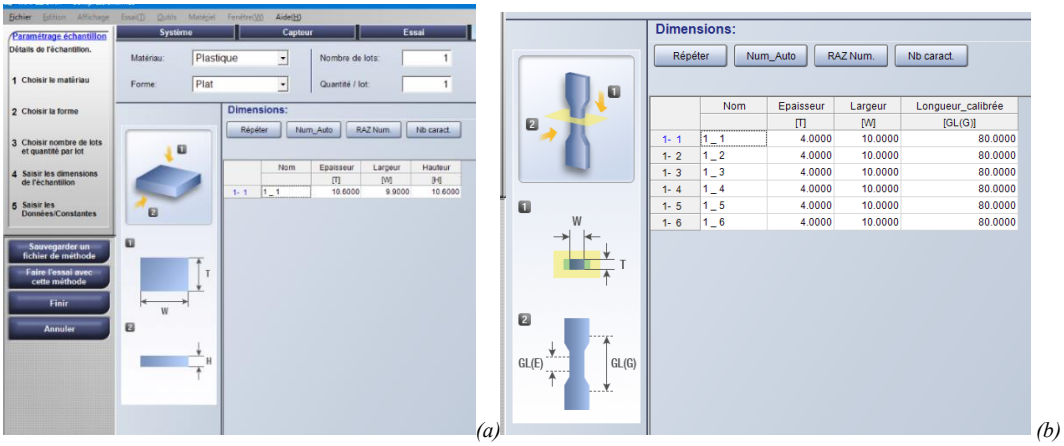

(a) *(b)*

Figure 3.31(a) Geometry setting for compression test (b) Geometry setting for tensile test

At the end of the test, the data is transmitted to the software so that it can be subsequently processed.

Using the TRAPEZIUM LITE X software, suitable for encoding of data, it is possible to display the characteristic stress-strain curves and force-displacement curves for each specimen in real time, and to obtain information on the elastic modulus and breaking points of the specific specimen.

As required by the ASTM standards, at least five samples are tested for each sample type and parameter.

- Compression test

The compression test consists of subjecting the scaffold to a compressive action, it is chosen a uniaxial downward force, by setting a moving crosshead speed of 1mm/min.

For compression test is useful to realize cubic scaffolds, in this thesis the scaffolds have dimensions of approximately 12mmx12mmx12mm, as represented in the Figure 3.32.

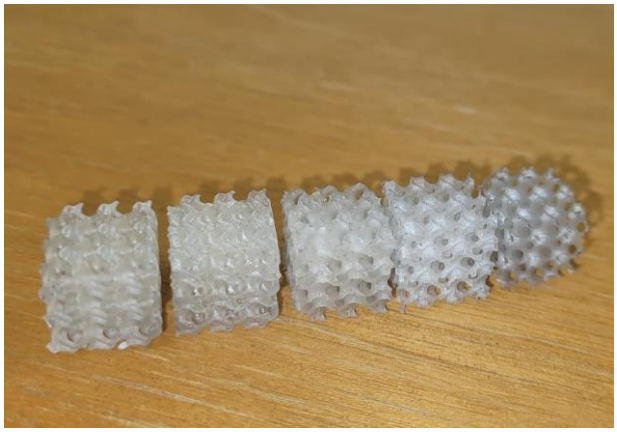

Figure 3.32 Cubic samples for compression test

Fixed-Type Compression Plates, with a diameter of ø50 × 25 mm of thickness, are used for the compression test; the scaffold is positioned in order to be in the centre of the plates.

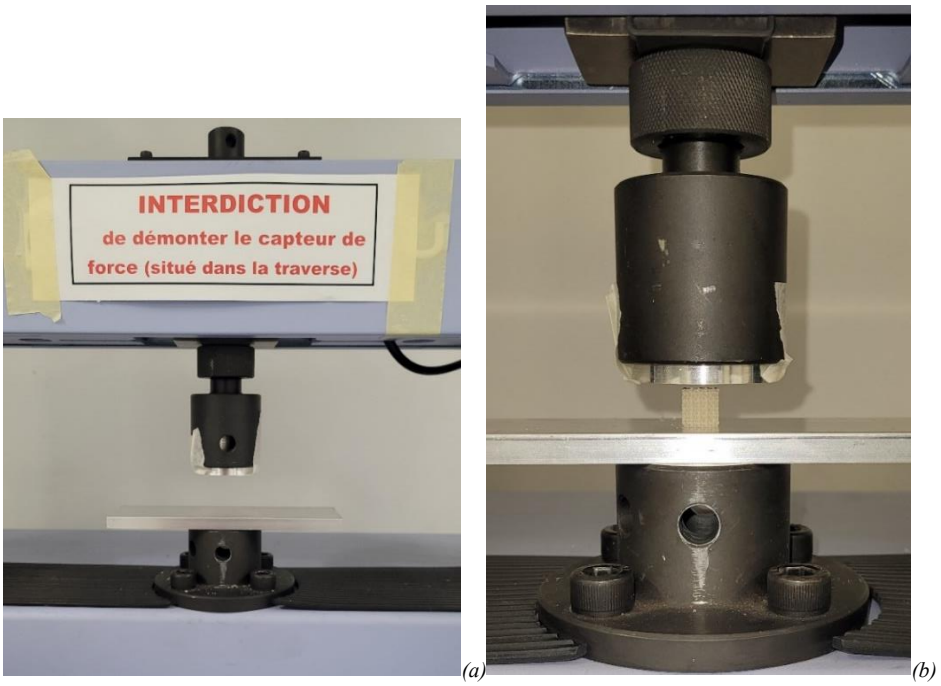

(a) (b)

Figure 3.33(a) Compression test plates (b) Positioning of the cubic specimen

- Tensile test

Tensile test consist of submit a specimen to a deformation at constant speed, through the action of a unidirectional tensile load force. The force is applied orthogonally to the specimen section. The speed set in the machine is 1mm/min.

The test specimen is brought to broke, and during the test, the values of the load applied to the test specimen and the associated deformation are measured.

For traction, dog-bone test specimens of the typical dimensions already used for the specific machine are moulded. The size of the test specimen are shown in the figures below.

In this test, it is not so much the size of the samples that is important as the shape of the sample. The middle part of the sample is always thinner than the ends, so that the deformation involves this area, away from the grips. That is why the porous structure, with similar parameters to the compression test, is placed in this middle part; also in order to have a better attachment of the non-porous part to the tensile hooks.

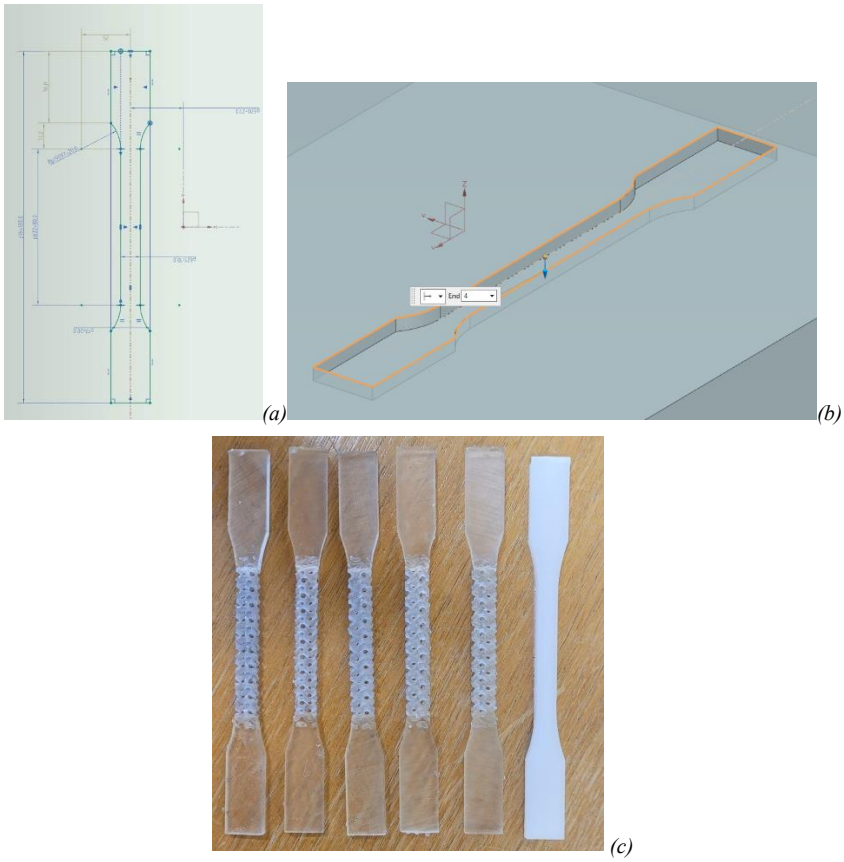

Figure 3.34(a)(b) CAD model of dog-bone specimen (c) Samples for tensile test

The tensile test requires specific couplings such as Non-Shift Wedge Type Grips. The specimen, placed vertically and centrally, is hooked into the clamps in the widest part of the outer section.

Figure 3.35(a) Tensile test grips (b) Positioning of the dog-bone specimen

The curve obtained from the two tests with the application of a uniaxial load has similar characteristics to that shown in Figure 3.36.

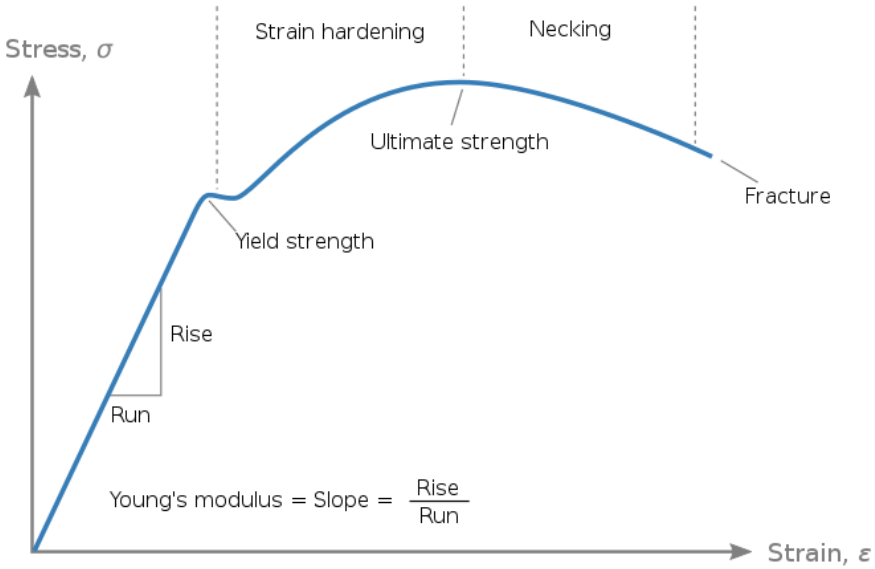

Figure 3.36 Curve stress-strain

The stress-strain curve is characterised firstly by a linear elastic zone, in which the stress and strain increase rapidly; the stress is proportional to the strain. In this zone, the material

obeys Hooke's law through which the slope of the curve allows the Young's Modulus to be calculated.

The formula below describe the calculation of stress and strain made to elaborate data.

$$\sigma = \frac{F}{\mathrm{Ao}}$$

σ is stress, F is the load applied to the specimen, Ao is the area of the section of the specimen before performing the test.

$$\varepsilon = \frac{l - lo}{\mathrm{l}}$$

ε is the deformation and is calculated as the ratio of the initial length of the specimen minus the length of the specimen during the test to the relative length of the specimen.

Using the two previous values, is possible to define Hooke's Law

$$\sigma = \mathrm{E} * \varepsilon$$

the constant E is the Young's modulus calculated in Mpa.

At the end of this region**,** plastic deformation begins. The stress in which the starting point of plastic deformation corresponds is called Yield stress.

Yield stress is that point where the transition from the elastic to the plastic field occurs.

The specimen continues to deform plastically until the breaking point.[58]

Chapter 4

Results and discussion

In this chapter there are the results, including comments, obtained in the characterization of the scaffold.

It is possible to note that surface that compose the scaffold in Pyvista are discretized better than the Pygmsh module, have a finer mesh that leads to a more accurate creation of the model.

4.1 Digital optical microscope

After removing supports created for printing, the different samples are analysed through the microscope to assess the accuracy of the printer and the minimum size in order that the lattice does not fail.

Through the microscope it can be measured pore size, the length of unit cell and thickness of scaffold.

The results obtained in the first test, printing the structure Schwarz P with five different scale factors are shown in the figures below. Each figure shows the measurements taken with the microscope software analysis tools and refers to a specific scale factor.

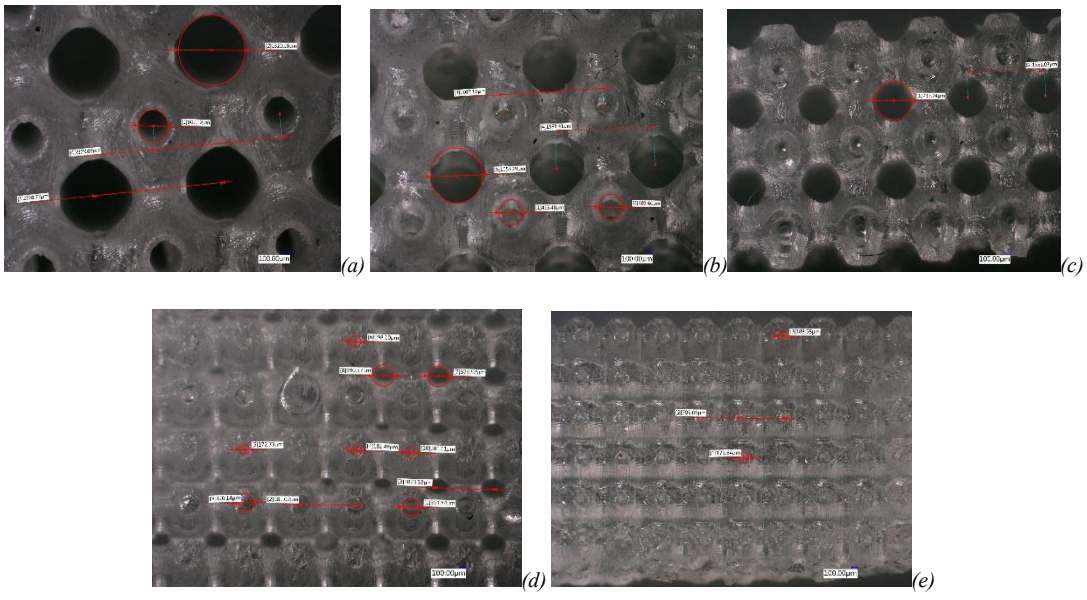

Figure 4.1 (a) Scale factor 0.5 (b) Scale factor 0.4 (c)Scale factor 0.3 (d)Scale factor0.2 (e)Scale factor 0.15

Table 4.1 shows the measurements made through the software of the digital optical microscope.

The calculation of each value in the table is the result of the average between the various measurements made in several images.

Scale factor	Little pore size(µm)	Pore size + thickness (µm)	Thickness (µm)	Big pore size(µm)	Cell length (µm)	Theoretical cell length(µm)	Theoretical thickness(µm)
0.5	598,15	870,36	136,10	1363,98	2519,21	2500	150
0.4	489,48	774,19	142,35	1069,11	2015,61	2000	120
0.3	314,92	519,27	102,18	734,29	1520	1500	90
0.2	194,57	382,98	94,21	357,69	995,08	1000	60
0.15	180,11	n.a	n.a	n.a	757,72	750	45

Table 4.1 Property of scaffold at different scale factor

Through these measurements, it can be seen that the scaling factor 0.15, not allowing the formation of pores, does not allow for valid measurements, as can already be seen from the pictures. Similarly for the scale factor 0.2, the values obtained are the result of measurements taken only on the easily visible pores, of which there are very few. The remaining scale factors allow a more accurate calculation of the set parameter values, which resulted a print accuracy value compared to the design settings of 17% for thickness values and 0.9% for element cell length values.

Similarly, the pore size obtained with scaling factors of 0.3 to 0.4 is comparable with the pore size for bone implants, the scale factor 0.5 is not accepted as it implies a pore size range of 600-1300 µm, large for bone scaffolds. Finally, it was stated that 0.3 is the minimum scale factor with which there is definitely less likelihood of lattice failure.

The same microscopic analysis is performed with the four types of TPMS, Schwarz P, Gyroid, Schwarz D and IWP.

Below is illustrated the characterisation for the Schwarz P type with different thickness values and with scale factor 0.4 in the first row, scale factor 0.3 the first two images in the second row and scale factor 0.2 the remainder.

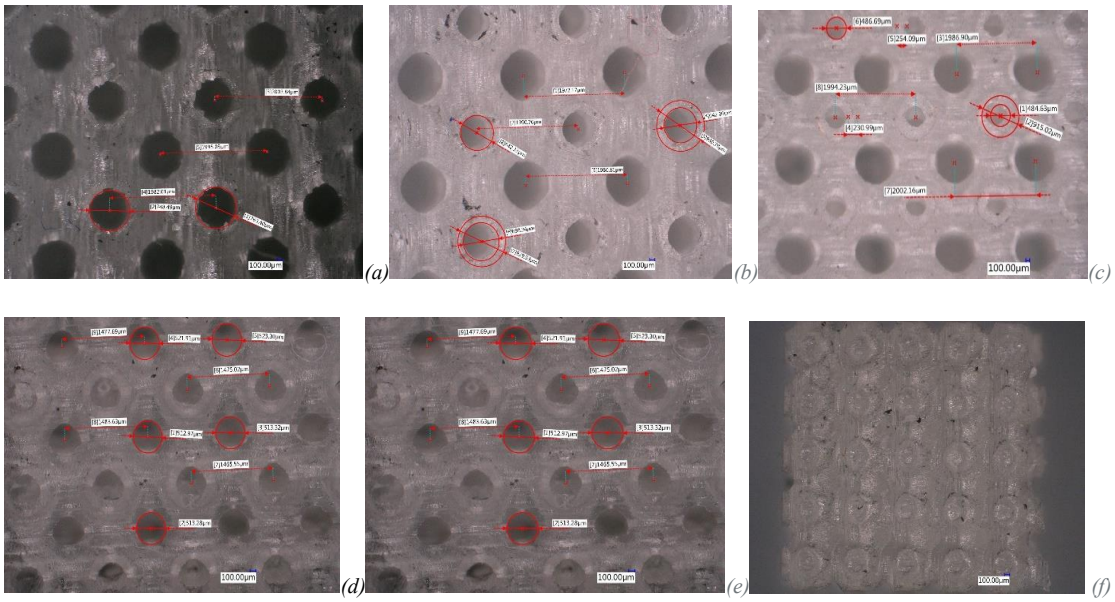

Figure 4.2 Schwarz P (a) scalefactor0.4thickness0.1mm (b)scalefactor0.4thickness0.25mm (c)scalefactor0.4thickness0.5mm (d)(e)scale factor 0.3 (f)scalefactor0.2

It can be visibly seen that the lattice with a scale factor of 0.2 is compact and has no porosity, and this is the case for all three thickness values.

Similarly, the images obtained with the microscope for the Gyroid type are shown with the same arrangement.

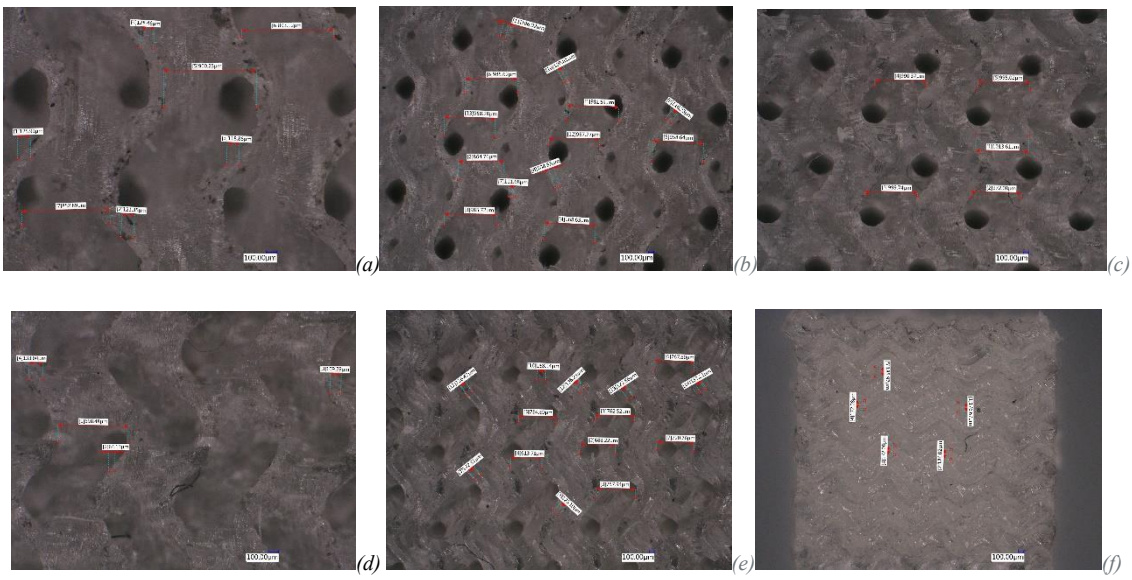

Figure 4.3 Gyroid (a) scalefactor0.4thickness0.1mm (b)scalefactor0.4thickness0.25mm (c)scalefactor0.4thickness0.5mm (d)(e)scalefactor0.3 (f)scalefactor0.2

As with the Schwarz P type, Gyroid with a scale factor of 0.2 does not produce a porous structure. In contrast, with scale factors of 0.3 and 0.4, it is possible to obtain porous structures through which pore size and thickness measurements can be made.

Below there are some images of the two remaining types, Schwarz D and IWP, through which completely porous structures could not be obtained with any of the scale factors.

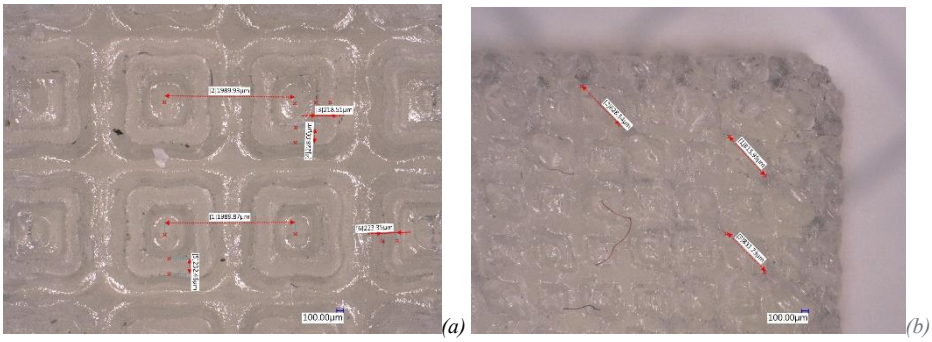

(a) (b)

Figure 4.4 (a) IWP scalefactor0.4thickness0.25 (b)Schwarz D scalefactor0.3thickness0.25

The failure of the two TPMS types led to their exclusion for subsequent characterisations. This is mainly due to their geometry, which was much more complex than the Schwarz P and Gyroid types. With such small dimensions, the parameters set, would have led to the formation of pores of a size useful for bone scaffolds, but the complex structure requires larger dimensions to produce better detail. For these reasons, the research goes on with the analysis of the Schwarz P and Gyroid types.

The following tables show the averaged values of the measurements obtained with the microscope and compared with the theorical values set in Python, in order to obtain the error values.

Scale Factor	Pore Size (µm)	Max Pore size (µm)	Cell length(µm)	Thickness measured (µm)	Theoretical Thickness (µm)	Theoretical cell length (µm)	Error thickness %	Error cell length %
0,4	483,34	972,17	2000,96	232,23	200	2000	16,11	0,05
0,4	660,92	879,71	1981,24	114,13	100	2000	14,13	0,94
0,4	789,20	843,26	1997,14	110,76	40	2000	176,90	0,14
0,3	398,52	622	1484,69	155,01	150	1500	3,34	1,02
0,3	437,41	571,58	1486,63	160,41	75	1500	113,88	0,89
0,3	518,54	515,15	1488,87	156,98	30	1500	423,27	0,74

Table 4.2 Measurements obtained for Schwarz P

Scale Factor	Pore Size(µm)	Cell length (µm)	Thickness measured (µm)	Theoretical thickness(µm)	Theoretical cell length(µm)	Error thickness %	Error cell length %
0,4	994,16	2005,35	172,07	200	2000	13,97	0,27

0,4	957,62	1978,34	112,67	100	2000	12,67	1,08
0,4	864,04	n.a.	124,52	40	2000	211,31	n.a
0,3	720,82	1494,24	135,87	150	1500	9,42	0,38
0,3	649,85	n.a.	92,67	75	1500	28,71	n.a
0,3	717,12	n.a.	64,13	30	1500	113,77	n.a

Table 4.3 Measurements obtained for Gyroid

The errors obtained between the value measured and set for the unit cell length are always less than 2%, obtained for a difference between the two values of approximately 20 μm.

As far as thickness is concerned, when it is a thickness of 0.5 mm, so as can be seen from the images it is clearly visible, there is an error of less than 20%; when, on the other hand, there is a limiting thickness of 0.1 mm, it is difficult to clearly distinguish the edges of the shapes, so the error increases considerably.

The absence of measurements in the Gyroid table is mainly due to an uncertainty in distinguishing the edges of the unit cell for small thicknesses and scale factors.

The first test carried out with Dental Clear resin consists of creating Schwarz P type and Gyroid type scaffolds by varying parameters such as C, element cell length and lattice thickness.

Among the scaffolds obtained, the successful scaffold are very few, as reported in the figures made with the microscope, it is seen that the lattices are not completely porous.

Figure 4.5 (a) Gyroid length3.2mm C0.6 thickness0.25mm (b)Gyroid length3.2mm C0.9 thickness0.25mm (c)Schwarz P length3.2mm C0.3 thickness0.5mm

At this point, therefore, only Schwarz P and Gyroid scaffolds with a C value of 0 were analysed in order to compare what happens when only the length of the unit cell and the thickness of the lattice are varied.

The measurements obtained with an initial unit cell length of 2mm are shown in the Figure 4.6(a)(b) for Gyroid and Figure 4.6(c)(d) for Schwarz P.

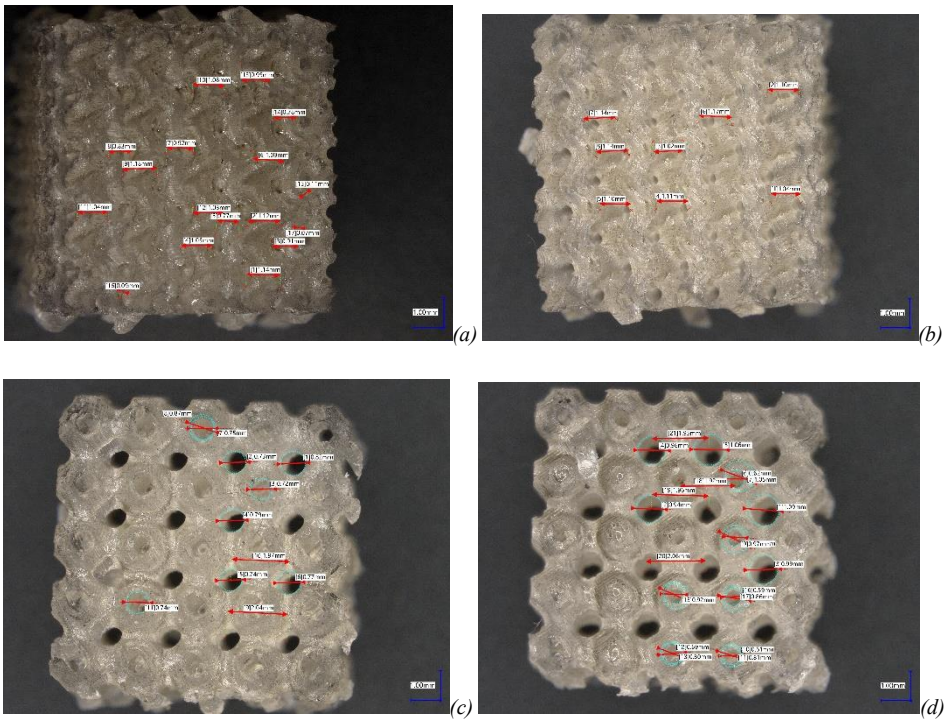

Figure 4.6 (a) Gyroid length2mm thickness0.1mm (b)Gyroid length2mm thickness0.2mm(c) Schwarz P length2mm thickness0.1mm (d)Schwarz P length2mm thickness0.2mm

As can be seen from the images there is a difference between the two types of geometry, the Gyroid with a cell length of 2mm does not allow the creation of a porous lattice as is the case with the Schwarz P.

The images taken with the microscope and the measurements taken for the two structures with a cell length of 3mm are shown in the Figure 4.7 for Gyroid and in the Figure 4.8 for Schwarz P.

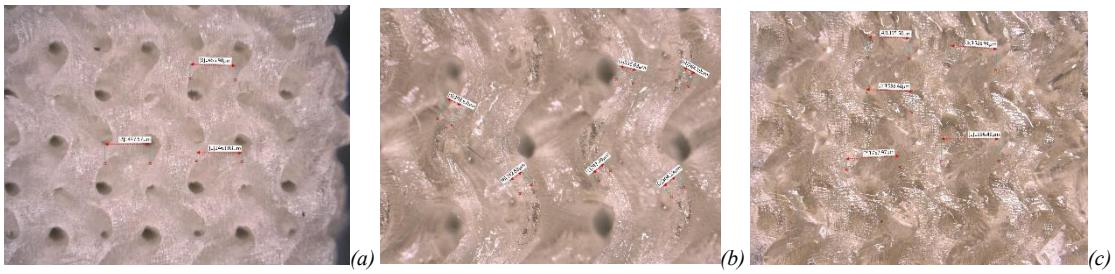

Figure 4.7 Gyroid Length 3mm (a) thickness 0.1mm (b) thickness 0.3mm (c) thickness 0.5mm

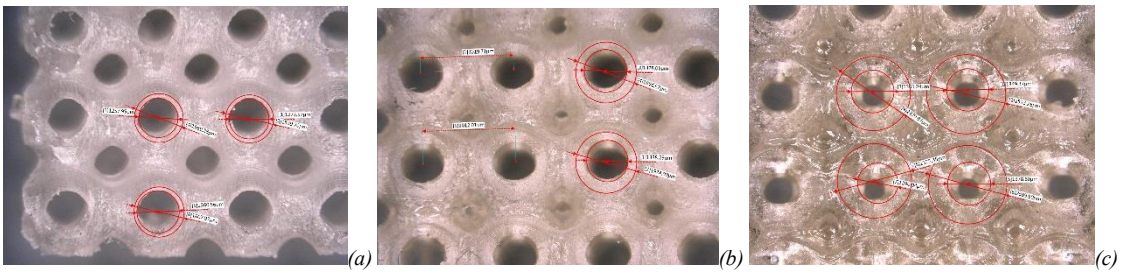

Figure 4.8 Schwarz P Length 3mm (a) thickness 0.1mm (b) thickness 0.3mm (c) thickness 0.5mm

For the unit length of 4mm, the images obtained with the digital optical microscope for both TPMS structures are shown with the same arrangement of the length of 3mm.

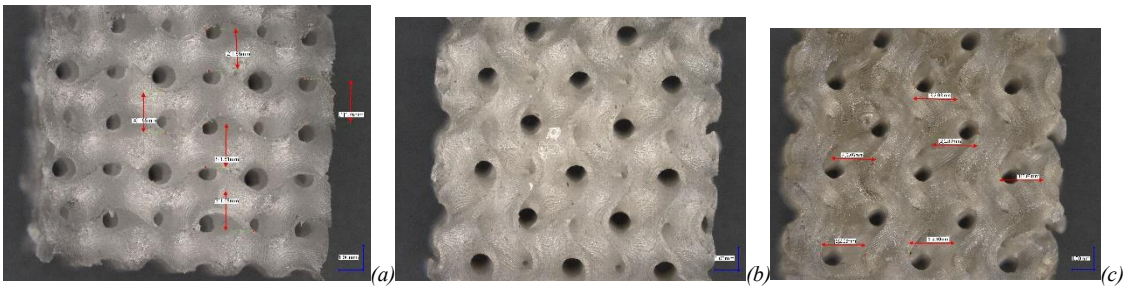

Figure 4.9 Gyroid Length 4mm (a) thickness 0.1mm (b) thickness 0.3mm (c) thickness 0.5mm

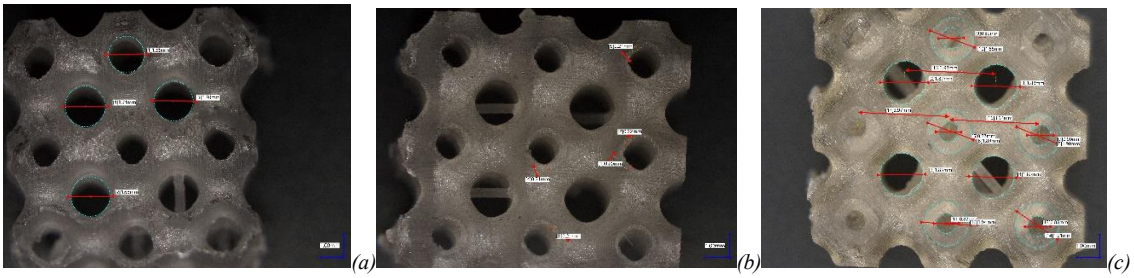

Figure 4.10 Schwarz P Length 4mm (a) thickness 0.1mm (b) thickness 0.3mm (c) thickness 0.5mm

Below there are the values obtained by averaging the various measurements for the Schwarz P in the Table 4.4 and Gyroid in the Table 4.5.

Theoretical Unit cell length (µm)	Theoetrical Thickness(µm)	Thickness (µm)	Pore size (µm)	Big pore size (µm)	Effective cell length(µm)	Error thickness %	Error cell length %
2000	100	115	594,68	763,86	2040	15	2
2000	200	255	361,09	818,7	1953,85	27,5	2,31
3000	100	137,36	1115,44	1296,67	2933,29	37,36	2,22
3000	200	217,98	806,54	1389,12	2941,08	8,99	1,96
3000	300	280,88	n.a	1337,34	2987,5	6,38	0,42
3000	400	393,5	n.a	1384,8	3008,73	1,63	0,29
3000	500	526,33	n.a	1371,5	2987	5,27	0,43

4000	100	66,67	890	1667,5	n.a	33,33	n.a
4000	200	110	n.a	1460	n.a	45	n.a.
4000	300	210	1312,5	1782	3976,67	30	0,58
4000	400	360	870	1885	4010	10	0,25
4000	500	508	882	1866,25	3963,33	1,6	0,92

Table 4.4 Measurements obtained for Schwarz P

Theoretical Unit cell length (μm)	Theoretical Thickness (μm)	Thickness (μm)	Pore size (μm)	Error thickness %
3000	100	132,59	1427,72	32,59
3000	200	179,60	1465,00	10,20
3000	300	293,33	1514,00	2,22
3000	400	382,50	1499,80	4,38
3000	500	486,33	1580,57	2,73
4000	100	86,00	1706,00	14,00
4000	200	178,89	1871,25	10,56
4000	300	248,33	1820,00	17,22
4000	400	362,00	1668,57	9,50
4000	500	462,50	2062,00	7,50

Table 4.5 Measurements obtained for Gyroid

The thickness for the two types of gratings is respected with an error of less than 10 % for the thickness with a value of 0.4mm and 0.5mm. On the contrary, for thinner thicknesses, the measurements are not accurate because the edges are not clearly distinguishable.

As regards pore sizes, the Gyroid presents pores with very high values compared to the size one would want for bone scaffolds. But having smaller elemental cell sizes, as seen with the 2mm of length unit cell, results in lattice failure.

Pore size obtained in the Schwarz P structure are similar to the pore size that characterize spongious bone, in the range of 500-1000 μm. For Gyroid structure the pore size is larger than that required for the bone.[25]

4.2 Electron scanning microscope

The scanning electron microscope allows further analysis of the sample morphology with better resolution than the digital optical microscope.

The scanning electron microscope images taken on the two types of TPMS structures for the unit cell length value of 3mm are shown in the figures below.

The pictures take the surface of the sample at different magnifications to assess its morphological characteristics.

Figures 4.11 show the images taken with the type Gyroide for the different values of thickness, in the rows there are different type of magnification to see better the morphology of the samples.

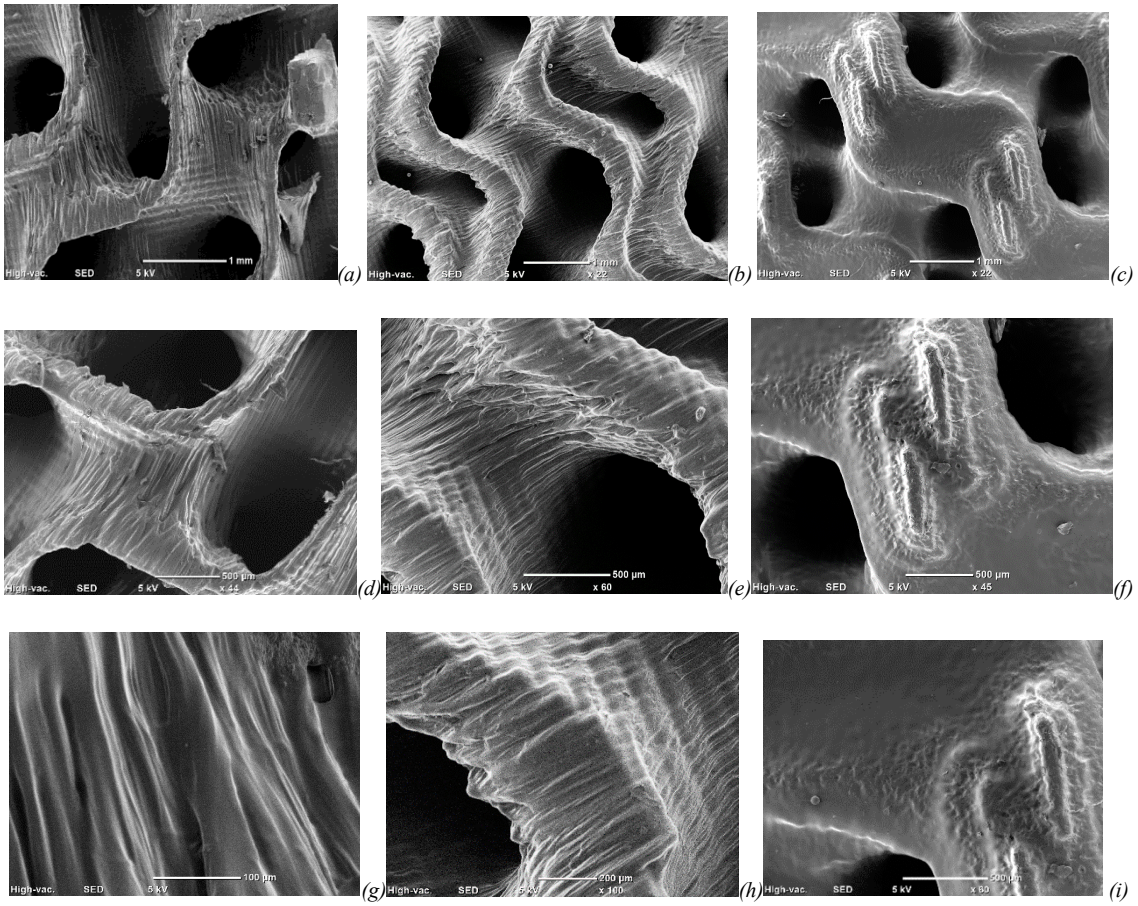

Figure 4.11 Gyroid (a)(d)(g)thickness0.1mm (b)(e)(h)thickness0.3mm(c)(f)(i)thickness0.5mm

The magnifications used equal to x22, x45, x60, x100, show structural variations due to different parameters in the preparation of the lattices.

Comparing the images obtained from different thicknesses for each structure, it is possible to note immediately a big difference in the morphology of the lattices.

In the lattice with thickness 0.1mm it can see the individual layers that compose the scaffold, from measurements made with SEM, the thickness of the layer is equal to 151µm.

It is possible to see that thickness equal to 0.1mm does not have defined edges. For thickness equal to 0.3mm it is possible to note the single layer that compose the structure, whick is visible and cause a deviation from the desired geometry at micrometric level. This deviation from the desired geometry is illustrated in the Figure 4.12.

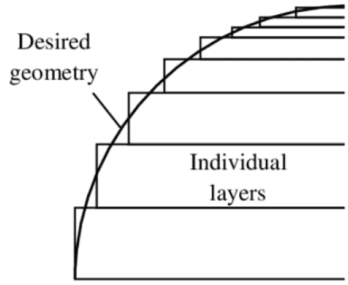

Figure 4.12 Deviation of the original geometry

The lattice with a thickness of 0.5mm presents a smooth, compact surface with no roughness. It is not possible to see the individual layers that compose the structure, everything appears without discontinuity, but rather than the other two thicknesses, the 0.5mm thickness does not allow the creation of pores in every part of the structure.

Measurements taken by SEM of pore thickness showed that the thickness is comparable to measurements taken by digital optical microscope. On the contrary, for the pore sizes with SEM a dimensional range of 700 to 1000 µm is obtained, much lower than the values obtained with digital optical microscope.

Schwarz P structure is characterized in the same way of the Gyroid, in the Figure 4.13 there are the images of Schwarz P refer to a different value of thickness.

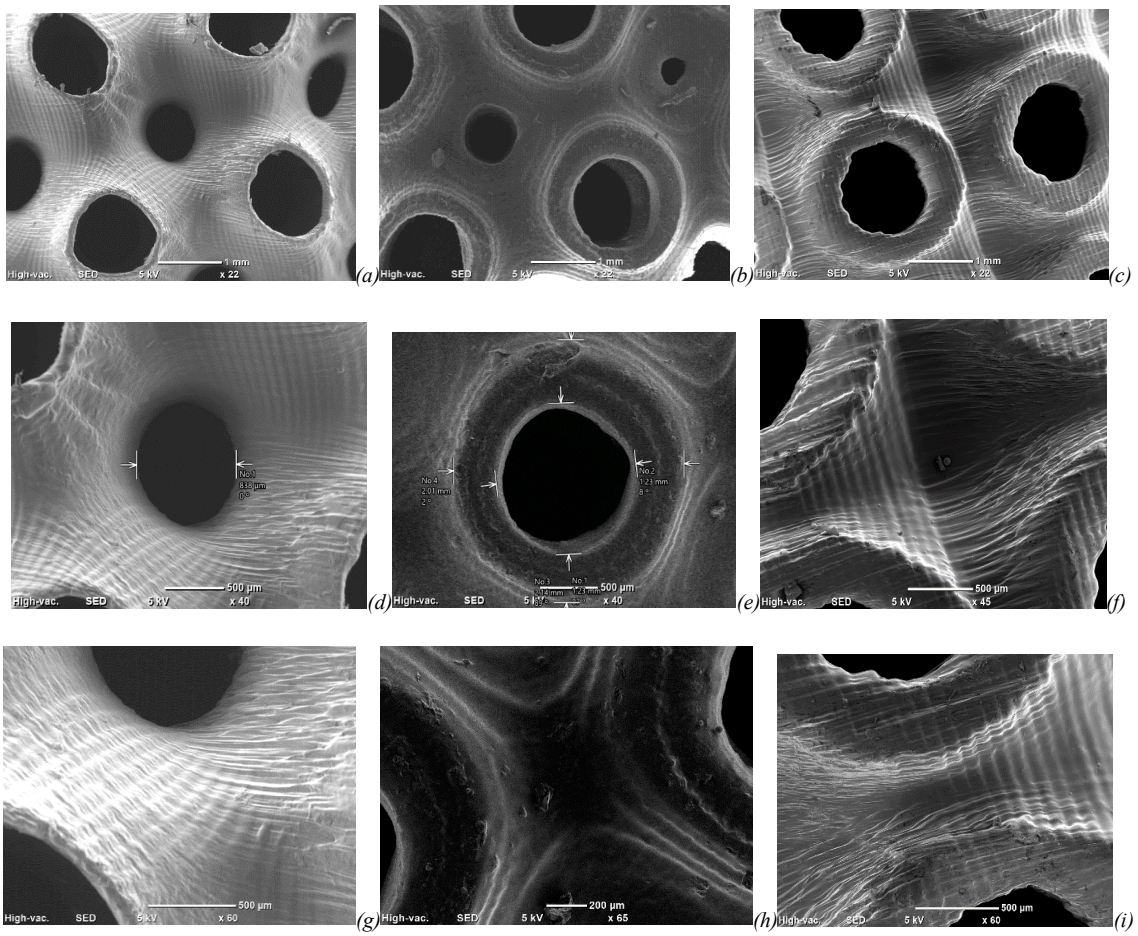

Figure 4.13 Schwarz P (a)(d)(g)thickness 0.1mm (b)(e)(h)thickness0.3mm(c)(f)(i)thickness0.5mm

The magnifications used for the Schwarz P type are the same for the Gyroid, and also in this analysis it can be seen how the variation in thickness induces structural changes.

Through the image with thickness 0.1mm it is possible to calculate the thickness of the single layer of the resin, in this TPMS structure this is equal to 98 µm.

In the images at x22 magnification, it can be seen immediately that a thickness of 0.1mm allows the formation of all the pores that characterise the TPMS type. With a thickness of 0.3mm the pores with smaller dimensions have differences in amplitude and some of these do not form, as the Figure 4.14 shows. Whereas for thickness of 0.5mm these pores fail to form. This may be due to the fact that a thickness of 0.5mm over a cell length of 3mm is very large and causes neighbouring surfaces to join.

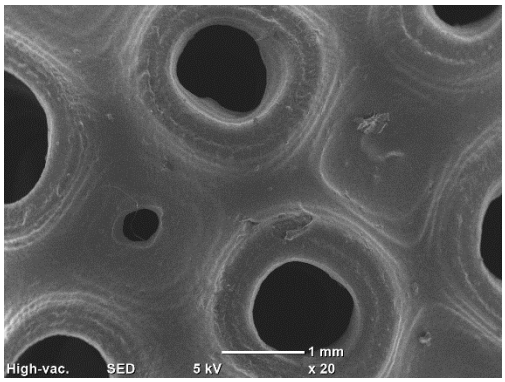

Figure 4.14 Schwarz P thickness 0.3mm

The values obtained through measurements of the pore amplitude are about 200µm lower than the values obtained with the digital optical microscope. The thickness as it happens for the Gyroid, has values similar to those obtained with the digital optical microscope.

4.3 Micro Computed Tomography

The use of Micro CT allows the 3D reconstruction of the virtual model of the Gyroid reticle with a length of 3mm and a thickness of 0.3mm, as shown in the Figure 4.15.

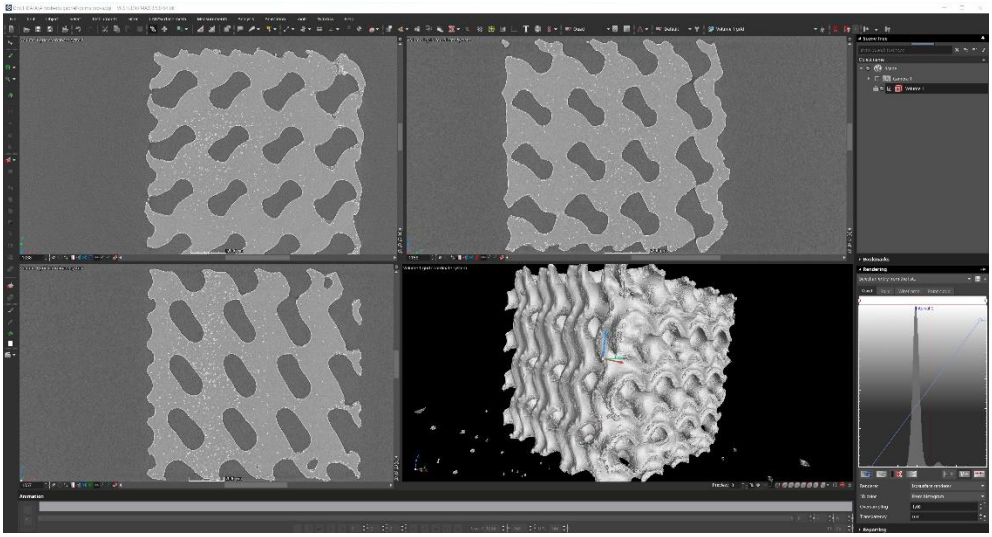

Figure 4.15 Reconstruction of Gyroid scaffold with MicroCT

It is possible to see how the 3D reconstruction of the model allows to analize all the sections of the sample, especially the internal ones that are not visible through the microscopes.

4.4 Mechanical results

Mechanical characterization of samples in tensile and compression is performed to determine the elastic modulus and yield stress of samples.

The creation of cubic and dog-bone scaffolds without any porosity serves to compare the behavior of the material subjected to compression and traction without the influence of the porosity. The behaviour of the cubic and dog-bone samples can be seen in the Figure 4.16.

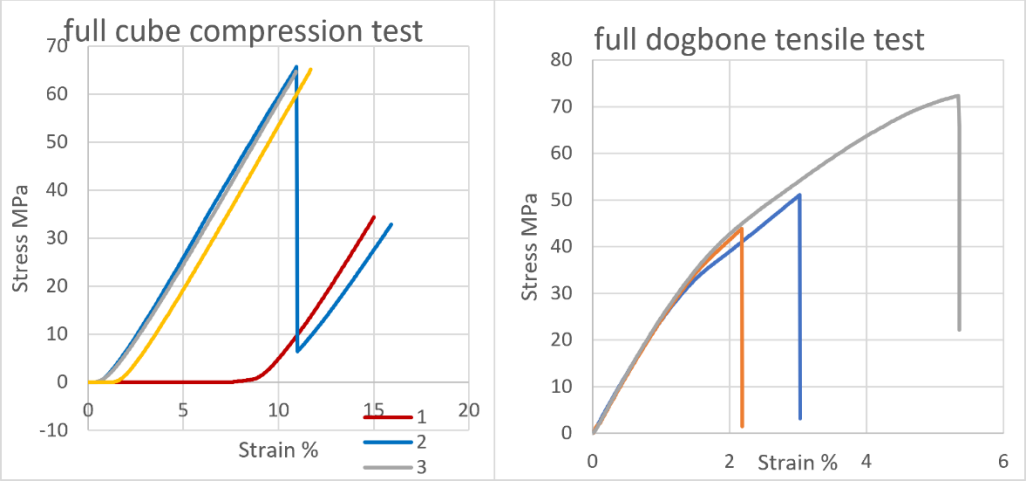

Figure 4.16 Graphs of compression and tensile tests for non porous structure

Name	Depth	Width	Height	Volume	Density	Young Modulus
dim	mm	mm	mm	mm³	kg/m³	MPa
1	12,1	12,02	12,7	1847,11	1168,96	583,05
2	11,9	12,8	11,98	1824,79	1168,02	648,92
3	12,8	12,1	12	1858,56	1169,45	624,45
4	12,8	12	12	1843,2	1168,62	639,39

Table 4.6 Compression test. Mechanical characteristics for non porous cube specimen

Name	Depth	Width	Height	Young Modulus
dim	mm	mm	mm	MPa
1	3,2	5,6	66,6	2626,4
2	3,2	5,6	66,6	2657,3
3	3,2	5,6	66,6	2676,3

Table 4.7 Tensile test. Mechanical characteristics for non porous dog-bone specimen

The Young Modulus obtained in the graphs for the specimen without porosity are different if the specimen is subjected to tension or compression; in particular for

compression the behaviour of the curve is similar to the behaviour of a brittle polymer, in tension the specimen has the behaviour of a plastic polymer with a high Young Modulus.

- Tensile test

The tensile tests were performed on the two types of microstructures selected. Six samples were created for each type and thickness.

In order to obtain accurate results the porous part is placed in the central linear part of the dog bone specimen.

Analysing the graphs of the samples, for each thickness value, it can be seen that the curves are different from each other. The behaviour of the tensile specimens is affected by variability, so the data obtained are not reliable.

The figures below represent the stress-strain curve for Schwarz P with thickness of 0.2mm, Figure 4.17, and for thickness 0.4mm, Figure 4.18.

It is possible to see that in six sample for thickness the slope of the curve is different and consequently the Young Modulus.

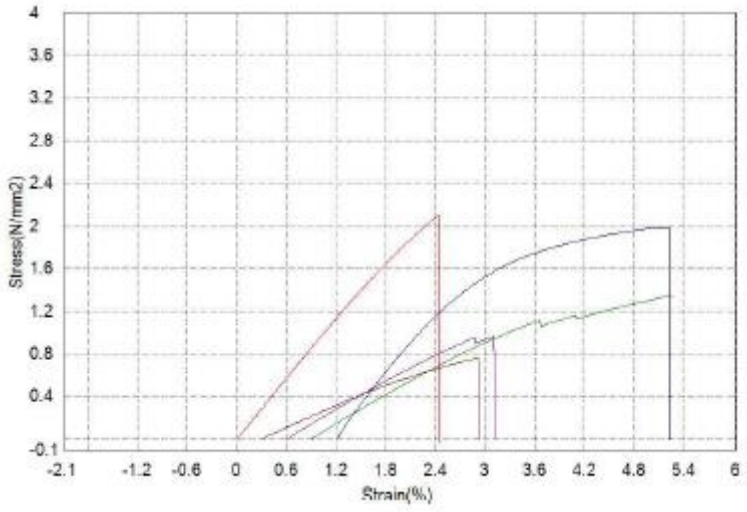

Figure 4.17 Stress-strain curve for thickness 0.2mm

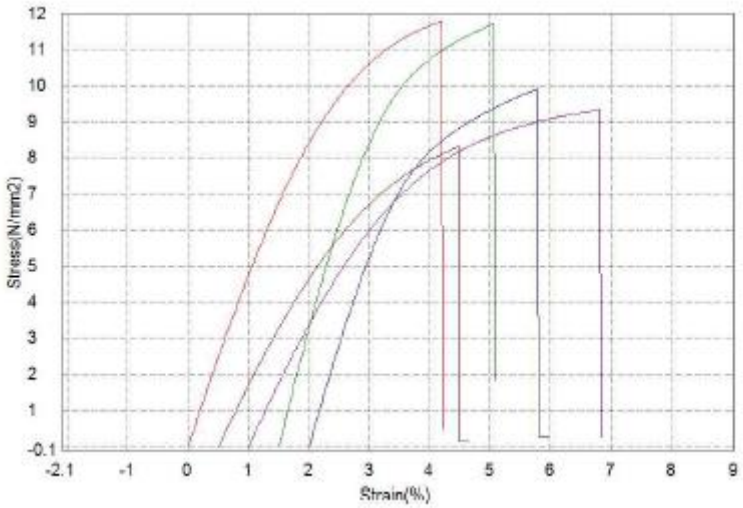

Figure 4.18 Stress-strain curve for thickness 0.4mm

The sample properties and in particular the load at break must not be influenced by the machinery used to grip the samples in the material testing machine.

The possibility of obtaining accurate data depends on the stress distribution along the sample cross-section, for this reason the cross section of the porous part must be uniform.

For the porous part it is difficult to obtain section width uniform, because fistrly the printer requires the use of support to print the sample and their removal is not precise. The presence of surface defects can facilitate fracture processes and cause errors in tensile measurements.

This problem is shown in the Figure 4.19.

Figure 4.19 Presence of surface defect

Also the machine could affect the sample properties. During the test without strain gauges it must be considered that the measurements can be affected by error, because the deformation calculated by the machine is likely to include not only the actual deflection of the specimen but also that caused by the grips.

For these reasons the mechanical tests continued with compression tests.

- Compression test

The figures below describe the stress-strain curves of the Gyroid scaffold for every thickness under the compression test. All the curves consisted of three stages: elastic stage, yield stage and plastic stage.

The tables below the graphs show the dimensional values of each sample, the volume and mass calculated to be able to obtain the density value. Then from the curves are obtained the values of Young Modulus, Yield stress and the corresponding Yield force, as explained in the Chapter Material and Methods.

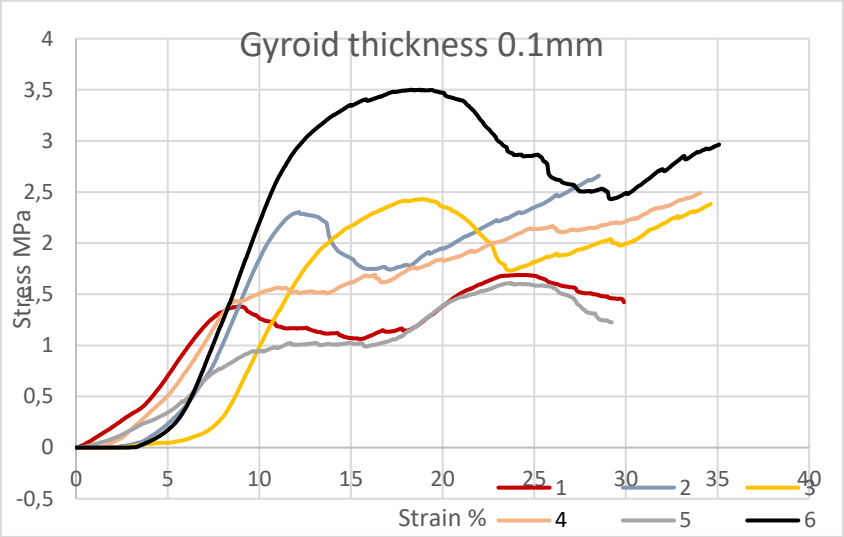

Figure 4.20 Curve stress-strain Gyroid with thickness 0.1mm and unit cell length 4mm

Name	Depth	Width	Height	Volume	Mass	Density
dim	mm	mm	mm	mm³	g	kg/m³
1	12	11,6	12	1670,4	0,3719	222,64
2	11,9	12	12,1	1727,88	0,351	203,14
3	12,3	12,2	11,78	1767,71	0,3262	184,53
4	12,1	11,6	12,1	1698,36	0,3121	183,76
5	11,8	11,9	12,2	1713,12	0,2941	171,67
6	12,2	12,1	11,88	1753,73	0,3592	204,82

Table 4.8(a) Structural property of Gyroid with thickness 0.1mm and length unit cell 4mm

Name	Young Mod	Mean Young	Yield Stress	Yield Force	Density relative
dim	MPa	MPa	MPa	N	%
1	25,68	29,68	1,03	143,52	19,0
2	26,44		1,89	269,87	17,3
3	35,18		1,61	241,56	15,8
4	20,87		1,13	158,73	15,7
5					14,7
6	40,22		2,61	384,62	17,5

Table 4.8(b) Mechanical property of Gyroid with thickness 0.1mm and length unit cell 4mm

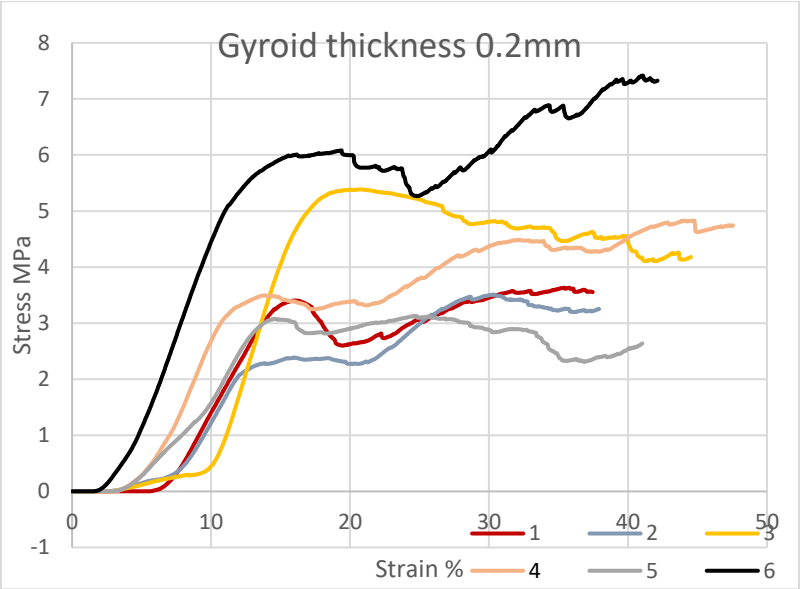

Figure 4.21 Curve stress-strain Gyroid with thickness 0.2mm and unit cell length 4mm

Name	Depth	Width	Height	Volume	Mass	Density
dim	mm	mm	mm	mm³	g	kg/m³
1	12,1	12,12	12,4	1818,48	0,6974	383,51
2	12,6	12,2	12,4	1906,13	0,4014	210,58
3	12,3	12,34	12,1	1836,56	0,4377	238,33
4	12,4	12,3	12,2	1860,74	0,4819	258,98
5	12,2	12,1	12,44	1836,39	0,4972	270,75
6	12,38	12,44	12,36	1903,53	0,4698	246,80

Table 4.9(a) Structural property of Gyroid with thickness 0.2mm and length unit cell 4mm

Name	Young Mod	Mean Young	Yield Stress	Yield Force	Density relative
dim	MPa	MPa	MPa	N	%
1	45,19	39,88	12,54	367,80	32,8
2	40,19		11,39	283,24	18,02
3			14,98	613,7	20,39
4	42,21		10,25	428,27	22,16
5	24,40		12,36	384,89	23,16
6	47,41		10,62	740,86	21,12

Table 4.9(b) Mechanical property of Gyroid with thickness 0.2mm and length unit cell 4mm

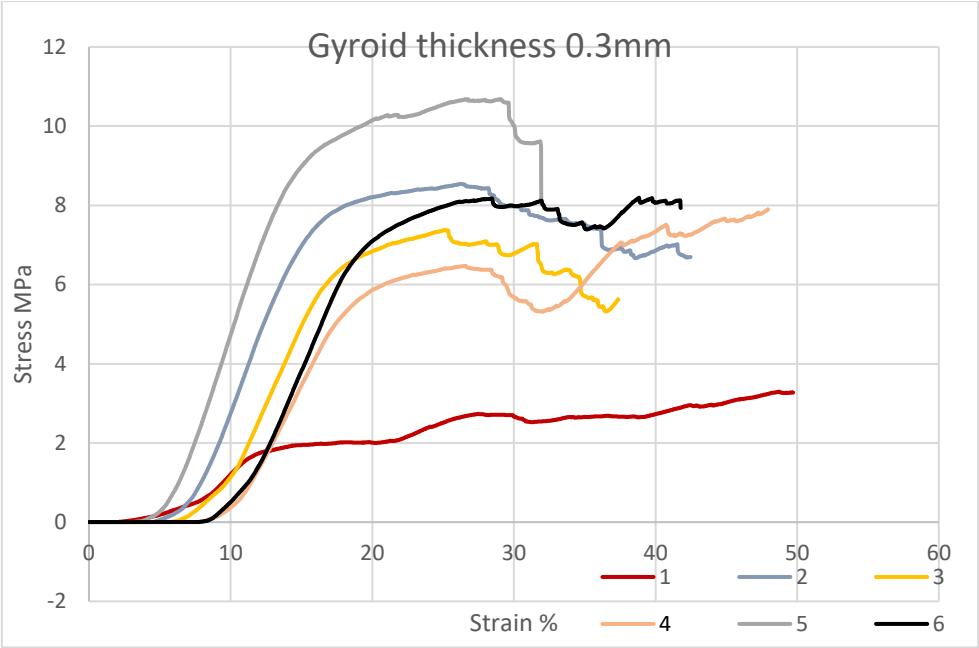

Figure 4.22 Curve stress-strain Gyroid with thickness 0.3mm and unit cell length 4mm

Name	Depth	Width	Height	Volume	Mass	Density
dim	mm	mm	mm	mm³	g	kg/m³
1	12,3	12,1	12,1	1800,84	0,7599	421,96
2	12,24	12,36	12,36	1869,9	0,6537	349,59
3	12,5	12,3	12,4	1906,5	0,7805	409,38
4	12,5	12,1	12,2	1845,25	0,7026	380,76
5	12,38	12,38	12,46	1909,67	0,6449	337,70
6	12,44	12,36	12,5	1921,98	0,7216	375,44

Table 4.10 (a) Structural property of Gyroid with thickness 0.3mm and length unit cell 4mm

Name	Young Mod	Mean Young	Yield Stress	Yield Force	Density relative
dim	MPa	MPa	MPa	N	%
1		80,38			36,10
2	86,08		5,91	893,96	29,91
3	77,15		4,99	768,03	35,03
4	67,81		3,78	571,71	32,58
5	97,08		7,91	1213,1	28,89
6	73,78		5,23	803,88	32,12

Table 4.10(b) Mechanical property of Gyroid with thickness 0.3mm and length unit cell 4mm

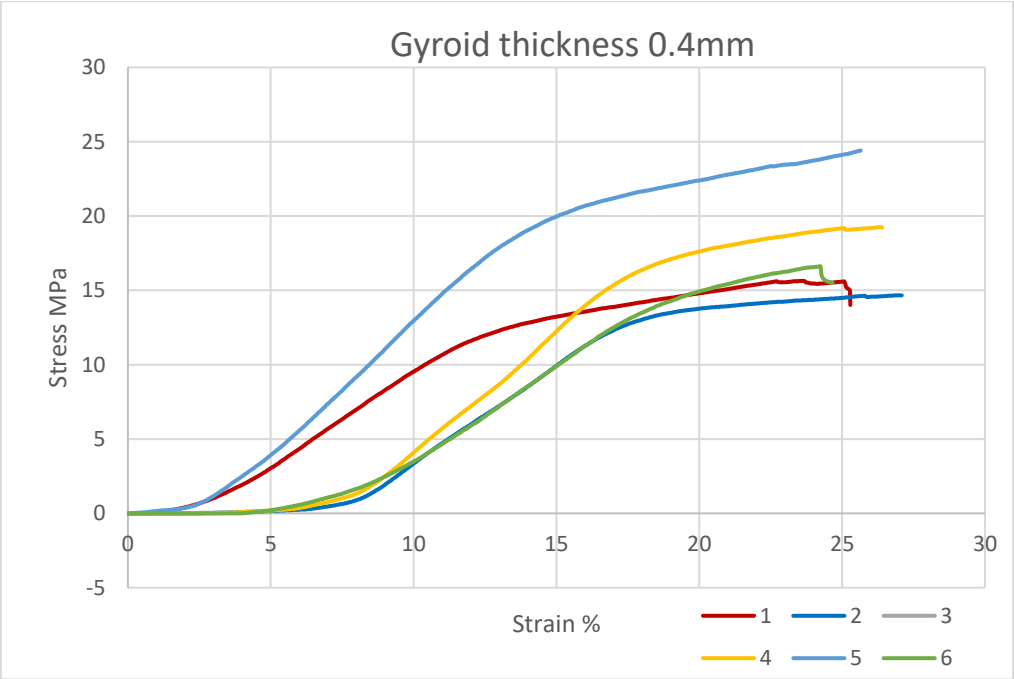

Figure 4.23 Curve stress-strain Gyroid with thickness 0.4mm and unit cell length 4mm

Name	Depth	Width	Height	Volume	Mass	Density
dim	mm	mm	mm	mm³	g	kg/m³
1	12,38	12,6	12,6	1965,45	1,0027	510,16
2	12,6	12,44	12,42	1946,76	0,9578	491,99
3	12,44	12,58	12,5	1956,19	1,0709	547,44
4	12,72	12,6	12,4	1987,37	1,0575	532,11
5	12,4	12,5	12,6	1953	1,156	591,91
6	12,64	12,42	12,6	1978,06	1,1186	565,50

Table 4.11(a) Structural property of Gyroid with thickness 0.4mm and length unit cell 4mm

Name	Young Mod	Mean Young	Yield Stress	Yield Force	Density relative
dim	MPa	MPa	MPa	N	%
1	133,33	145,27	11,45	1786,76	43,65
2	136,69		12,08	1894,14	42,09
3					46,84
4	163,40		15,40	2468,26	45,53
5	177,70		17,39	2696,11	50,64
6	115,20		12,47	1958,19	48,38

Table 4.11(b) Mechanical property of Gyroid with thickness 0.4mm and length unit cell 4mm

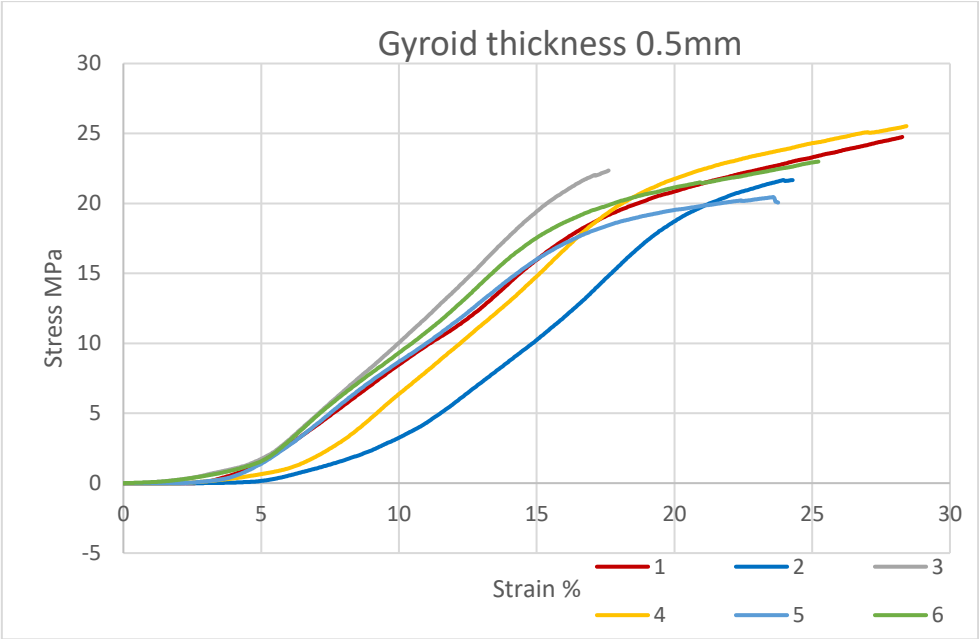

Figure 4.24 Curve stress-strain Gyroid with thickness 0.5mm and unit cell length 4mm

Name	Depth	Width	Height	Volume	Mass	Density
dim	mm	mm	mm	mm³	g	kg/m³
1	12,78	12,7	12,6	2045,06	1,2056	589,52
2	12,7	12,7	12,8	2064,51	1,1506	557,32
3	12,7	12,8	12,55	2040,13	1,2054	590,84
4	12,8	12,55	12,5	2008	1,1678	581,57
5	12,7	12,6	12,4	1984,25	1,1286	568,77
6	12,45	12,55	12,68	1981,22	1,1069	558,69

Table 4.12(a) Structural property of Gyroid with thickness 0.5mm and length unit cell 4mm

Name	Young Mod	Mean Young	Yield Stress	Yield Force	Density relative
dim	MPa	MPa	MPa	N	%
1	146,08	156	16,09	2612,3	50,44
2	148,84		18,17	2930,16	47,68
3	172,2		21,06	3423,34	50,55
4	164,91		17,07	2741,81	49,76
5	150,28		16,31	2809,6	48,66
6	153,70		17,44	2725,43	47,80

Table 4.12(b) Mechanical property of Gyroid with thickness 0.5mm and length unit cell 4mm

The same graphs and tables related to different thickness values are reported for the Schwarz P type with an elementary cell length of 4mm.

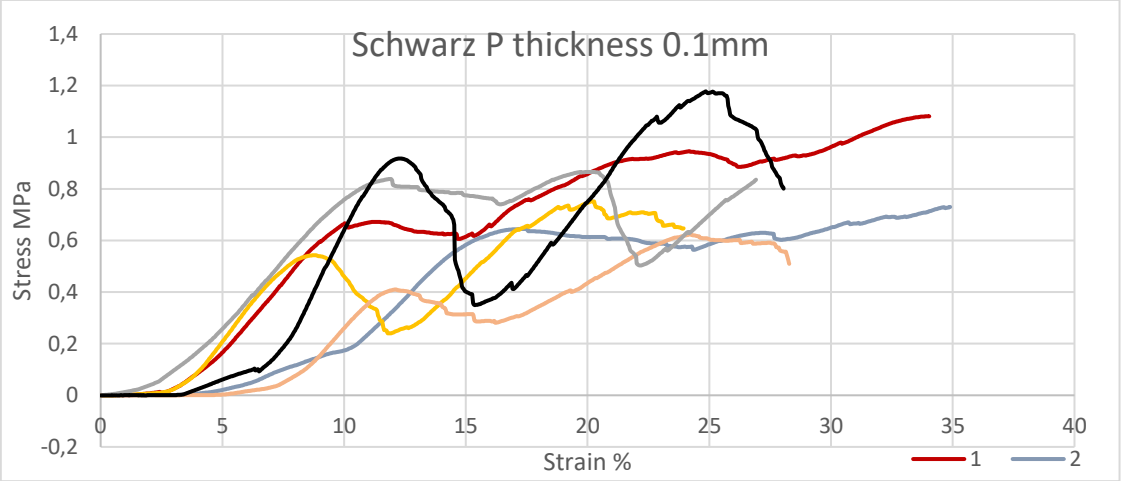

Figure 4.25 Curve stress-strain Schwarz P with thickness 0.1mm and unit cell length 4mm

Name	Depth	Width	Height	Volume	Mass	Density
dim	mm	mm	mm	mm³	g	kg/m³
1	11,94	11,84	11,8	1668,16	0,2451	146,92
2	11,9	11,7	11,7	1628,99		
3	12	11,8	11,6	1642,56	0,2305	140,33
4	11,6	11,76	11,7	1596,06	0,25	156,63
5	11,82	11,9	11,6	1631,63	0,2608	159,84
6	12,2	11,9	11,8	1713,12		

Table 4.13(a) Structural property of Schwarz P with thickness 0.1mm and length unit cell 4mm

Name	Young Mod	Mean Young	Yield Stress	Yield Force	Density relative
dim	MPa	MPa	MPa	N	%
1	9,69	10,1	0,56	79,08	12,57
2					
3	12,25		0,49	70,03	12
4	10,02		0,37	50,05	13,40
5	8,44		0,75	106,48	13,67
6					

Table 4.13(b) Mechanical property of Schwarz P with thickness 0.1mm and length unit cell 4mm

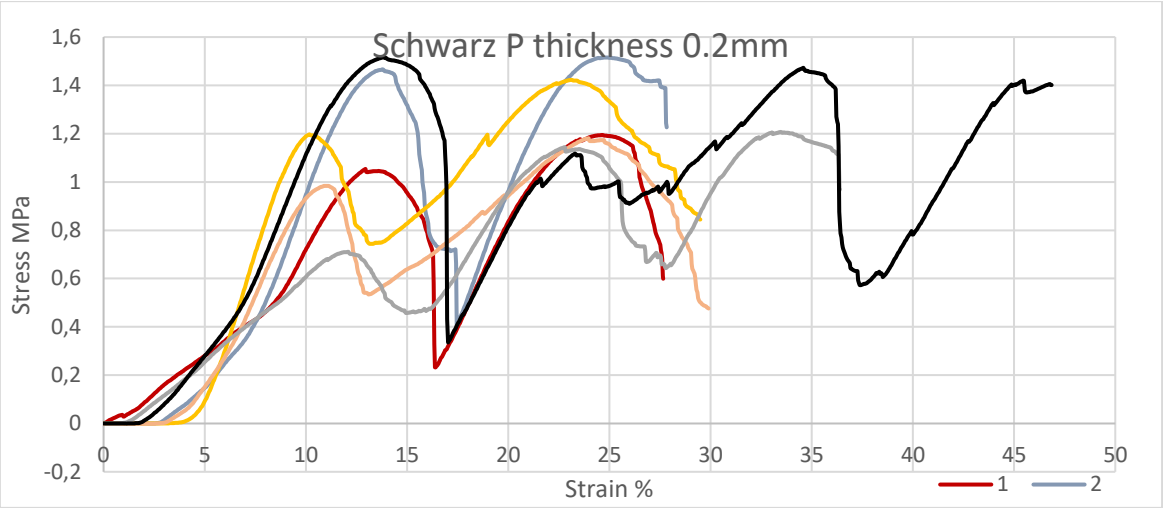

Figure 4.26 Curve stress-strain Schwarz P with thickness 0.2mm and unit cell length 4mm

Name	Depth	Width	Height	Volume	Mass	Density
dim	mm	mm	mm	mm³	g	kg/m³
1	12,26	11,86	12,24	1779,74	0,2782	156,31
2	12,14	11,88	12,08	1742,21	0,2782	159,68
3	11,9	12,1	12,08	1739,39	0,2793	160,57
4	11,88	11,8	12,1	1696,22	0,3071	181,05
5	11,8	12	12,3	1741,68	0,3169	181,95
6	12,04	11,96	12	1727,98	0,3004	173,84

Table 4.14(a) Structural property of Schwarz P with thickness 0.2mm and length unit cell 4mm

Name	Young Mod	Mean Young	Yield Stress	Yield Force	Density relative
dim	MPa	MPa	MPa	N	%
1		19,10			
2	30,29		1,28	180,95	13,66
3	25,98		1,06	157,7	13,74
4	14,01		0,92	125	15,49
5	7,14		0,64		15,56
6	18,13		1,43	196,4	

Table 4.14(b) Mechanical property of Schwarz P with thickness 0.2mm and length unit cell 4mm

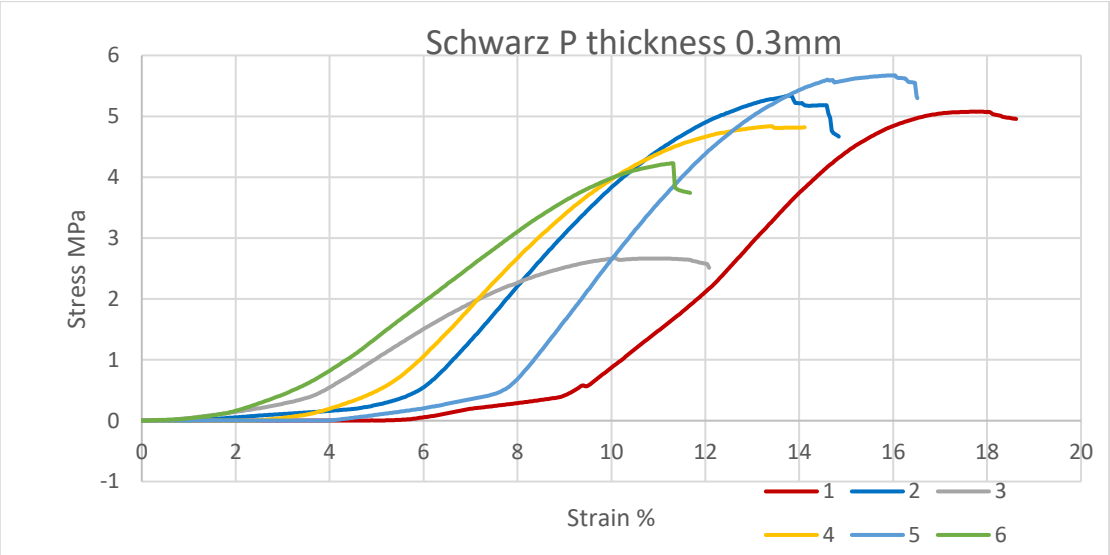

Figure 4.27 Curve stress-strain Schwarz P with thickness 0.3mm and unit cell length 4mm

Name	Depth	Width	Height	Volume	Mass	Density
dim	mm	mm	mm	mm³	g	kg/m³
1	11,84	12,2	12,1	1747,82	0,5132	293,62
2	12,08	12,14	11,86	1739,28	0,5033	289,37
3	12,2	12,08	11,7	1724,29	0,3702	214,69
4	12,1	11,96	11,98	1733,69	0,4722	272,36
5	12,16	12	11,9	1736,44	0,5042	290,36
6	11,78	12,2	12,3	1767,70	0,4786	270,74

Table 4.15(a) Structural property of Schwarz P with thickness 0.3mm and length unit cell 4mm

Name	Young Mod	Mean Young	Yield Stress	Yield Force	Density relative
dim	MPa	MPa	MPa	N	%
1		56,28			25,12
2					24,75
3					18,37
4	64,71		3,57	517,05	23,30
5					24,84
6	47,83		3,66	525,91	23,16

Table 4.15(b) Mechanical property of Schwarz P with thickness 0.3mm and length unit cell 4mm

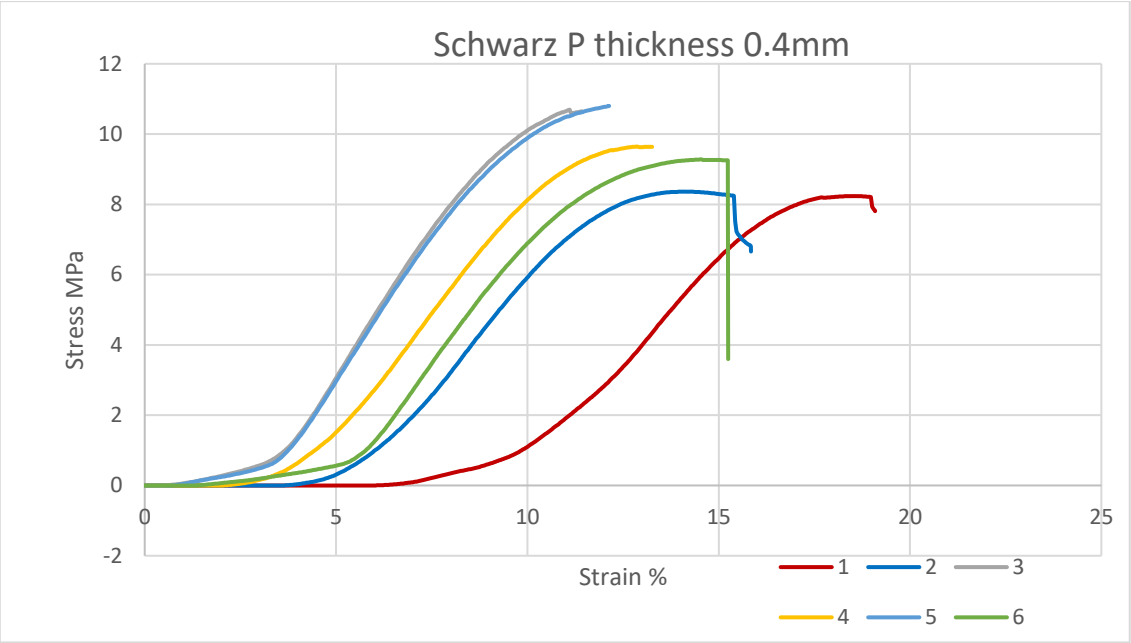

Figure 4.28 Curve stress-strain Schwarz P with thickness 0.4mm and unit cell length 4mm

Name	Depth	Width	Height	Volume	Mass	Density
dim	mm	mm	mm	mm³	g	kg/m³
1	12,08	12,2	12,1	1783,25	0,6408	359,34
2	12,08	12,16	12,1	1777,40	0,6218	349,84
3	12,16	12,12	12,16	1792,13	0,7105	396,45
4	12,1	12	12,2	1771,44	0,6533	368,79
5	12,16	12,08	12,08	1774,46	0,6784	382,31
6	12,12	12,26	12,26	1821,73	0,659	361,74

Table 4.16(a) Structurall property of Schwarz P with thickness 0.4mm and length unit cell 4mm

Name	Young Mod	Mean Young	Yield Stress	Yield Force	Density relative
dim	MPa	MPa	MPa	N	%
1	87,15	129,26	6,74	993,45	30,74
2	113,08		6,86	1007,21	29,93
3	162,72		8,81	1298,33	33,92
4	119,03		8,46	1228,93	31,55
5	164,34		8,8	1293,04	32,71
6					30,95

Table 4.16(b) Mechanical property of Schwarz P with thickness 0.4mm and length unit cell 4mm

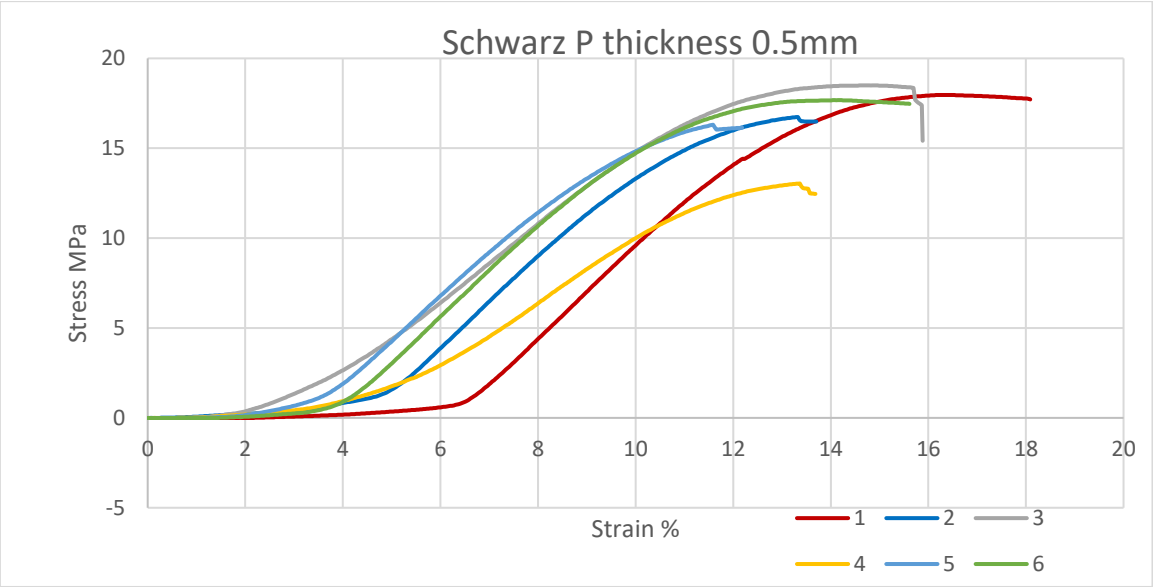

Figure 4.29 Curve stress-strain Schwarz P with thickness 051mm and unit cell length 4mm

Name	Depth	Width	Height	Volume	Mass	Density
dim	mm	mm	mm	mm³	g	kg/m³
1	12,35	11,98	12,1	1790,23	0,8838	493,67
2	12,1	12,1	12,2	1786,20	0,844	472,51
3	12,15	12,2	12,4	1838,05	0,894	486,38
4	12,08	12,22	12,35	1823,07	0,8109	444,79
5	12,2	12	11,98	1753,87	0,82	467,53
6	12,16	12,2	12,08	1792,09	0,8836	493,06

Table 4.17(a) Structural property of Schwarz P with thickness 0.5mm and length unit cell 4mm

Name	Young Mod	Mean Young	Yield Stress	Yield Force	Density relative
dim	MPa	MPa	MPa	N	%
1	261,79	231	12,74	1884,39	42,2
2	258,31		11,30	1654,9	40,43
3	187,07		13,88	2058	41,61
4	168,34		9,71	1432,69	38,05
5	248,9		11,22	1642,64	40
6	261,65		12,55	1861,55	42,18

Table 4.17(b) Mechanical property of Schwarz P with thickness 0.5mm and length unit cell 4mm

As it can be seen in the graphs, the lattices subjected to compression exhibit behaviour initially characterised by linear elastic deformation, followed by non-linear elastic deformation until the point of yield stress. From this point onwards, the lattices exhibit plastic deformation with the presence of rupture of internal parts of the scaffold.

It should be noted that no specimen were completely broken during the compression tests. This is due to the presence of micro-breaking of the lattice that occurs immediately after

its elastic deformation, which indicates that the lattice is breaking internally. For elastic modulus evaluations, it is not necessary to break the sample. The Figure 4.30 shows the lattices in the Gyroid type after the compression test.

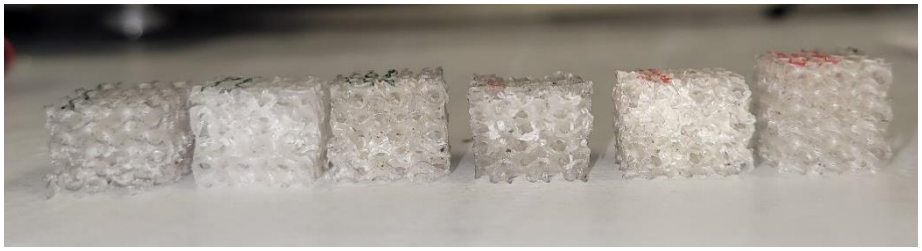

Figure 4.30 Gyroid scaffold after compression tests

The same graphs and tables were also obtained for the elementary cell lengths of 3mm and 2mm. Stress-strain behaviour and curves are similar to those obtained with a length of 4mm.

In the tables below are summarized the relevant characteristics for this type of characterisation, through which comparisons can be made between all scaffolds.

Thickness	mm	0,1	0,2	0,3	0,4	0,5
Density	kg/m³	150,93	168,9	271,86	369,75	476,33
Reative Density	%	12,91	14,45	23,26	31,64	40,75
Porosity	%	87,09	85,55	76,74	68,36	59,25
YoungMod	MPa	10,1	19,11	56,28	129,27	231
Yieldstress	MPa	0,54	1,07	3,62	7,93	11,89

Table 4.18 Schwarz P Unit cell length 4mm

Thickness	mm	0,1	0,2	0,3	0,4	0,5
Density	kg/m³	195,1	268,16	379,14	539,85	574,46
Reative Density	%	16,69	22,94	32,44	46,19	49,15
Porosity	%	83,31	77,06	67,56	53,81	50,85
YoungMod	MPa	29,68	39,88	80,38	145,26	156
Yieldstress	MPa	1,65	3,1	5,57	13,76	17,69

Table 4.19 Gyroid Unit cell length 4mm

Thickness	mm	0,1	0,2	0,3	0,4	0,5
Density	kg/m³	192,39	291,88	441,54	589,59	631,71
Reative Density	%	16,46	24,97	37,78	50,44	54,05
Porosity	%	83,54	75,03	62,22	49,56	45,95
YoungMod	MPa	17,19	52,73	150,66	321,71	317,99
Yieldstress	MPa	0,82	2,89	6,92	15,48	19,91

Table 4.20 Schwarz P Unit cell length 3mm

Thickness	mm	0,1	0,2	0,3	0,4	0,5

Density	kg/m³	354,53	404,25	605,41	706,41	690,57
Reative Density	%	30,33	34,59	51,8	60,44	59,09
Porosity	%	69,67	65,41	48,2	39,56	40,91
YoungMod	MPa	77,46	92,74	171	291,23	213,05
YieldStress	MPa	3,34	5,26	14,86	22,86	20,06

Table 4.21 Gyroid Unit cell length 3mm

Thickness	mm	0,1	0,2
Density	kg/m³	571,28	668,09
Reative Density	%	48,87	57,16
Porosity	%	51,13	42,84
YoungMod	MPa	192,58	383,86
YieldStress	MPa	9,9	24,31

Table 4.22 Schwarz P Unit cell length 2mm

It is possible to note that there is a similar pattern behavior for the various types of elementary cell length. As the thickness of the lattice increases, the density of the lattice increases because there is more material composing it in spite of porosity.

Yield stress increases slowly as the lattice thickness increases. This is due to the greater applied force that the material can withstand, as it is denser with increasing thickness.

Young modulus has an increasing trend with increasing thickness, because the material is characterized by a minimum deformation during the application of the load that increases in proportion to the thickness of the scaffold.

The TPMS structure developed show a porosity between 85% and 45%, less for the Schwarz P with a unit cell length equal to 2mm. This range of porosity is within the porosity values that characterise spongious bone, between 50-90%.

The Young Modulus values obtained in the compression tests are in the range of Elastic Modulus of spongious bone; in the test it is obtained values between 10-320 MPa including in the range 0.01-0.5 GPa of the spongious bone. [25]

Yield stress value for the scaffold with a porosity between 0.1-0.2mm is less than the value that caracterize cancellous bone, this happens because the resin is not ideal for applications in bone tissue despite being biocompatible.

Through the analyzed trends it is possible to create a relationship between the mechanical properties of the lattices with their own density.

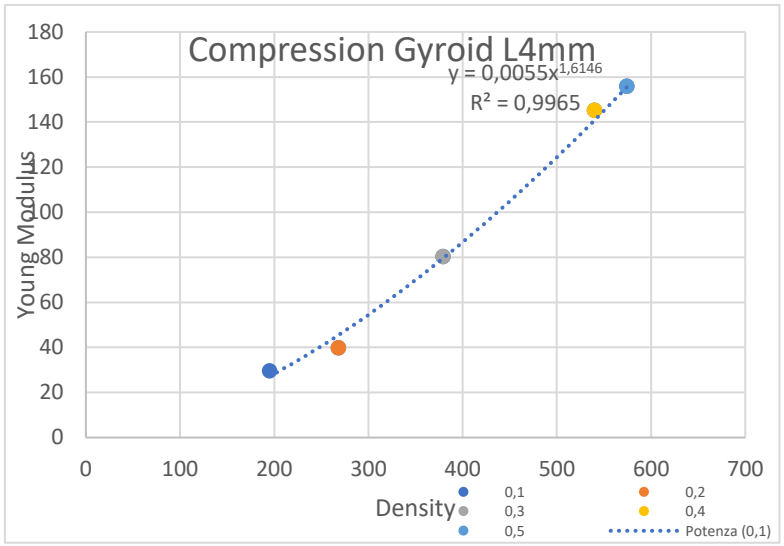

Figure 4.31 Relationship between Young Modulus and Density of Gyroid

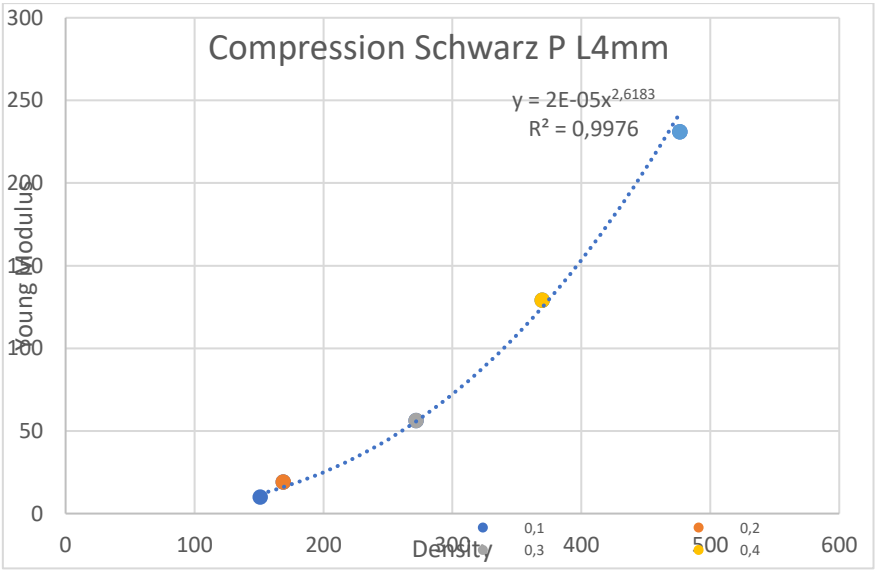

Figure 4.32 Relationship between Young Modulus and Density of Schwarz P

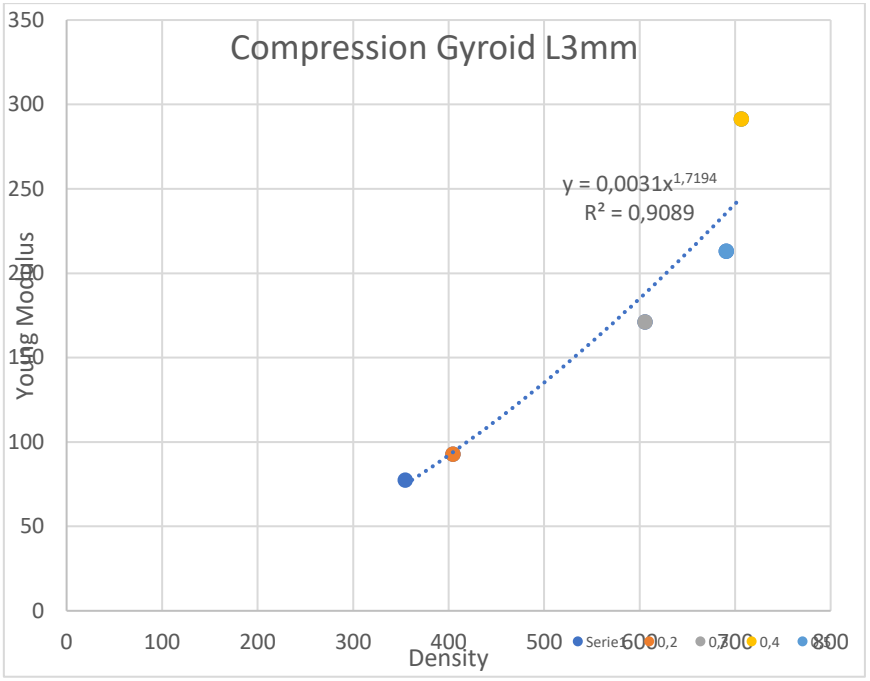

Figure 4.33 Relationship between Young Modulus and Density of Gyroid

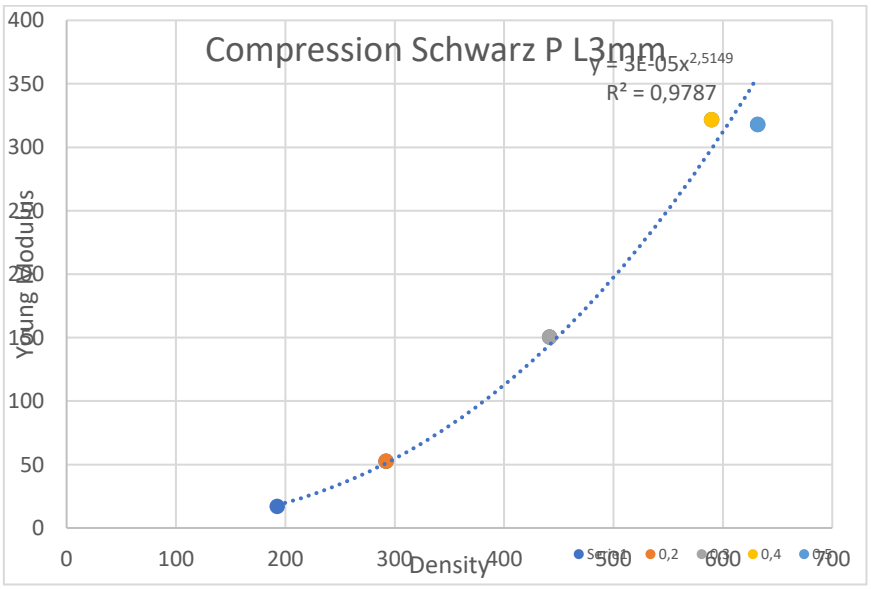

Figure 4.34 Relationship between Young Modulus and Density of Schwarz P

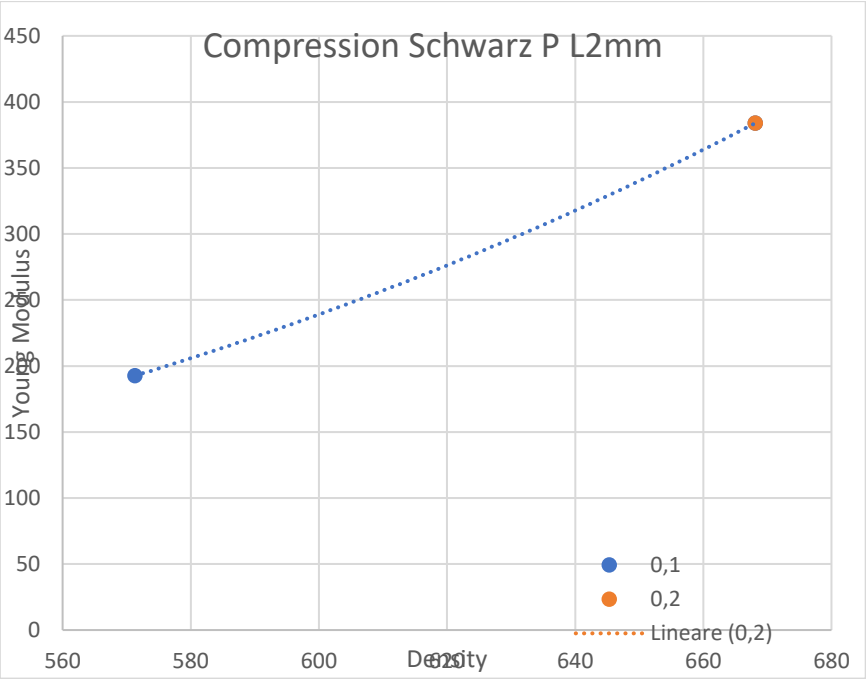

Figure 4.35 Relationship between Young Modulus and Density of Schhwarz P

The obtained graphs show that it is possible to obtain a relationship between Young Modulus and density for each scaffold.

The law which connects the mechanical and structural properties is similar to a power law but it is not possible to quantify it and to find a universal relation for each type of parameter.

Chapter 5

Conclusions

The research activity developed is aimed at the creation of scaffolds for bone tissue engineering applications through 3D printing.

The main purpose is to create a scaffold that can reproduce the mechanical and structural characteristics of bone.

The first phase of the study was dedicated to the creation of the scaffold structure through 3D modeling and the realization developed with the stereolithographic technique.

The second part of the thesis focused to the mechanical and structural characterization of the created lattices.

3D modelling using Python has enabled the creation of complex surface lattices simply by using trigonometric formulas. Despite being easy to use and free, Python is characterised by modules that do not allow high resolutions for the creation of 3D models in limited computational time. Another limitation found in Python is the inability to have information on the dimensional characteristics of the chosen elementary cells, among them the diameter of the pores and/or their interconnection.

The production of the scaffolds is done through stereolithography, a technique belonging to additive manufacturing. It has excellent mechanical qualities that are necessary in the biomedical field for the realisation of this type of scaffold, such as accuracy and impermeability, thus allowing the creation of objects with the best tolerance in the field of additive manufacturing and continuous in all their parts.

This technique is used for 3D printing of scaffolds mainly because it has the ability to produce high-precision components with small, complex internal features and a smooth surface finish.

These characteristics were demonstrated using the SEM microscope and the digital optical microscope.

The measurements made with microscopes for the calculation of the elementary cell length do not differ more than 1.1% from those programmed in Python. This error corresponds to a length deviation of 20-30μm, which may be due to measurement errors in the human-machine interface.

In fact, when comparing the thickness values measured with the microscopes and set in Python, there is a significant increase in the error between the two values as the size decreases, sometimes the measurement was not reported because of difficult acquisition.

According to the dimensional analysis of the pores, the average pore size was greater than those required for bone application specially for Gyroid structure.

Despite this, the structures developed showed a degree of porosity comparable to the range of porosity that characterizes the spongious bone, between 40-85%.

From images taken under the digital optical microscope, structures with a thickness of 0.1-0.2mm appear to have low mechanical stability and the edges of which are difficult to distinguish, with the SEM microscope, on the other hand, they show to be structures with defined shapes and continuous in all their parts.

It can be concluded that the electron scanning microscope, in addition to returning a more three-dimensional image, allows to have better resolutions, that provide more precise measurements, than the digital optical microscope.

Structural tests were followed by mechanical characterisation tests. The stress-strain curves obtained from the uniaxial compression tests for each sample reproduce the mechanical behaviour of the polymers.

The resin chosen has a behaviour comparable to that of a brittle polymer; it is characterised by an initial elastic behaviour, with a high slope of the curve, thus able to absorb little energy before breaking. Consequently, once the yield stress is exceeded, the samples fail internally by breaking. The rupture of the samples occurs without any noticeable plastic change.

From the curve, Young Modulus and Yield stress values were obtained for each of the specimens.

It can be seen that the values obtained for Young Modulus are within the range of values for spongious bone, between 0.5-0.05 Gpa. On the contrary, the Yield stress values are

lower than those that bone can withstand; this is due to the fact that the resin used, despite being biocompatible, is not suitable for applications in the bone field, and therefore has a lower compressive strength than that which would be obtained for bone.

A different choice of resin type, for example a polymer-ceramic composite resin, could lead to better results in the mechanical field.

In terms of Young Modulus and porosity, it can be ended that the scaffolds produced, despite the limitations of the various methods, satisfy the properties of spongious bone.

Given that the porosity and Young Modulus for individual scaffolds were derived, an attempt was made to describe and predict the relationship between them.

Quantifying a relationship linking mechanical properties and porosity for brittle and porous scaffolds as in this case, based on microstructural information such as the parameters set in the elementary cell, requires further research analysis.

Further analysis in terms of biocompatibility could be conducted on the scaffolds, in order to first assess the interaction between the biomaterial and the cells, and then whether the pore size and structural stability are able to favour cell attachment and promote cell proliferation.

Bibliography

[1] «Stampa 3D, la quarta rivoluzione industriale», *Coesum.it*, 19 gennaio 2021. https://coesum.it/stampa-3d-la-terza-rivoluzione-industriale/ (consultato 12 luglio 2022).

[1] admin, «History of 3D Printing in Medicine | Resources | Fast Radius». https://www.fastradius.com/resources/3d-printing-medicine.

[3] D. M. Bini, «Stampa 3D in medicina: didattica, protesi e biopriting», *InSalute*, 2 luglio 2018. https://blogunisalute.it/stampa-3d-medicina/ (consultato 12 luglio 2022).

[4] «5 casi di utilizzo innovativi della stampa 3D nel settore medico», *Formlabs*. https://formlabs.com/it/blog/stampa-3d-medicina-settore-sanitario/ (consultato 12 luglio 2022).

[5] R. Langer e J. P. Vacanti, «Tissue engineering», *Science*, vol. 260, n. 5110, pagg. 920–926, mag. 1993, doi: 10.1126/science.8493529.

[6] R. Langer, «Tissue Engineering», *Mol. Ther.*, vol. 1, n. 1, pagg. 12–15, gen. 2000, doi: 10.1006/mthe.1999.0003.

[7] P. Chocholata, V. Kulda, e V. Babuska, «Fabrication of Scaffolds for Bone-Tissue Regeneration», *Materials*, vol. 12, n. 4, pag. 568, feb. 2019, doi: 10.3390/ma12040568.

[8] F. J. O'Brien, «Biomaterials & scaffolds for tissue engineering», *Mater. Today*, vol. 14, n. 3, pagg. 88–95, mar. 2011, doi: 10.1016/S1369-7021(11)70058-X.

[9] H. Abukawa *et al.*, «The Engineering of Craniofacial Tissues in the Laboratory: A Review of Biomaterials for Scaffolds and Implant Coatings», *Dent. Clin. North Am.*, vol. 50, n. 2, pagg. 205–216, apr. 2006, doi: 10.1016/j.cden.2005.11.006.

[10] N. Grizzuti, L. Ambrosio, e P. A. Netti, «MATERIALI E TECNOLOGIE PER LA REALIZZAZIONE DI SOSTITUTI OSSEI NELL'INGEGNERIA DEI TESSUTI», pag. 270.

[11] F. Guillemot, V. Mironov, e M. Nakamura, «Bioprinting is coming of age: report from the International Conference on Bioprinting and Biofabrication in Bordeaux (3B'09)», *Biofabrication*, vol. 2, n. 1, pag. 010201, mar. 2010, doi: 10.1088/1758-5082/2/1/010201.

[12] «Tessuto osseo | Atlante di Istologia». http://www.istologia.unige.it/page13/page35/page42/ (consultato 29 settembre 2021).

[13] Ž. Perić Kačarević *et al.*, «An introduction to bone tissue engineering», *Int. J. Artif. Organs*, vol. 43, n. 2, pagg. 69–86, feb. 2020, doi: 10.1177/0391398819876286.

[14] A. P. Moreno Madrid, S. M. Vrech, M. A. Sanchez, e A. P. Rodriguez, «Advances in additive manufacturing for bone tissue engineering scaffolds», *Mater. Sci. Eng. C*, vol. 100, pagg. 631–644, lug. 2019, doi: 10.1016/j.msec.2019.03.037.

[15] P. Chocholata, V. Kulda, e V. Babuska, «Fabrication of Scaffolds for Bone-Tissue Regeneration», *Materials*, vol. 12, n. 4, pag. 568, feb. 2019, doi: 10.3390/ma12040568.

[16] «0003-3219%281994%29064%3C0175%3AWLABSA%3E2.0.CO%3B2.pdf». https://meridian.allenpress.com/angle-orthodontist/article/64/3/175/57155/Wolff-s-Law-and-bone-s-structural-adaptations-to

[17] «Malattia dell'osso | ICS Maugeri». https://www.icsmaugeri.it/patologie/malattia-dellosso (consultato 12 luglio 2022).

[18] G. Scandelli, «Caratterizzazione meccanica scaffold per tessuti ossei realizzati con stampa 3D e validazione modello computazionale», pag. 87.

[19] A. J. Salgado, O. P. Coutinho, e R. L. Reis, «Bone Tissue Engineering: State of the Art and Future Trends», *Macromol. Biosci.*, vol. 4, n. 8, pagg. 743–765, ago. 2004, doi: 10.1002/mabi.200400026.

[20] T. Ghassemi, A. Shahroodi, M. H. Ebrahimzadeh, A. Mousavian, J. Movaffagh, e A. Moradi, «Current Concepts in Scaffolding for Bone Tissue Engineering», . *NUMBER*, vol. 6, n. 2, pag. 10, 2018.

[21] «science.8493529.pdf». R. Langer, J.P. Vacanti, «Tissue engineering», *Articles, SCIENCE*, vol.260

[22] Y.-Z. Huang, H.-Q. Xie, e X. Li, «Scaffolds in Bone Tissue Engineering: Research Progress and Current Applications», in *Encyclopedia of Bone Biology*, Elsevier, 2020, pagg. 204–215. doi: 10.1016/B978-0-12-801238-3.11205-X.

[23] N. Abbasi, S. Hamlet, R. M. Love, e N.-T. Nguyen, «Porous scaffolds for bone regeneration», *J. Sci. Adv. Mater. Devices*, vol. 5, n. 1, pagg. 1–9, mar. 2020, doi: 10.1016/j.jsamd.2020.01.007.

[24] A. Wubneh, E. K. Tsekoura, C. Ayranci, e H. Uludağ, «Current state of fabrication technologies and materials for bone tissue engineering», *Acta Biomater.*, vol. 80, pagg. 1–30, ott. 2018, doi: 10.1016/j.actbio.2018.09.031.

[25] S. Zhang, S. Vijayavenkataraman, W. F. Lu, e J. Y. H. Fuh, «A review on the use of computational methods to characterize, design, and optimize tissue engineering scaffolds, with a potential in 3D printing fabrication», *J. Biomed. Mater. Res. B Appl. Biomater.*, vol. 107, n. 5, pagg. 1329–1351, lug. 2019, doi: 10.1002/jbm.b.34226.

[26] G. Turnbull *et al.*, «3D bioactive composite scaffolds for bone tissue engineering», *Bioact. Mater.*, vol. 3, n. 3, pagg. 278–314, set. 2018, doi: 10.1016/j.bioactmat.2017.10.001.

[27] B. Thavornyutikarn, N. Chantarapanich, K. Sitthiseripratip, G. A. Thouas, e Q. Chen, «Bone tissue engineering scaffolding: computer-aided scaffolding techniques», *Prog. Biomater.*, vol. 3, n. 2–4, pagg. 61–102, dic. 2014, doi: 10.1007/s40204-014-0026-7.

[28] B. Stevens, Y. Yang, A. Mohandas, B. Stucker, e K. T. Nguyen, «A review of materials, fabrication methods, and strategies used to enhance bone regeneration in engineered bone tissues», *J. Biomed. Mater. Res. B Appl. Biomater.*, vol. 85B, n. 2, pagg. 573–582, mag. 2008, doi: 10.1002/jbm.b.30962.

[29] Y.-Z. Huang, H.-Q. Xie, e X. Li, «Scaffolds in Bone Tissue Engineering: Research Progress and Current Applications», in *Encyclopedia of Bone Biology*, Elsevier, 2020, pagg. 204–215. doi: 10.1016/B978-0-12-801238-3.11205-X.

[30] L. Roseti *et al.*, «Scaffolds for Bone Tissue Engineering: State of the art and new perspectives», *Mater. Sci. Eng. C*, vol. 78, pagg. 1246–1262, set. 2017, doi: 10.1016/j.msec.2017.05.017.

[31] R. Ambu e A. E. Morabito, «Modeling, Assessment, and Design of Porous Cells Based on Schwartz Primitive Surface for Bone Scaffolds», *Sci. World J.*, vol. 2019, pagg. 1–16, giu. 2019, doi: 10.1155/2019/7060847.

[32] «Python», *Wikipedia*. 7 giugno 2022. Consultato: 13 luglio 2022. [Online]. Disponibile su: https://it.wikipedia.org/w/index.php?title=Python&oldid=127791465

[33] «Libraries in Python», *GeeksforGeeks*, 16 ottobre 2021. https://www.geeksforgeeks.org/libraries-in-python/ (consultato 13 luglio 2022).

[34] «PyPI · The Python Package Index», *PyPI*. https://pypi.org/ (consultato 13 luglio 2022).

[35] C. Sullivan e A. Kaszynski, «PyVista: 3D plotting and mesh analysis through a streamlined interface for the Visualization Toolkit (VTK)», *J. Open Source Softw.*, vol. 4, n. 37, pag. 1450, mag. 2019, doi: 10.21105/joss.01450.

[36] «Blender 3.2 Python API Documentation — Blender Python API». https://docs.blender.org/api/current/index.html (consultato 13 luglio 2022).

[37] «Welcome to pygmsh's documentation! — pygmsh documentation». https://pygmsh.readthedocs.io/en/latest/ (consultato 13 luglio 2022).

[38] A. S. Whitehead, «Triply Periodic Minimal Surfaces», *WeWantToLearn.net*, 3 febbraio 2019. https://wewanttolearn.wordpress.com/2019/02/03/triply-periodic-minimal-surfaces/ (consultato 14 luglio 2022).

[39] O. Al-Ketan e R. K. Abu Al-Rub, «MSLattice: A free software for generating uniform and graded lattices based on triply periodic minimal surfaces», *Mater. Des. Process. Commun.*, vol. 3, n. 6, dic. 2021, doi: 10.1002/mdp2.205.

[40] E. A. Ramírez, N. Béraud, F. Pourroy, F. Villeneuve, e M. Museau, «Design parameters effects on relative density of triply periodic minimal surfaces for additive manufacturing», *Procedia CIRP*, vol. 100, pagg. 13–18, 2021, doi: 10.1016/j.procir.2021.05.002.

[41] O. Al-Ketan, D.-W. Lee, R. Rowshan, e R. K. Abu Al-Rub, «Functionally graded and multi-morphology sheet TPMS lattices: Design, manufacturing, and mechanical properties», *J. Mech. Behav. Biomed. Mater.*, vol. 102, pag. 103520, feb. 2020, doi: 10.1016/j.jmbbm.2019.103520.

[42] «La guida definitiva alla stampa 3D stereolitografica (SLA)», *Formlabs*. https://formlabs.com/it/blog/guida-definitiva-stampa-3d-stereolitografia-sla/ (consultato 14 luglio 2022).

[43] «Buy Dental LT Clear Resin», *Formlabs*. https://dental.formlabs.com/store/dental-lt-clear-resin/ (consultato 14 luglio 2022).

[44] «Form 2», *Formlabs*. https://formlabs.com/it/3d-printers/form-2/ (consultato 14 luglio 2022).

[45] «Form Wash and Form Cure: Automated Post-Processing», *Formlabs*. https://formlabs.com/it/post-processing/wash-cure/ (consultato 14 luglio 2022).

[46] «Tech Specs for the Form 2», *Formlabs*. https://formlabs.com/it/3d-printers/form-2/tech-specs/ (consultato 14 luglio 2022).

[47] «Che cosa significa risoluzione nella stampa 3D?» https://formlabs.com/it/blog/risoluzione-stampa-3d/ (consultato 12 ottobre 2021).

[48] «Keyence VHX-6000 Digital Microscopes Rentals | ATEC». https://www.atecorp.com/products/keyence/vhx-6000 (consultato 14 luglio 2022).

[49] «Microscopio digitale - VHX-6000 | KEYENCE Italia». https://www.keyence.it/products/microscope/digital-microscope/vhx-6000/models/vhx-6000/ (consultato 14 luglio 2022).

[50] «Microscopia elettronica a scansione (SEM) | ALFATEST Materials science». https://www.alfatest.it/tecniche/sem-microscopia-elettronica-scansione/ (consultato 14 luglio 2022).

[51] G. Höflinger, «Brief Introduction to Coating Technology for Electron Microscopy», ago. 2013, Consultato: 14 luglio 2022. [Online]. Disponibile su: https://www.leica-microsystems.com/science-lab/brief-introduction-to-coating-technology-for-electron-microscopy/

[52] «Che cos'è il SEM? Spieghiamo la tecnologia del Microscopio elettronico a scansione | Microscopia Elettronica da banco». https://www.microscopiaelettronicadabanco.it/come-funziona-il-sem (consultato 14 luglio 2022).

[53] «SEM: i vari tipi di elettroni, rilevazione e informazioni ottenute | Microscopia Elettronica da banco». https://www.microscopiaelettronicadabanco.it/sem_vari_elettroni_rilevazione_informazioni_ottenute (consultato 14 luglio 2022).

[54] «1055_jcm-6000_catalog_en.pdf».

[55] «What is Micro-CT? An Introduction», *Micro Photonics*, 23 febbraio 2018. https://www.microphotonics.com/what-is-micro-ct-an-introduction/ (consultato 14 luglio 2022).

[56] S. Bertoldi, S. Farè, e M. C. Tanzi, «Assessment of scaffold porosity: the new route of micro-CT», *J. Appl. Biomater. Biomech.*, vol. 9, n. 3, pagg. 165–175, 2011, doi: 10.5301/JABB.2011.8863.

[57] «BR_AMS_Dinamometri_AGS-X-Series_21.pdf». Consultato: 15 luglio 2022. [Online]. Disponibile su: https://www.newprojectsrl.com/allegati/BR_AMS_Dinamometri_AGS-X-Series_21.pdf

[58] «Stress–strain curve», *Wikipedia*. 6 luglio 2022. Consultato: 15 luglio 2022. [Online]. Disponibile su: https://en.wikipedia.org/w/index.php?title=Stress%E2%80%93strain_curve&oldid=1096782857

Acknowledgements